Modal and SEA Parameters of Ribbed Plates

master thesis

Dickow, Kristoffer Ahrens

Publication date:
2009

Document Version
Publisher's PDF, also known as Version of record

Technical University of Denmark

Kristoffer Ahrens Dickow

Modal and SEA parameters of ribbed plates

Master's thesis, August 2009

DTU Electrical Engineering
Department of Electrical Engineering

Modal and SEA parameters of ribbed plates

Report written by:
Kristoffer Ahrens Dickow

Advisor(s):
Jonas Brunskog
Mogens Ohlrich

DTU Elektro
Technical University of Denmark
2800 Kgs. Lyngby
Denmark

studieadministration@elektro.dtu.dk

Project period:	2009-02-09 – 2009-08-07
ECTS:	35
Education:	M.Sc. Engineering Acoustics
Field:	Engineering Acoustics
Class:	Public
Edition:	1. edition
Remarks:	This report is submitted as partial fulfillment of the requirements for graduation in the above education at the Technical University of Denmark.

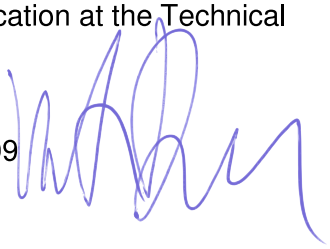

Modal and SEA parameters of ribbed plates

Technical University of Denmark

Modal and SEA Parameters of Ribbed Plates

Kristoffer Ahrens Dickow

M.Sc. Thesis
Engineering Acoustics
2009

DTU Electrical Engineering
Department of Electrical Engineering

Modal and SEA parameters of ribbed plates

Typesetting and graphical layout by the author using PDFLaTeX and the *memoir*-class
Font: Utopia (text) and Fourier (math) 11pt / 13.6pt
Printed at DTU, Electrical Engineering, Acoustic Technology, Building 352, August 2009
Figures and graphics are created using InkScape, LaTeX and MATLAB ®
Numerical computations and simulations are done using MATLAB version 7.7.0.471 (R2008b)
running on a linux server at DTU (gbar)
MATLAB is a registered trademark of MathWorks™

Technical University of Denmark

Master's thesis in Engineering Acoustics

Title:	Modal and SEA parameters of ribbed plates
– Danish title:	*Modale- og SEA parametre i afstivede plader*
Author:	Kristoffer Ahrens Dickow
– Student ID:	071324
	s071324@student.dtu.dk
Supervisors:	Jonas Brunskog
	Mogens Ohlrich
ECTS:	35 points
Number of copies:	4
Pages:	89
Appendices:	A-C
Date:	August 7th 2009

DTU Electrical Engineering
Department of Electrical Engineering

Abstract

When predicting the vibrational behavior of structures several different approaches can be used. One approach is to use differential analysis and the wave equation. This however, can be rather cumbersome and computationally demanding. Another approach is to consider the modal density and the statistical distribution of energies in the structure. This latter approach will be the main topic of the present thesis.

Rib reinforced plates are often used in lightweight building structures, vehicles, ships, aircrafts and so forth. In lightweight building elements the materials may be different kinds of wood, or perhaps wooden plates on steel frames, whereas constructions like vehicles, ships and aircrafts would more likely be made from some kind of metal or fiber material. What these otherwise different structures have in common, is that the reinforcing ribs are very often periodically spaced.

Existing simplified prediction tools, such as Statistical Energy Analysis (SEA) are not always suitable for these kinds of constructions, as for instance standard SEA is based on diffuse field assumptions, which do not apply to rib reinforced plates.

In order to adapt SEA theory to spatially periodic structures, the modal density of such structures need to be investigated. It the present thesis a modal model of a rib reinforced plate is presented and the modal density is investigated. The model is introduced by Chung [3] and is based on Hamilton's Principle by considering the kinetic and elastic potential energies in bending plates and beams. The model, which is made ready for parallel computing, is implemented in MATLAB.

It is shown that the modes of a spatially periodic ribbed plate can be divided into two groups; one showing periodic behavior in terms of pass bands and stop bands, and another that does not show such behavior. It is demonstrated that the rotational mass moment of inertia and the rotational stiffness are important to the pass band/stop band behavior. Further, simulations showing that the frequencies of the pass bands are determined primarily by the distance between the beams are performed. The period of the modal density of the perpendicular modes is seen to be proportional to kl.

The hope is that the implemented model and the findings regarding the grouping of modes may help the process of developing an SEA based prediction tool for spatially periodic constructions.

Preface

About the thesis

The present Master's thesis is the culmination of two years studying M.Sc. Engineering Acoustics at the Technical University of Denmark, Department of Electrical Engineering, Acoustic Technology. The work is submitted as partial fulfillment of the requirements for the Master of Science degree, and has been carried out between February 9th and August 7th 2009.

The prerequisites for reading this thesis is a basic knowledge withing the area of sound and vibration, as well as some theory on acoustics in general. Further, as the present work involves quite a bit of math, the reader should be acquainted with the topics of linear algebra, partial differential equations and complex analysis. I have made use of references [11], [1], and [35] to refresh my memory, but any basic mathematical textbook on each of these subjects should do.

During the development of the work at hand, many hours, days, and sometimes even weeks, have been spent working out mathematical details and optimizing MATLAB algorithms. Furthermore, it has been necessary to study several principles within both math and physics, as it is crucial to understand how tools work before they are applied.

It is my goal to convey the knowledge, that I have gained during my thesis studies, in such a way, that it will be understandable – though at times perhaps challenging – for my fellow students at the acoustics department.

Before getting started I was told, that one might want to use a quote of some famous person in the introductory material of a thesis. But, in the often frustrating process of writing, all that I could think of, was a quote of Kurt Cobain (*Nirvana - Very Ape* on the 1993 album *In Utero*):

> If you ever need anything please don't hesitate to ask someone else first.

However, looking back at the past six months, it has been a lot of work, but at the same time, it has been both intriguing and a great relief to become immersed in the studies of a single topic.

I hope, that other students will become interested in continuing the development of an SEA model, as described in the present thesis. If so, they should not hesitate to contact

me, regarding questions to my work. I would appreciate any kind of feedback, so please feel free to send me an email at s071324@student.dtu.dk.

Acknowledgements

I thankfully acknowledge the support and guidance by my supervisors, Assoc. Prof. Jonas Brunskog and Assoc. Prof. Mogens Ohlrich, at the Technical University of Denmark, the Department of Electrical Engineering, Acoustic Technology, Building 352. Without the project proposal and the enthusiastic commitment of Jonas Brunskog this thesis would not have been.

Further, I would like to thank Dr. Hyuck Chung, University of Otago, Dept. of Physics, New Zealand, who introduced me to the implemented modal model, and willingly offered his help in case I had any questions.

In addition to those, who have been involved directly in the development of the present thesis, I owe my gratitude to my employer, AkustikNet A/S (for teaching me things that cannot be taught in a class room), Lars Madsen (for writing a good introduction [24] to LaTeX), the open source community (for providing alternative software that students can afford), friends & family (for being there) and most of all my beloved and understanding girlfriend Anne, without whom I would probably never have started studying at DTU.

Kristoffer Ahrens Dickow
Kgs. Lyngby
August 2009

Contents

Part I

Introduction

CHAPTER

1 Introduction

When predicting the vibrational behavior of structures several different approaches can be used. One approach is to use differential analysis and the wave equation. This however, can be rather cumbersome and computationally demanding. Another approach is to consider the modal density and the statistical distribution of energies in the structure. This latter approach will be the main topic of the present thesis.

Rib reinforced plates are often used in lightweight building structures, vehicles, ships, aircrafts and so forth. In lightweight building elements the materials may be different kinds of wood, or perhaps wooden plates on steel frames, whereas constructions like vehicles, ships and aircrafts would more likely be made from some kind of metal or fiber material. What these otherwise different structures have in common, is that the reinforcing ribs are very often periodically spaced.

Existing simplified prediction tools, such as Statistical Energy Analysis (SEA), originally proposed by R.H. Lyon [21], are not always suitable for these kinds of constructions, as for instance standard SEA is based on diffuse field assumptions, which do not apply to rib reinforced plates. The reason for this being that a greater stiffness is introduced in the direction parallel to the ribs, which makes the plate act more as an orthotropic system (i.e., the system has different properties in two orthogonal directions) rather than an isotropic one. Secondly, in the direction perpendicular to the ribs, the spatial periodicity of the ribs introduce non-uniform distribution of the natural modes of the system, as it is well-known, that spatial periodicity results in so-called pass bands where waves can propagate, and stop bands where no wave propagation can occur. Further, the spatial attenuation of periodic structures is highly directional, as demonstrated by Sjökvist [33].

Adapting SEA to ribbed structures, however, is outside the scope of the present thesis. Our focus will be introducing and implementing a modal model, that can later be used to investigate the modal densities needed for SEA adaptation.

1.1 Goal

The main goal of the work carried out during this project is, to introduce and implement a modal model describing the behavior of a simple ribbed structure. The model will be using the theory of thin plates and slender beams and is based on Hamilton's Principle, which will be introduced later.

Speaking in terms of numerically investigating the properties of a system, a theoretical model is rather useless if it is not practical to implement in a computer. Thus, a basic requirement of success is, that the model can be used on an ordinary desktop computer, without requiring weeks of CPU time. As we will be dealing with matrices literally having billions of entries, this is not a trivial task.

In the present thesis a modal model is implemented such that the criterions described above are fulfilled. Further, the steps and theory behind the model are explained, so that other students interested in continuing the work on adapting SEA to ribbed structures need not go through several months of investigating for instance the calculus of variations, complex analysis and linear algebra, as applied in the work at hand.

1.2 General notation

When studying literature within acoustics and structural dynamics, many different (more or less consistent) notations are encountered. To avoid confusion, we wish to make a few initial remarks regarding the use of notation in the present thesis. A list of symbols can be found in the back on page 125.

Remark 1.1 (Conventions). In this thesis, the following conventions are applied (exceptions are explicitly noted in the respective sections):

- Non-bold italic describes a scalar or a real-valued function
- Regular boldface describes a matrix or a vector, where uppercase letters represent matrices and lowercases are vectors. Exceptions do occur when using greek letters and reshaping of vectors into matrices in chapters 5 and 6.
- A tilde is used for complex quantities. Excepted are the complex coefficients occurring in Fourier series as well as Young's moduli and other parameters becoming complex because of added damping.
- Time and spatial averaging are denoted by $\bar{\ }$ and $\langle\ \rangle$, respectively.
- Differentiation with respect to time is indicated by Newton's notation (a dot):

$$\dot{x}(t) = \frac{\mathrm{d}}{\mathrm{d}t}x(t). \tag{1.1}$$

- Spatial differentiation will be written explicitly as we are dealing with more than one spatial dimension.
- When making use of orthogonality a $\perp$ will be placed above the equals sign.
- An asterisk is used to denote the complex conjugate.
- $^{\mathrm{T}}$ is used for the transpose of matrices and vectors.

1.2.1 References and citations

Equations are numbered subsequently within each chapter, and are referred to using parenthesis. Citations and references to other peoples work are given using square brackets, with a number referring to the reference list in the back of the thesis on page 131. Proofs and techniques that are not referenced to specific sources are either considered general knowledge or, especially in chapter 6, derived in the process of writing this thesis. All figures are made from scratch. If based on similar figures from other sources it will be stated in the caption ('Redrawn from [ref]'). Excepted are figures in appendix A.

CHAPTER

2 The basics

In the following chapter, a short introduction to the basic principles behind structural analysis and acoustics will be given. It is assumed that the reader – to some extend – is familiar with these principles. Further reading can be found in most textbooks within acoustics and/or sound and vibration, such as references [13], [15] or [10].

2.1 Fundamental elements of vibration

We start by introducing the fundamental idealized mechanical elements; the mass, the spring, and the damper, following Hixson [12]. By using the term *idealized* we imply that the real-world properties of masses, springs and dampers may not be exactly as described in the following. For instance, we assume a spring to be massless, a mass to be non-deformable and the resistance of a damper to be perfectly proportional the velocity. Neither of these assumptions will be completely true in a real-world situation. However, they are good approximations when describing systems by their mechanical configurations.

In the following we list the fundamental equations of these elements, but we will not treat the elementary mechanical properties in further detail, as the only part in the present thesis, where we think in terms of masses, springs, and dampers is when validating our MATLAB implementation by looking at the phase of the point mobility in our model.

We make use of the fact that for a linear system, differentiation and integration with respect to time corresponds to multiplying and dividing by $\mathrm{i}\omega$ respectively. Linearity and complex exponential notation will be explained in sections 2.2 and 2.3.

2.1.1 Impedance and mobility

We define the mechanical impedance to be the complex ratio between the driving force and the response velocity. We often express it as a function of the angular frequency:

$$\tilde{Z}(\omega) = \frac{\tilde{F}\mathrm{e}^{\mathrm{i}\omega t}}{\tilde{v}\mathrm{e}^{\mathrm{i}\omega t}}, \tag{2.1}$$

where $\tilde{F}$ is the complex driving force and $\tilde{v}$ is the complex velocity.

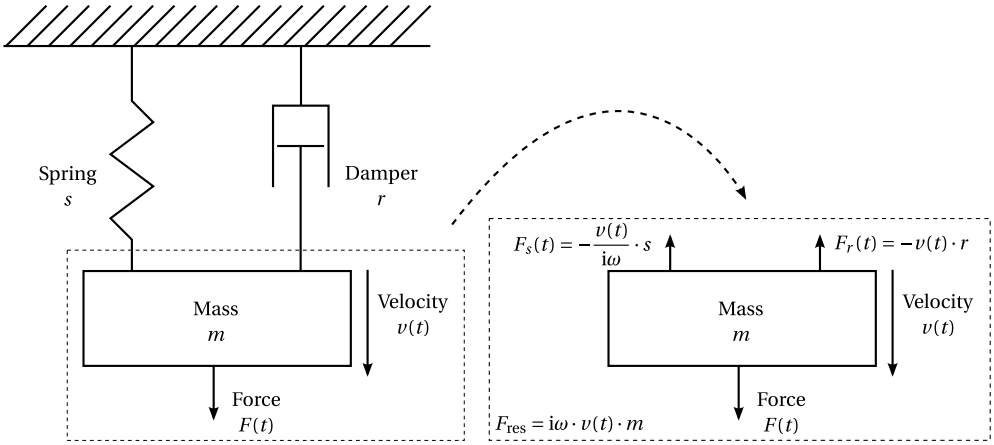

Figure 2.1: A viscously damped forced resonator on the left. On the right the forces acting on the mass are depicted. The forces of the spring and the damper act opposite the external force applied to the system. When dominated by the mass, the point mobility of a system will have a 90° phase lag, whereas for a spring dominated system it will have a 90° lead. When dominated by the damping, the phase of the point mobility is zero. We use the terms *mass-like*, *spring-like*, and *damping controlled*.

The reciprocal of the impedance is called the mobility:

$$\tilde{Y}(\omega) = \frac{\tilde{v}e^{i\omega t}}{\tilde{F}e^{i\omega t}}. \tag{2.2}$$

The magnitude of mobility can be thought of as a measure of how much force is needed to obtain a certain vibration level of a given structure; that is, a high mobility implies that the structure is easy to move at the given frequency.

In figure 2.1 a viscously damped forced resonator is shown. The system depicted includes both mass, spring and damper. Before deriving the mobilities of each, we need to introduce Newton's Laws of Motion and Hooke's Law of Elasticity.

Theorem 2.1 (Newton's Laws of Motion). Newton's three laws of motion states:

- The velocity of a moving body remains constant unless an external force is exerted on it.
- The acceleration of a body is directly proportional to the resulting force acting on it. The constant of proportionality is the mass of the body.
- Every action has an equal and opposite reaction.

The above laws can be found in most books dealing with motion of mechanical systems. See for instance Young and Freedman [41].

Newton's Laws are the foundations of the topic of classical mechanics, which is why the term *Newtonian mechanics* is often used to describe this branch of physics.

Theorem 2.2 (Hooke's Law of Elasticity). The simplest form of Hooke's Law of Elasticity is the spring equation. It states that the force exerted by the string is directly proportional to the displacement (compression or elongation) of the string [41]. The direction

of the spring force is opposite that of the displacement.

$$F_s = -sx, \tag{2.3}$$

where F_s is the force exerted by the string, s is the spring constant, and x is the displacement.

Now that we are familiar with the governing principles of motion, we can describe the behavior of the fundamental elements of vibration.

2.1.1.1 Masses

As we are assuming both springs and dampers to be massless, the total mass of the system shown in figure 2.1 is equal to the mass of the rigid body. By Newton's second law we get

$$F_{\text{res}}(t) = m\dot{v}(t) = \mathrm{i}\omega m v(t), \tag{2.4}$$

where m is the mass and the dot denotes differentiation with respect to time. The mobility of a mass can also be derived from Newton's second law:

$$Y_m(\omega) = \frac{1}{\mathrm{i}\omega m}. \tag{2.5}$$

Thus, if a system is dominated by a mass, the frequency response will show a 90° phase lag.

2.1.1.2 Springs

Similarly we can apply Hooke's law for the spring and obtain:

$$F_s(t) = \frac{sv(t)}{\mathrm{i}\omega}, \tag{2.6}$$

where s is the spring constant. By rearranging we find the mobility:

$$Y_s(\omega) = \frac{\mathrm{i}\omega}{s}, \tag{2.7}$$

which tells us that the phase of the velocity of a spring is leading the force by 90°.

2.1.1.3 Dampers

Finally, by definition the viscous damper is a device for which the applied force is directly proportional to the relative velocity between the end points. That is,

$$F_r(t) = r\,v(t), \tag{2.8}$$

where r is the damping constant of a viscous damper. The mobility is:

$$Y_r(\omega) = \frac{1}{r}. \tag{2.9}$$

Thus for a system of pure damping, the applied force is in phase with the vibration velocity.

2.1.2 Equation of motion

Knowing the forces related to masses, springs and dampers, we can express the equation of motion of a viscously damped forced resonator, such as the one shown in figure 2.1. Keep in mind that the resultant force equals the sum of force components, and therefore we have the following expression for the applied force:

$$F(t) = F_{\text{res}}(t) - F_r(t) - F_s(t) = v(t)\left(\mathrm{i}\omega m + r + \frac{1}{\mathrm{i}\omega}s\right), \tag{2.10}$$

where F is the applied force. From the above equation, we see that at lower frequencies the spring part is dominating, whereas at high frequencies the mass is dominating. Further introduction to simple mechanics can be found in Ohlrich [29].

In the next two sections we provide a brief description of linearity, and a more detailed introduction to the complex exponential notation.

2.2 Linear acoustics

In acoustics and structural vibration it is often assumed that the system behaves in a linear way; that is, the principle of superposition applies:

Theorem 2.3 (Principle of superposition). Quoting Hixson [12] we get the following theorem of superposition:

> If a mechanical system of linear bilateral elements includes more than one vibration source, the force or velocity response at a point in the system can be determined by adding the response to each source, taken one at a time (the other sources supplying no energy but replaced by their internal impedances).

Here, Hixson defines i linear bilateral element to be one, for which

- the magnitude of the basic elements (mass, spring and damper) are constant and do not depend on the amplitude of the motion of the system
- forces are transmitted equally well in either direction.

Both these assumptions are applied in the present thesis.

In simple terms this implies that if a system is described by the function $f(x)$, then

$$f(x_1 + x_2) = f(x_1) + f(x_2), \quad f(ax) = af(x). \tag{2.11}$$

Further, the principle of superposition is an important assumption in solving partial differential equations, as it implies that any linear combination of solutions to the governing differential equation of the system is in itself a solution, see Courant and Hilbert [8]. In modal analysis we make use of linearity to divide the system into a frequency part with time dependence and a mode shape depending only on position, as we shall see later on.

2.3 Complex notation

In the present thesis we make use of polar representation of complex numbers, based on Euler's formula:

Theorem 2.4 (Euler). For any real number x the following identity is true:

$$e^{ix} = \cos x + i \sin x, \tag{2.12}$$

where e is the base of the natural logarithm, and i is the imaginary unit. The above relation between the complex exponential and the trigonometric functions (sin and cos) can be extended into the complex domain such that:

$$e^{i\tilde{z}} = \cos \tilde{z} + i \sin \tilde{z}, \tag{2.13}$$

where $\tilde{z}$ is any complex number. See Kusse and Westwig [16].

Figure 2.2 illustrates how to think of harmonic signals in terms of phasors. In the figure, $\tilde{A}$ represents a complex amplitude having length A and initial phase angle φ. When multiplied by the time varying phasor $e^{i\omega_0 t}$ it represents time harmonic motion with angular speed ω_0. The magnitude of the complex amplitude is referred to simply as the amplitude.

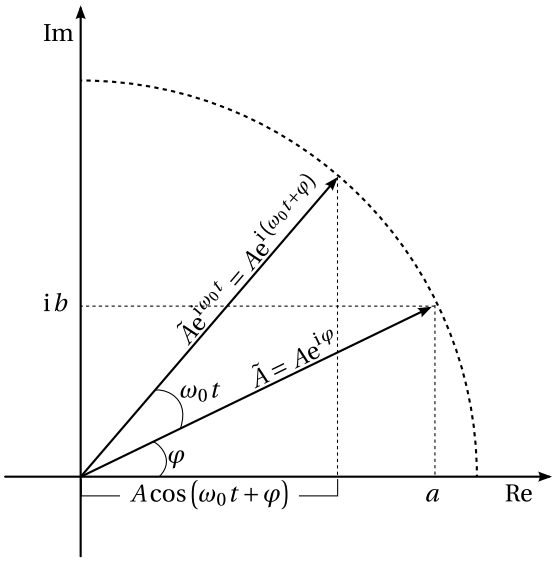

$$\tilde{A} = a + ib = Ae^{i\varphi}$$
$$A = |\tilde{A}| = \sqrt{a^2+b^2} = \sqrt{\tilde{A}\tilde{A}^*}$$

Figure 2.2: The complex plane. $\tilde{A}$ represents a complex amplitude having length A and initial phase angle φ. When multiplied by the time varying phasor $e^{i\omega_0 t}$ it represents time harmonic motion with angular speed ω_0. When using the complex exponential method, care must be taken to obtain the real part when seeking the correct physical equation. Redrawn from Kinsler et al. [15]

Using the complex exponential notation turns out to be very convenient when considering time harmonic motion. Multiplication of two complex numbers is easy as

$$A_1 e^{i\varphi_1} A_2 e^{i\varphi_2} = A_1 A_2 e^{i(\varphi_1+\varphi_2)}, \tag{2.14}$$

and similarly with division:

$$\frac{A_1 e^{i\varphi_1}}{A_2 e^{i\varphi_2}} = \frac{A_1}{A_2} e^{i(\varphi_1-\varphi_2)}. \tag{2.15}$$

Finally, the sum of two harmonic signals having the same frequency becomes a harmonic signal (keeping the frequency) with an amplitude equal to the magnitude of the sum of complex amplitudes:

$$\tilde{A}_1 e^{i\omega_0 t} + \tilde{A}_2 e^{i\omega_0 t} = \left(\tilde{A}_1 + \tilde{A}_2\right) e^{i\omega_0 t}. \tag{2.16}$$

Differentiation and integration of time harmonic signals are easily carried out when using the complex exponential notation:

$$\frac{d}{dt} e^{i\omega_0 t} = i\omega_0 e^{i\omega_0 t}, \tag{2.17}$$

and

$$\int e^{i\omega_0 t}\, dt = \frac{1}{i\omega_0} e^{i\omega_0 t} + C. \tag{2.18}$$

Thus, differentiation with respect to time is merely a matter of multiplying by $i\omega_0$, while integration is dividing by $i\omega_0$.

The only catch of using the complex exponential method is, that special care must be taken to obtain the real part when seeking the correct physical equation. That is, if we represent a vibrational displacement by a complex exponential, then the physical displacement equals the real part of the complex expression:

$$w(t) = \mathrm{Re}\left\{\tilde{w} e^{i\omega_0 t}\right\} = |\tilde{w}| \cos\left(\varphi + \omega_0 t\right), \tag{2.19}$$

where $w(t)$ is the displacement function, $\tilde{w} = |\tilde{w}| e^{i\varphi}$ is the complex amplitude, and $e^{i\omega_0 t}$ is the time harmonic frequency part.

The magnitude can conveniently be expressed by introducing the complex conjugate.

$$\text{if} \quad \tilde{A} = A_r + i A_i \quad \text{then} \quad \tilde{A}^* = A_r - i A_i \Rightarrow \tilde{A}\tilde{A}^* = A_r^2 + A_i^2, \tag{2.20}$$

where the asterisk denotes the complex conjugate. Thus, $\left|\tilde{A}\right|^2 = AA^* = A^* A$ by the theorem of Pythagoras.

2.4 The Dirac delta function

Later in the present thesis, we will be modelling beams of a ribbed plate as discrete disturbances. In the model, the effect of the beams will be introduced simply along lines at certain positions. Further, we will be using point excitation. For this we need to introduce the Dirac delta function. Strictly speaking, the Dirac delta function is not a function, but rather a distribution or a *generalized function*; that is, it cannot be defined pointwise, but is instead defined by the value of its integral against other functions. Without going into different mathematical aspects and definitions of the Dirac delta function, we define it as follows:

Definition 2.5 (The Dirac delta function). Let $f(x)$ be a continuous function on the interval $(-\infty,\infty)$. The Dirac delta function about zero, δ_0, is defined as the generalized function fulfilling

$$\int_{-\infty}^{\infty} f(x)\delta_0(x) = f(0). \tag{2.21}$$

Thus,

$$\int_a^b f(x)\delta_0(x-x_0) = \begin{cases} f(x_0) & \text{if } a < x_0 < b, \\ 0 & \text{otherwise.} \end{cases} \tag{2.22}$$

The derivative of the Dirac delta function is defined as:

Definition 2.6 (Derivative of the Dirac delta function). The derivative of the Dirac delta function has the following property:

$$\int_{-\infty}^{\infty} f(x)\delta_0'(x) = -\int_{-\infty}^{\infty} f'(x)\delta_0(x) = -f'(0), \tag{2.23}$$

where the prime denotes the derivative.

2.5 Vibration level

As often within sound and vibration, we will express the vibration by the vibrational velocity. The vibration velocity level is calculated from the displacement as follows:

$$L_v = 10\log\left(\frac{|\mathrm{i}\omega w|^2}{2v_{\text{ref}}^2}\right), \tag{2.24}$$

where $v_{\text{ref}} = 10^{-9}$ m/s is the reference velocity and the division by two is to obtain the root mean square value. Throughout this thesis $\log(\cdot)$ refers to the logarithm to the base 10.

CHAPTER

3 Plate analysis

Bending waves are the dominant wave type in terms of sound radiation from plates, as they give rise to significant displacement of the plate in the normal direction to the surface, giving rise to sound waves propagating away from the plate, see Mørkholt [25].

In the following section the general theory of bending waves (also known as flexural waves) in plates is described. Time harmonic motion and thin plates are assumed throughout the thesis. We define a plate as follows:

Definition 3.1 (Plate). The term *plate* refers to a homogeneous (isotropic) elastic continuum, bounded by two parallel planes [9]. The adjective *thin* is used when it is assumed that the wavelength is much larger than the thickness of the plate.

We usually denote the thickness of the plate h and place it in a Cartesian coordinate system such that the plate is located in the (x, y)-plane with the two bounding planes at $z = \pm h/2$ respectively. In chapter 5 we model the plate as a surface with no height, but described in terms of mass per unit area and bending stiffness per unit width.

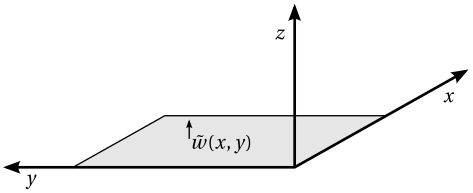

Figure 3.1: We use the convention of plates located in the (x, y) plane of a Cartesian coordinate system.

3.1 Bending waves in thin plates

Throughout this thesis, plates are assumed to be isotropic (i.e. having equal properties in all directions) unless otherwise is clearly stated. When the properties of a plate differs in two orthogonal directions, the plate is termed *orthotropic*. This may be the case with for instance plates of laminated wood. By adding stiffeners to an isotropic plate, the bending stiffness of the system changes. In the case of periodically spaced stiffeners the system

will behave as an orthotropic plate whenever the wavelength in the plate is considerably larger than the stiffener separation distance, see Mace [22]. In the present section we will look at the governing differential equations of bending waves in plates. The theory is based on Szilard [36], and we start by listing the assumptions used in the following (quoting [36]):

- The material is homogeneous, isotropic and linear elastic; that is, it follows Hooke's law.
- The plate is initially flat.
- The middle surface of the plate remains unstrained during bending.
- The *constant* thickness of the plate, h, is small compared to its other dimensions; that is, the smallest lateral dimension of the plate is at least 10 times larger than its thickness.
- The transverse deflections $w(x,t)$ are small compared to the plate thickness. A maximum deflection of one-tenth of the thickness is considered the limit of the small-deflection theory.
- Slopes of the deflected middle surface are small compared to unity.
- Sections taken normal to the middle surface before deformation remain plane and normal to the deflected middle surface. Consequently shear deformations are neglected.
- The normal stress σ_z in the direction transverse to the plate surface can be neglected.

We will not derive the plate equation, but such derivation can be found in [36]. The governing differential equation of bending waves in a thin plate excited by an external pressure distribution normal to the surface is:

$$B'_p\left(\frac{\partial^4 w}{\partial x^4}+2\frac{\partial^4 w}{\partial x^2 y^2}+\frac{\partial^4 w}{\partial y^4}\right)+m''_p\ddot{w}=p, \tag{3.1}$$

where B'_p is the bending stiffness per unit width, $w=w(x,y,t)$ is the transverse displacement of the plate and $p=p(x,y,t)$ is the external excitation, see Ohlrich [30]. Note that a plate is by definition 3.1 assumed to be homogeneous.

The bending stiffness per unit width (sometimes referred to as the flexural rigidity) can be calculated from the material properties; that is, Young's Modulus (E), the thickness (h) and the Poisson ratio (ν) [30].

$$B'_p=\frac{E_p h_p^3}{12\left(1-\nu^2\right)}. \tag{3.2}$$

Equation (3.1) can be written using the *Laplacian operator* (in two dimensions) by recognizing the following definitions: First, we define the *del operator*:

Definition 3.2 (Del operator). Using Cartesian coordinates in three dimensions, the del operator is defined as:

$$\nabla = \left(\frac{\partial}{\partial x}, \frac{\partial}{\partial y}, \frac{\partial}{\partial z} \right). \tag{3.3}$$

When applied to a scalar field, the del operator is called the *gradient*. When applied to a vector field it is called the *divergence*.

We can then define the Laplacian operator as:

Definition 3.3 (Laplacian in Cartesian coordinates).

$$\Delta = \nabla \cdot \nabla = \left(\frac{\partial^2}{\partial x^2} + \frac{\partial^2}{\partial y^2} + \frac{\partial^2}{\partial z^2} \right). \tag{3.4}$$

From this we can express equation (3.1) simply as

$$B'_p \nabla^4 w + m''_p \ddot{w} = p, \tag{3.5}$$

where ∇ is the two-dimensional (Cartesian) del operator and the biharmonic operator is defined as:

$$\nabla^4 = \Delta \cdot \Delta. \tag{3.6}$$

By introducing the structural wavenumber for bending waves and assuming time harmonic motion, the bending wave equation can be expressed as in terms of complex amplitudes:

$$\nabla^4 \tilde{w} - k_{b,p}^4 \tilde{w} = \frac{\tilde{p}}{B'_p}, \tag{3.7}$$

where $\tilde{w} = \tilde{w}(x, y)$ and $\tilde{p} = \tilde{p}(x, y)$ are the complex amplitudes such that

$$w(x, y, t) = \mathrm{Re}\left\{ \tilde{w}(x, y) \mathrm{e}^{\mathrm{i}\omega t} \right\}, \qquad p(x, y, t) = \mathrm{Re}\left\{ \tilde{p}(x, y) \mathrm{e}^{\mathrm{i}\omega t} \right\}. \tag{3.8}$$

The structural wavenumber for bending waves is defined by:

$$k_{b,p}^4 = \frac{\omega^2 \rho h_p}{B'_p} = \frac{\omega^2 m''_p}{B'_p}, \tag{3.9}$$

where the subscript p indicates that we are dealing with a plate (as later on we will be considering both beams and plate at the same time, hence the need for a subscript). From the wavenumber we can determine the bending wave speed, see Mørkholt [25]:

$$c_b = \frac{\omega}{k_b}, \tag{3.10}$$

and thus for a rectangular plate we have:

$$c_{b,p} = \sqrt[4]{\omega^2 \frac{B'_p}{m''_p}}. \tag{3.11}$$

3.1.1 Modal density

The modal density of a plate; that is, the number of modes per frequency, is found to be constant if disregarding the range of the lowest natural frequencies. From Ohlrich [30] we have:

$$\frac{\Delta N}{\Delta f} = \frac{S m_p''}{2\sqrt{B_p' m_p''}}, \tag{3.12}$$

where N is the number of modes, f is the frequency, and S is the plate area.

3.2 Bending waves in beams

Bending waves in beams are just like those of plates, except missing one dimension. Instead of *thin* we use the adjective *slender* when discussing beams.

3.2.1 Material properties of beams

The bending stiffness of a beam is defined as:

$$B_b = E_b I, \tag{3.13}$$

where I is the second area moment of inertia

$$I = I_y = \int z^2 \, \mathrm{d}S, \tag{3.14}$$

where z is the distance to the y-axis and S is the area. It is understood that it is the area moment of inertia about the (vertically centered) y-axis as depicted in figure 3.2. For a beam with rectangular cross section, the area moment of inertia is:

$$I = \frac{bh^3}{12}, \tag{3.15}$$

where b is the width and h is the height [30].

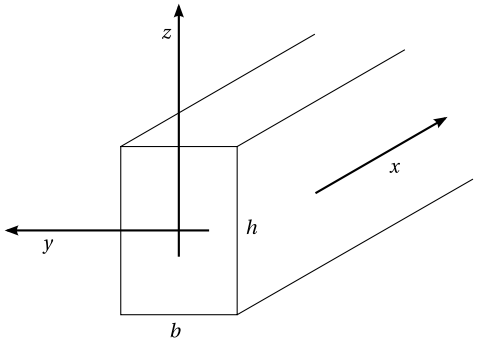

$$I_y = \int z^2 \, \mathrm{d}S, \quad \mathrm{d}S = b\,\mathrm{d}z$$
$$= \int_{-\frac{h}{2}}^{\frac{h}{2}} b z^2 \, \mathrm{d}z$$
$$= \frac{bh^3}{12}$$

Figure 3.2: The second moment of area, or the *area moment of inertia*, here calculated of a beam about the y-axis.

If we assume pure bending and time harmonic motion, and denote the transverse deflection of a beam by

$$w_b(x,t) = \mathrm{Re}\left\{\tilde{w}_b(x) \mathrm{e}^{\mathrm{i}\omega t}\right\}, \tag{3.16}$$

then the homogeneous bending wave equation for the beam can be expressed as

$$B_b \frac{\partial^4 w_b}{\partial x^4} + m'_b \ddot{w}_b = 0, \tag{3.17}$$

which we rewrite using the complex displacement amplitude and the bending wavenumber we obtain a fourth order homogeneous ordinary differential equation:

$$\frac{\mathrm{d}\tilde{w}_b}{\mathrm{d}x^4} - k_{b,b}^4 \tilde{w}_b = 0, \tag{3.18}$$

where the bending wavenumber is similar to the case of plates

$$k_{b,b}^4 = \frac{\omega^2 m'_b}{B_b}. \tag{3.19}$$

To keep plates and beams apart we use the extra subscript b to indicate that we are dealing with beams.

3.2.2 A Fourier sine series solution

Using the general solution of a n-th order linear homogeneous ordinary differential equation (with constant coefficients) we have the characteristic equation

$$\lambda^4 = k_{b,b}^4, \tag{3.20}$$

with roots

$$\lambda = \pm k_{b,b}, \pm \mathrm{i}\, k_{b,b}. \tag{3.21}$$

Thus, the general solution to equation (3.18) is:

$$\tilde{w}_b = c_1 \mathrm{e}^{k_{b,b}x} + c_2 \mathrm{e}^{-k_{b,b}x} + d_1 \cos\left(k_{b,b}x\right) + d_2 \sin\left(k_{b,b}x\right), \tag{3.22}$$

where the coefficients may include both real and imaginary terms, see Asmar [1]. To determine the coefficients, we need boundary conditions. Throughout this thesis we are assuming simply supported boundaries.

3.2.2.1 Applying the boundary conditions

The boundary conditions for a simply supported beam of length l_x are:

$$\tilde{w}_b(0) = \tilde{w}_b(l_x) = 0 \tag{3.23}$$

$$\left.\frac{\mathrm{d}^2\tilde{w}_b}{\mathrm{d}x^2}\right|_{x=0} = \left.\frac{\mathrm{d}^2\tilde{w}_b}{\mathrm{d}x^2}\right|_{x=l_x} = 0. \tag{3.24}$$

Applying the boundary conditions to the general solution (3.22) gives:

$$\tilde{w}_b(0) = 0 \quad \Rightarrow \quad c_1 + c_2 + d_1 = 0, \tag{3.25}$$

$$\begin{aligned} \tilde{w}_b(l_x) = 0 \quad \Rightarrow \quad & c_1 \mathrm{e}^{k_{b,b}l_x} + c_2 \mathrm{e}^{-k_{b,b}l_x} \\ & + d_1 \cos\left(k_{b,b}l_x\right) + d_2 \sin\left(k_{b,b}l_x\right) = 0, \end{aligned} \tag{3.26}$$

and

$$\left.\frac{\mathrm{d}^2\tilde{w}_b}{\mathrm{d}x^2}\right|_{x=0} = 0 \quad \Rightarrow \quad c_1 + c_2 - d_1 = 0, \tag{3.27}$$

$$\left.\frac{\mathrm{d}^2\tilde{w}_b}{\mathrm{d}x^2}\right|_{x=l_x} = 0 \quad \Rightarrow \quad c_1 \mathrm{e}^{k_{b,b}l_x} + c_2 \mathrm{e}^{-k_{b,b}l_x} - d_1 \cos\left(k_{b,b}l_x\right) - d_2 \sin\left(k_{b,b}l_x\right) = 0, \tag{3.28}$$

where we make use of the fact that $k_{b,b}^2 \neq 0$. Combining equations (3.25) and (3.27) gives

$$d_1 = 0 \quad \text{and} \quad c_2 = -c_1. \tag{3.29}$$

Thus (3.26) and (3.28) become

$$2c_1 \sinh\left(k_{b,b}l_x\right) + d_2 \sin\left(k_{b,b}l_x\right) = 0, \tag{3.30}$$

$$2c_1 \sinh\left(k_{b,b}l_x\right) - d_2 \sin\left(k_{b,b}l_x\right) = 0. \tag{3.31}$$

If $d_2 = 0$ that would force $c_1 = 0$ (the trivial solution) as $\sinh(x) \neq 0$ for $x \neq 0$. Thus we may assume that $d_2 \neq 0$. This implies that

$$\sin\left(k_{b,b}l_x\right) = 0 \quad \Rightarrow \quad k_{b,b} = \frac{m\pi}{l_x}, \quad m = 1,2,3,\ldots, \tag{3.32}$$

and thus that

$$c_1 = 0. \tag{3.33}$$

By the principle of superposition we can now express $\tilde{w}_b$ using the convergent infinite series [8]:

$$\tilde{w}_b(x) = \sum_{m=1}^{\infty} c_m \sin\left(\frac{m\pi x}{l_x}\right). \tag{3.34}$$

Such a series is known as a half-range expansion or a Fourier sine series expansion. In a similar manner a double expansion may be used to describe the solution to the homogeneous plate equation:

$$\tilde{w}(x,y) = \sum_{m,n=1}^{\infty} c_{mn} \sin\left(\frac{m\pi x}{l_x}\right) \sin\left(\frac{n\pi x}{l_y}\right), \tag{3.35}$$

where $\tilde{w}(x,y)$ is the complex amplitude of the transverse plate deflection.

3.3 Normal modes of vibration

We now move on to the topic of modal analysis. Modal analysis means describing a structure by modal parameters, namely the natural frequencies and corresponding mode-shapes, along with damping properties of the structure. The following introduction to modal analysis is based on Rossing [31], Cremer et al. [9], and Ohlrich [30]. We only deal with the mathematical methods of modal analysis, in contrary to experimental determination of the properties of a given structure. In the mathematical approach, the idea is to describe the modal properties of a combined structure by considering simple elements such as beams and plates, for which the modal properties are known. Then, the laws of physics are used to couple these simple elements together in order to obtain a modal model of the combined structure. Often, as in the present thesis, a solution will be found using numerical methods as an exact analytic solution to the problem is not possible to obtain.

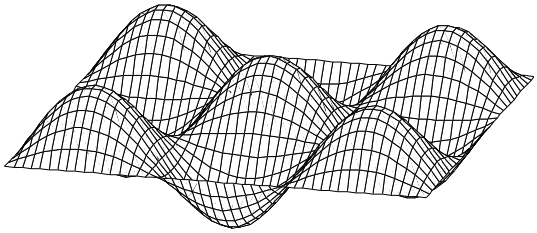

Figure 3.3: Mode shape of a simply supported plate

3.3.1 Natural frequencies and mode shapes

As we saw in the previous section, the homogeneous partial differential equation of a beam (or a plate) has a frequency dependant solution. The frequencies that correspond to the general solutions of the homogeneous governing wave equation are called the *natural frequencies* or *eigenfrequencies* of a system. In the case of a simply supported beam these solutions are on the form (3.32). The corresponding solutions are called *mode shapes* or *eigenfunctions*. If ω_n is a natural frequency of a system we say that the system has *normal mode* at ω_n. Figure 3.3 shows a mode shape of a finite thin plate simply supported along all four of its edges. Usually the modes are numbered by the indeces, m and n; that is, the mode shape in figure 3.3 corresponds to the mode $(3,3)$. By the term *normal* it is implied that the modes are orthogonal, and thus by linearity any forced vibration response of the system can be described as a linear combination of normal modes (as there are infinitely many normal modes). The concept of orthogonality will be introduced in the following.

3.3.1.1 Orthogonality

To define orthogonality, we must first introduce the concept of an inner product of two functions:

Definition 3.4 (Inner product). Let f and g be real-valued functions defind on the interval (a,b). The inner product of f and g is defined as

$$\langle f,g\rangle = \int_a^b f(x)g(x)\,\mathrm{d}x. \tag{3.36}$$

From Asmar [1].

Then, we define orthogonality as follows:

Definition 3.5 (Orthogonality). We say that two functions, f and g are orthogonal if

$$\langle f,g\rangle = 0. \tag{3.37}$$

A sequence of functions is orthogonal if

$$\langle \varphi_m,\varphi_n\rangle = \Lambda_n\delta_{m,n}, \tag{3.38}$$

where $\Lambda_n = \langle \varphi_n,\varphi_n\rangle$ is the squared norm of φ_n and $\delta_{m,n}$ is the Kronecker delta:

$$\delta_{i,j} = \begin{cases} 1 & \text{for } i = j \\ 0 & \text{otherwise.} \end{cases} \tag{3.39}$$

If the norm of each function, φ_m in the sequence is unity, the set of functions is called an orthonormal set.

In the following we shall explain the orthogonality of arbitrary mode shapes.

3.3.1.2 Natural frequencies of complex shapes

Not only 'simple' structures as those described in the previous section exhibit natural frequencies. According to Cremer et al. [9] structures of arbitrary shape have infinite sequences of natural frequencies. However, unlike the plate and beam described above, the distribution of these natural frequencies may be considerably more irregular, as they are rarely integral multiples of a fundamental frequency, as in the case of the simply supported beam.

At first sight it may seem problematic, as the key feature of mode shapes is the orthogonality used to describe any vibration response as a linear combination of mode shapes. However, the orthogonality of mode shapes still holds, even for complex shapes. Following Cremer et al. [9] we consider the kinetic energy of a structure excited such that it is vibrating precisely at modes with mode shapes $\varphi_n(x,y)$ and $\varphi_m(x,y)$ respectively.

$$\mathcal{K}_n = \frac{1}{2}\int_S v_n^2 m'' \varphi_n^2(x,y)\,\mathrm{d}x\,\mathrm{d}y, \tag{3.40}$$

and likewise

$$\mathcal{K}_m = \frac{1}{2}\int_S v_m^2 m'' \varphi_m^2(x,y)\,\mathrm{d}x\,\mathrm{d}y, \tag{3.41}$$

where $\mathcal{K}$ is the kinetic energy, S is the surface of the structure, v is the velocity amplitude corresponding to the mode shape, and m'' is the mass per unit area. Now, we excite the structure at both these modes simultaneously, keeping the excitation exactly as when exciting the modes one by one. Thus, by linearity and conservation of energy, the total kinetic energy equals the sum of (3.40) and (3.41).

$$\frac{1}{2}\int_S m''\left(v_n\varphi_m(x,y) + v_m\varphi_m(x,y)\right)^2\,\mathrm{d}x\,\mathrm{d}y \tag{3.42}$$

$$= \frac{1}{2}\int_S v_n^2 m'' \varphi_n^2(x,y)\,\mathrm{d}x\,\mathrm{d}y + \frac{1}{2}\int_S v_m^2 m'' \varphi_m^2(x,y)\,\mathrm{d}x\,\mathrm{d}y. \tag{3.43}$$

We conclude that this can only be true if the cross term disappears; that is, if

$$\int_S m''\varphi_m(x,y)\varphi_n(x,y)\,\mathrm{d}x\,\mathrm{d}y = 0, \quad \text{for} \quad m \neq n. \tag{3.44}$$

If the system has a uniform mass distribution the term m'' can be removed from the equation to simplify it even further.

3.3.2 Damping

Strictly speaking, the normal modes of vibration are only solutions to undamped systems, and thus they may prove to be imprecise for highly damped systems. However, in cases where the damping is proportional to either the structural stiffness of the system or to its mass distribution, the normal modes of vibration provide exact solutions according

to Rossing [31]. In these cases the structure is said to be proportionally damped, and the damping matrix can be described as a linear combination of the mass and stiffness matrices.

In the present thesis, we will not be dealing with damping matrices, but instead we will be using complex mode shapes. The damping is introduced by applying an imaginary part to the Young's modulus, following Ohlrich [30]. We assume the complex Young's modulus to be constant; that is the complex part representing the damping is assumed to be independent of frequency.

3.3.3 Modal density

As will be explained in chapter 7, the modal density is an important parameter in SEA. Throughout this text, the modal density is denoted $\Delta N/\Delta f$ with N being the number of modes and Δf being the bandwidth. Thus, the modal density is simply calculated by counting the number of modes occurring within a given frequency band and dividing by the bandwidth.

It is well known that for periodic structures, the modes are non-uniformly distributed; they tend to group together in so-called pass bands where waves propagate, contrary to the stop bands, where no wave propagation occurs. See Cremer et al. [9].

Part II

Theory and implementation

CHAPTER

4 An introduction to Hamilton's Principle

In the following chapter, a brief introduction to the calculus of variations and Hamilton's Principle will be given. These techniques are deployed in the present thesis in the development of a modal model describing the behavior of a ribbed plate. We will not provide proofs of the validity of these principles and techniques, but such proofs can be found in the referenced literature along with more detailed mathematical definitions.

4.1 Calculus of variations

Hamilton's Principle is an extremely powerful tool based on energy relations of a system. It is also known as *The Principle of Least Action*, and states that [17, ch. 5]:

Theorem 4.1 (Hamilton's Principle). In any conservative field, the *action*, $\mathcal{S}$, is stationary, i.e.

$$\delta\mathcal{S} = \delta\int_{t_1}^{t_2} \mathcal{L} = 0, \tag{4.1}$$

where $\mathcal{L}$ is the *Lagrangian* describing the difference between the kinetic energy, $\mathcal{K}$ and the potential energy, $\mathcal{P}$.

$$\mathcal{L} = \mathcal{K} - \mathcal{P}. \tag{4.2}$$

The operator δ is called the *first variation* and will be introduced shortly.

Note that Hamilton's Principle does not actually require the least action. It only states that the action is stationary; that is, either a minimum, a maximum or a saddle point.

To understand the physical nature of the principle, we use the words of Morse and Ingard [26, p. 197]:

> Hamilton's Principle of dynamics states, that the displacement of a system adjusts itself in shape and velocity, such that the integral of this Lagrange function over time, from some initial time t_0 to a specified final time t_1, is minimal.

In order to apply Hamilton's Principle, we need tools to find stationary values of an integral of functions. Such tools can be found in most textbooks dealing with calculus of variations. The following introduction is based on Tang [37], but references [17] and [39] should be mentioned as well. In the following, and throughout this thesis in general, things are assumed to be sufficiently smooth and differentiable where needed.

4.1.1 The δ operator

In mathematics a function can be thought of as a mapping that produces a unique output (the dependant variable) to each argument (the independant variable) in its domain. A mapping assigning a real value to each function within a given class of functions is called a functional [2].

Localizing minima of functions is a widely used task within ordinary calculus. In physics this task is often extended to minima of certain functionals:

$$I = \int_{x_1}^{x_2} F(y, y', x)\,\mathrm{d}x, \tag{4.3}$$

where F is a function of $y(x)$, $y'(x)$ and x, determined by the physical nature of the problem at hand. The prime in this case denotes the derivative of y with respect to x.

As F is fixed by physics, the value of the definite integral can only be varied by varying the curve $y(x)$, and thus I is a functional of $y(x)$. Our goal is to find a curve that minimizes the integral of equation (4.3). The arguments carried out in the present section are mainly based on [37, ch. 7].

Assume that $y(x)$ minimizes (4.3). Then, any neighboring curve should have an integral value greater than or equal to that of $y(x)$. Let ε be a very small value, and let $\gamma(x)$ be an arbitrary (smooth) function bounded by $\gamma(x_1) = \gamma(x_2) = 0$. The family of neighboring curves having the same endpoints as $y(x)$ can be expressed as:

$$Y(x) = y(x) + \varepsilon\gamma(x). \tag{4.4}$$

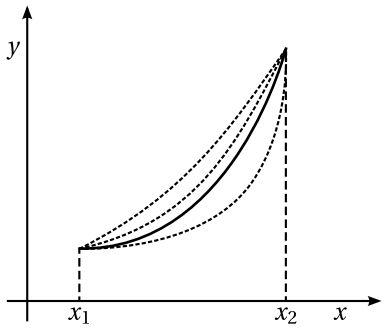

Figure 4.1: Variations of a curve. The solid line is the curve along which the integral is stationary, the dotted lines are small variations from the solid path. Redrawn from [37, p. 368].

The difference between $y(x)$ and its neighboring curves are called variations of $y(x)$. Such variations of a curve are shown in figure 4.1.

Now, the integral of a given member of the family of neighbouring curves can be written using the parameter ε:

$$I(\varepsilon) = \int_{x_1}^{x_2} F(Y, Y', x)\,\mathrm{d}x, \tag{4.5}$$

where $I(0)$ by definition is the minimal integral as

$$Y(x)\Big|_{\varepsilon=0} = y(x). \tag{4.6}$$

We then expand equation (4.5) using Taylor series about $\varepsilon = 0$.

$$I(\varepsilon) = I(0) + \frac{\mathrm{d}I}{\mathrm{d}\varepsilon}\Big|_{\varepsilon=0} \varepsilon + \text{higher order terms}, \tag{4.7}$$

and observe that the variation of I due to the variation (4.4) is the difference between $I(\varepsilon)$ and $I(0)$.

$$I(\varepsilon) - I(0) = \frac{\mathrm{d}I}{\mathrm{d}\varepsilon}\Big|_{\varepsilon=0} \varepsilon + \text{higher order terms}. \tag{4.8}$$

Note that the higher order terms become negligible as ε is very small. From this we define the *first variation* of I and denote it δI:

$$\delta I = \frac{\mathrm{d}I}{\mathrm{d}\varepsilon}\Big|_{\varepsilon=0} \varepsilon. \tag{4.9}$$

As we require that $I(\varepsilon)$ takes on a minimum for $\varepsilon = 0$ for any $\gamma(x)$, we know that

$$\frac{\mathrm{d}I}{\mathrm{d}\varepsilon}\Big|_{\varepsilon=0} = 0. \tag{4.10}$$

This is a necessary but not sufficient condition of a minimum, but as we are only seeking stationary values, it can be shown that such points can be identified by a vanishing first variation.

Theorem 4.2 (Stationary values). The integral (4.3) has a stationary value when

$$\delta I = 0, \tag{4.11}$$

that is, when its first variation vanishes.

4.1.1.1 Properties of the δ-operator

Lanczos [17] proves the following properties of the δ-operator:

Theorem 4.3 (Properties of the δ-operator). The variational operator has the following properties regarding differentiation and integration:

- Variation and differentiation are permutable processes.
- Variation and integration are permutable processes.

From [17, p.57].

These properties are fundamental and will be used without further notice. Later on we shall need the following theorem, also derived by Lanczos:

Theorem 4.4 (Stationary values of functions of multiple variables). A necessary and sufficient condition that a function F of n variables shall have a stationary value at a certain point P is that the n partial derivatives of F with respect to all n variables shall vanish at that point P [17, p.40].

4.2 Euler-Lagrange principles

Consider the integral

$$\mathcal{S} = \int_{t_1}^{t_2} F(x(t), \dot{x}(t), t)\, \mathrm{d}t. \tag{4.12}$$

It can be proven that equation (4.12) is stationary whenever the *Euler-Lagrange equation* is fulfilled, see e.g. [37]:

Theorem 4.5 (Euler-Lagrange). A necessary but not sufficient condition of a minimum of $\mathcal{S}$ is

$$\frac{\partial F}{\partial x} - \frac{\mathrm{d}}{\mathrm{d}t}\left(\frac{\partial F}{\partial \dot{x}}\right) = 0, \tag{4.13}$$

where $\mathcal{S}$ is defined as in equation (4.12).

The Euler-Lagrange equations (plural in the case of several generalized coordinates in the Lagrangian) are often referred to simply as the *Lagrangian equations*, and can be used to derive differential equations of motion.

4.3 Hamilton's Principle

Proving Hamilton's Principle as stated in theorem 4.1 is outside the scope of this thesis, but inspired by Tang [37] we will provide an example based on a simple harmonic oscillator.

Consider a mass m and a spring with spring constant s. If no external force is applied the relation between forces is

$$m\ddot{x} + sx = 0, \tag{4.14}$$

as the spring acts opposite the direction of movement. We will now derive the same result by applying Hamilton's Principle.

Let the Lagrangian be the difference between kinetic and potential energy:

$$\mathcal{L}(x, \dot{x}, t) = \frac{1}{2}m\dot{x}^2 - \frac{1}{2}sx^2, \tag{4.15}$$

In order for the action integral to be stationary, the Euler-Lagrange equation must be fulfilled:

$$\frac{\partial \mathcal{L}}{\partial x} - \frac{\mathrm{d}}{\mathrm{d}t}\left(\frac{\partial \mathcal{L}}{\partial \dot{x}}\right) = m\ddot{x} + sx = 0, \tag{4.16}$$

which we recognize as (4.14).

4.3.1 Hamilton's Principle for complex fields

Hamilton's Principle is applicable only to purely real functionals, since it describes energy relations which must be real. However, later in the present thesis, we shall describe the motion of a structure using complex Fourier sine-series.

For this reason we will tailor a formulation of Hamilton's Principle extending it to work within complex fields, by defining a real valued Lagrangian from complex variables. The way we do so, is simply by recognizing that the Lagrangian of our system is a quadratic functional:

$$\mathcal{L} = \mathcal{L}(w^2, \dot{w}^2), \tag{4.17}$$

of real deflections,

$$w = w(x,y,t) = \mathrm{Re}\left\{\tilde{w}(x,y)\mathrm{e}^{\mathrm{i}\omega t}\right\}. \tag{4.18}$$

Let $\tilde{w} = w_R + \mathrm{i}\, w_I$, where w_R and w_I are real functions of x and y. Consider the squared deflection:

$$\begin{aligned} w^2 &= \left(\mathrm{Re}\left\{\tilde{w}(x,y)\mathrm{e}^{\mathrm{i}\omega t}\right\}\right)^2 && (4.19)\\ &= \left(w_R\cos(\omega t) - w_I\sin(\omega t)\right)^2 && (4.20)\\ &= w_R^2\cos^2(\omega t) + w_I^2\sin^2(\omega t) - 2w_R w_I\cos(\omega t)\sin(\omega t). && (4.21) \end{aligned}$$

Now, the integral of the squared deflection over one period (of length T) is:

$$\begin{aligned} I &= \int_0^T w^2\,\mathrm{d}t && (4.22)\\ &= \int_0^T w_R^2\cos^2(\omega t) + w_I^2\sin^2(\omega t) - 2w_R w_I\cos(\omega t)\sin(\omega t)\,\mathrm{d}t && (4.23)\\ &= w_R^2\int_0^T \cos^2(\omega t)\,\mathrm{d}t + w_I^2\int_0^T \sin^2(\omega t)\,\mathrm{d}t - 2w_R w_I\int_0^T \cos(\omega t)\sin(\omega t)\,\mathrm{d}t && (4.24)\\ &= \frac{T}{2}\left(w_R^2 + w_I^2\right) && (4.25)\\ &= \frac{T}{2}\tilde{w}\tilde{w}^*, && (4.26) \end{aligned}$$

where $\tilde{w}$ is the complex deflection amplitude and the asterisk is the complex conjugate. In the derivation that leads from (4.24) to (4.25) we made use of the following identities:

$$\int \cos^2(\omega t)\,\mathrm{d}t = \frac{t}{2} + \frac{1}{4\omega}\sin(2\omega t) + C, \qquad \int \sin^2(\omega t)\,\mathrm{d}t = \frac{t}{2} - \frac{1}{4\omega}\sin(2\omega t) + C, \tag{4.27}$$

and

$$2\int \cos(\omega t)\sin(\omega t)\,\mathrm{d}t = \frac{1}{\omega}\sin^2(\omega t), \tag{4.28}$$

which can be derived using integration by parts. In a similar manner to the derivation (4.22)-(4.26) , we see that

$$\int_0^T \dot{w}^2\,\mathrm{d}t = \frac{T}{2}\omega^2\tilde{w}\tilde{w}^*. \tag{4.29}$$

Thus, we can safely apply Hamilton's Principle to our system.

CHAPTER

5 A modal model

In the following chapter we implement a modal model, that will be used to calculate the vibrational behavior of a thin plate supported by periodically spaced beams and exerted to a harmonic point force excitation. First, the model is implemented as described by Brunskog and Chung [3]. Later on we shall expand it by including twisting of the beams, as done in a slightly different approach by Sjökvist, Brunskog, and Jacobsen [34]. The implementation is based on Hamilton's Principle, as described in chapter 4. The model is used in references [4] and [5] as well. In references [6] and [7], Chung et al. use the same basic principles, but without specifying what numerical methods are used to solve the problem – in the latter of the two, different theoretical approaches of modelling wooden joist floors are discussed.

A mentioned previously, we are assuming the system to be linear and simply supported along all plate edges and at beam ends. Further, we will be applying theory based on the assumption of thin plates and slender beams. The pressure from the surrounding air is neglected, and we are only considering bending wave motion.

5.1 The subject of investigation

Figure 5.1 shows a thin plate supported by equally spaced parallel beams. A rectangular coordinate system is introduced having its origin at one of the corners of the plate, such that the plate is located in the (x, y)-plane and the beams are parallel to the x-axis. When at rest it is assumed that $z = 0$ anywhere on the surface of the plate.

In the model developed in the present thesis, we shall assume that the plate is simply supported along all four edges, and that the beams are simply supported at both ends. Further, we are assuming that the system is excited in the transverse direction by a time harmonic point force, as depicted in figure 5.1. In the following, the plate has dimension $l_x \times l_y$ [m^2], and is supported by S beams.

5.2 Energy considerations

In the model we make use of Hamilton's principle as introduced in chapter 4, to find the displacement of the plate, by minimizing the total energy in the structure. The verti-

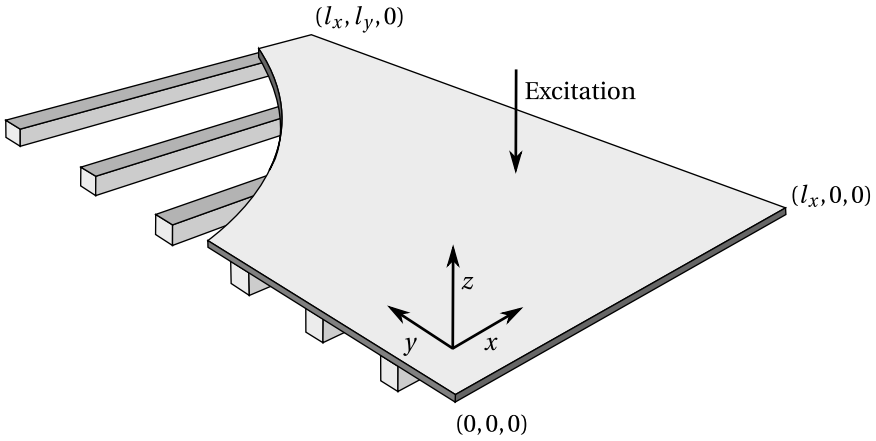

Figure 5.1: A ribbed plate. Redrawn from [3]

cal displacement of the plate is denoted $w(x, y, t)$ and the displacement of the beams by $w_b(x, j, t)$, where $j = 1, 2, \ldots, S$.

Following Brunskog and Chung [3], we consider the action integral over the time period $[0, T]$:

$$\mathcal{S} = \int_0^T \mathcal{L}(t)\,\mathrm{d}t \tag{5.1}$$

$$= \int_0^T \mathcal{K}(t) + \mathcal{W}(t) - \mathcal{P}(t)\,, \tag{5.2}$$

where $\mathcal{K}$ is the kinetic energy, $\mathcal{W}$ is the work and $\mathcal{P}$ is the potential strain energy. Shames and Dym [32] derive expressions for the involved energies of both plate and beams, and it is seen that the kinetic energy depends on the squared time derivative of the displacement, whereas the work depends on the product of the applied force and the displacement. Finally, the potential energy depends on the squared displacement. This is based on the principles of Hooke's Law and Newtonian mechanics.

The plate is modelled simply as a surface and the beams as lines acting as discrete disturbances.

Modelling potential and kinetic energies imposes no direct restriction to the movement of neither beams nor plate. The movement of the plate is only *restricted* by the (simple) support, but is *affected* by the energies in the beams, such that if torsional energies in the beams are neglected, this does not impose a restriction to the system. It does, however, mean that there is no torsional coupling between the plate and the beams, and therefore no torsional excitation of the beams (i.e. the beams move only in the vertical direction). Thus, one must carefully consider which energies are needed in the model to ensure sufficient accuracy for a given system.

5.2.1 Energy of the beams

From Shames and Dym [32] we get the kinetic and potential energies for a single beam. Thus we describe the total energies of all the beams by introducing a summation:

$$\mathcal{K}_b = \frac{m_b'}{2} \sum_{j=1}^{S} \int_0^{l_x} \dot{w}_b^2 \,\mathrm{d}x, \tag{5.3}$$

and

$$\mathcal{P}_b = \sum_{j=1}^{S} \frac{B_b}{2} \int_0^{l_x} \left(\frac{\partial^2 w_b}{\partial x^2} \right)^2 \mathrm{d}x, \tag{5.4}$$

where m'_b is the mass per unit length of the beams [kg/m], B is the bending stiffness [Nm^2] and w_b is the transverse deflection.

5.2.2 Energy of the plate

Very similar to the expressions of the beams we have those of the plate [32]:

$$\mathcal{K}_p = \frac{m''_p}{2} \int_0^{l_x} \int_0^{l_y} \dot{w}^2 \, \mathrm{d}y \, \mathrm{d}x, \tag{5.5}$$

and

$$\mathcal{P}_p = \frac{B'_p}{2} \int_0^{l_x} \int_0^{l_y} \left((\nabla^2 w)^2 + 2(1-\nu) \left(\frac{\partial^2 w}{\partial x^2} \frac{\partial^2 w}{\partial y^2} - \left(\frac{\partial^2 w}{\partial x \partial y} \right)^2 \right) \right) \mathrm{d}y \, \mathrm{d}x, \tag{5.6}$$

where m''_p is the mass per unit area [kg/m^2], D is the flexural rigidity of the plate [Nm], and ν is the Possion ratio. Szilard [36] shows that for a simply supported plate, equation (5.6) is reduced to:

$$\mathcal{P}_p = \frac{B'_p}{2} \int_0^{l_x} \int_0^{l_y} \left((\nabla^2 w)^2 \right) \mathrm{d}y \, \mathrm{d}x, \tag{5.7}$$

This reduction is straight forward when considering the boundary conditions of simple support.

5.2.3 Applied force

As we are assuming time harmonic point force excitation in (x_0, y_0) and linearity, the force can be described by using the Dirac delta function, which we denote δ_0 to avoid confusion with the variational delta-operator:

$$F(x, y, t) = \mathrm{Re} \left\{ \int_0^{l_x} \int_0^{l_y} F_0 \delta_0(x - x_0, y - y_0) \mathrm{e}^{\mathrm{i}\omega t} \, \mathrm{d}y \, \mathrm{d}x \right\}. \tag{5.8}$$

F_0 is the force amplitude [N]. The work equals the product of force and displacement:

$$\mathcal{W} = F w \tag{5.9}$$

$$= \mathrm{Re} \left\{ \int_0^{l_x} \int_0^{l_y} F_0 \delta_0(x - x_0, y - y_0) \mathrm{e}^{\mathrm{i}\omega t} w \, \mathrm{d}y \, \mathrm{d}x \right\} \tag{5.10}$$

$$= \mathrm{Re} \left\{ F_0 w(x_0, y_0, t) \mathrm{e}^{\mathrm{i}\omega t} \right\}, \tag{5.11}$$

by the properties of the Dirac delta function.

5.3 The model

Now that we are given expressions for the considered energies, we wish to describe the transverse displacement of the plate, by applying Hamilton's Principle with numerical solveability in mind. That is, we will set up a system of equations using Fourier series expansions, that can be truncated such, that the coefficients can be determined by using numerical analysis tools like MATLAB.

First, as we are assuming a linear behavior of the system, the vibration can be decomposed into a complex mode shape and a frequency part. The physical displacement is, of course, purely real:

$$w(x,y,t) = \mathrm{Re}\left\{\tilde{w}(x,y)\mathrm{e}^{\mathrm{i}\omega t}\right\}, \tag{5.12}$$

$$w_b(x,j,t) = \mathrm{Re}\left\{\tilde{w}_b(x,j)\mathrm{e}^{\mathrm{i}\omega t}\right\}, \tag{5.13}$$

where the tilde denotes complex amplitude. As in section 4.3.1 we define $\tilde{w} = w_R + \mathrm{i}\, w_I$, where w_R and w_I are real functions of x and y. Then,

$$w(x,y,t) = w_R \cos(\omega t) - w_I \sin(\omega t), \tag{5.14}$$

and similarly for $w_b(x,y,t)$.

5.3.1 Boundary conditions

The boundary conditions for a simply supported plate are:

$$\tilde{w}(0,y) = \tilde{w}(l_x,y) = 0, \quad \tilde{w}(x,0) = \tilde{w}(x,l_y) = 0, \tag{5.15}$$

$$\left.\frac{\partial^2\tilde{w}}{\partial x^2}\right|_{x=0} = \left.\frac{\partial^2\tilde{w}}{\partial x^2}\right|_{x=l_x} = 0, \quad \left.\frac{\partial^2\tilde{w}}{\partial y^2}\right|_{y=0} = \left.\frac{\partial^2\tilde{w}}{\partial y^2}\right|_{y=l_y} = 0, \tag{5.16}$$

and likewise for a simply supported beam. It is well known, that the wave equation for beams and plates respectively, can be solved by using a Fourier sine-series expansion. We shall use this in our model.

5.3.1.1 Fourier sine-series solution

For simple support along all edges (plate) and both ends (beams), the complex Fourier sine-series solution to the wave equation is:

$$\tilde{w}(x,y) = \sum_{m=1}^{\infty}\sum_{n=1}^{\infty} c_{mn}\varphi_m(x)\psi_n(y), \tag{5.17}$$

and

$$\tilde{w}_b(x,j) = \sum_{m=1}^{\infty} c^b_{mj}\varphi_m(x), \tag{5.18}$$

where c_{mn} and c_{mj} are (possibly) complex coefficients. Still following Brunskog and Chung [3], the modes are:

$$\varphi_m(x) = \sqrt{\frac{2}{l_x}}\sin k_m x, \quad \psi_n(y) = \sqrt{\frac{2}{l_y}}\sin\kappa_n y, \tag{5.19}$$

where

$$k_m = \frac{\pi m}{l_x}, \quad \kappa_n = \frac{\pi n}{l_y}. \tag{5.20}$$

Note that:

$$\int_0^{l_x} \varphi_m^2(x)\,\mathrm{d}x = \int \frac{2}{l_x}\sin^2\left(\frac{m\pi x}{l_x}\right)\mathrm{d}x \tag{5.21}$$

$$= \frac{2}{l_x}\left[\frac{x}{2} - \frac{4l_x}{m\pi}\sin\left(\frac{2m\pi x}{l_x}\right)\right]_0^{l_x} \tag{5.22}$$

$$= \frac{2}{l_x}\left(\frac{l_x}{2} - \sin(2\pi m)\right) = 1, \tag{5.23}$$

since m is an integer. Likewise

$$\int_0^{l_y} \psi_n^2(y)\,\mathrm{d}y = 1, \tag{5.24}$$

and thus we see that the modes form an orthonormal basis, which will be used in the following.

5.3.2 Applying Hamilton's Principle

Before we perform the variation described by Hamilton's Principle, the action integral of the Lagrangian must be derived. For simplicity we shall consider the different terms of the integral one by one. Recall from equation (5.3) and (5.4) that

$$\mathcal{K}_b = \frac{m_b'}{2}\sum_{j=1}^{S}\int_0^{l_x} \dot{w}_b^2\,\mathrm{d}x, \quad \mathcal{P}_b = \frac{B_b}{2}\sum_{j=1}^{S}\int_0^{l_x}\left(\frac{\partial^2 w_b}{\partial x^2}\right)^2\mathrm{d}x. \tag{5.25}$$

Take the definite integral over one period of time $[0, T]$, and insert the decomposition (5.13) using equation (4.29) and the Fourier sine-series solution (5.18):

$$\int_0^T \mathcal{K}_b\,\mathrm{d}t = \int_0^T \frac{m_b'}{2}\sum_{j=1}^{S}\int_0^{l_x}\dot{w}_b^2\,\mathrm{d}x\,\mathrm{d}t \tag{5.26}$$

$$= \frac{m_b'}{2}\sum_j\int_0^{l_x}\int_0^T \dot{w}_b^2\,\mathrm{d}t\,\mathrm{d}x \tag{5.27}$$

$$= \frac{m_b'}{2}\sum_j\int_0^{l_x}\frac{T}{2}\omega^2\tilde{w}_b\tilde{w}_b^*\,\mathrm{d}x \tag{5.28}$$

$$= \frac{T}{2}\frac{m_b'\omega^2}{2}\sum_j\int_0^{l_x}\left(\sum_m c_{mj}^b\varphi_m(x)\right)\left(\sum_m c_{mj}^{b*}\varphi_m(x)\right)\mathrm{d}x \tag{5.29}$$

$$\overset{\perp}{=} \frac{T}{2}\frac{m_b'\omega^2}{2}\sum_m\sum_j c_{mj}^b c_{mj}^{b*}, \tag{5.30}$$

where the $\perp$ above the equals sign indicates that the orthonormality is being used. Perform the same procedure for the potential strain energy of the beams:

$$\int_0^T \mathcal{P}_b \,\mathrm{d}t = \int_0^T \frac{B_b}{2} \sum_{j=1}^{S} \int_0^{l_x} \left(\frac{\partial^2 w_b}{\partial x^2} \right)^2 \mathrm{d}x \,\mathrm{d}t \tag{5.31}$$

$$= \frac{T}{2} \frac{B_b}{2} \sum_j \int_0^{l_x} \left(\sum_m -k_m^2 c_{mj}^b \varphi_m(x) \right) \left(\sum_m -k_m^2 c_{mj}^{b*} \varphi_m(x) \right) \mathrm{d}x \tag{5.32}$$

$$\overset{\perp}{=} \frac{T}{2} \frac{B_b}{2} \sum_m \sum_j k_m^4 c_{mj}^b c_{mj}^{b*}. \tag{5.33}$$

Regarding the plate, we recall from (5.5) and (5.7) that

$$\mathcal{K}_p = \frac{m_p''}{2} \int_0^{l_x} \int_0^{l_y} \dot{w}^2 \,\mathrm{d}y \,\mathrm{d}x, \quad \mathcal{P}_p = \frac{B_p'}{2} \int_0^{l_x} \int_0^{l_y} \left((\nabla^2 w)^2 \right) \mathrm{d}y \,\mathrm{d}x. \tag{5.34}$$

Again, the definite time integral of each is evaluated (we skip some of the steps, as the procedure is identical to that of the beams):

$$\int_0^T \mathcal{K}_p \,\mathrm{d}t = \int_0^T \frac{m_p''}{2} \int_0^{l_x} \int_0^{l_y} \dot{w}^2 \,\mathrm{d}y \,\mathrm{d}x \,\mathrm{d}t \tag{5.35}$$

$$= \frac{T}{2} \frac{m_p'' \omega^2}{2} \int_0^{l_x} \int_0^{l_y} \left(\sum_{m,n} c_{mn} \varphi_m(x) \psi_n(y) \right) \tag{5.36}$$

$$\times \left(\sum_{m,n} c_{mn}^* \varphi_m(x) \psi_n(y) \right) \mathrm{d}y \,\mathrm{d}x \,\mathrm{d}t \tag{5.37}$$

$$\overset{\perp}{=} \frac{T}{2} \frac{m_p'' \omega^2}{2} \sum_m \sum_n c_{mn} c_{mn}^*, \tag{5.38}$$

and

$$\int_0^T \mathcal{P}_p \,\mathrm{d}t = \int_0^T \frac{B_p'}{2} \int_0^{l_x} \int_0^{l_y} \left((\nabla^2 w)^2 \right) \mathrm{d}y \,\mathrm{d}x \,\mathrm{d}t \tag{5.39}$$

$$= \frac{T}{2} \frac{B_p'}{2} \int_0^{l_x} \int_0^{l_y} \left(\sum_{m,n} -\left(k_m^2 + \kappa_n^2\right) c_{mn} \varphi_m(x) \psi_n(y) \right) \tag{5.40}$$

$$\times \left(\sum_{m,n} -\left(k_m^2 + \kappa_n^2\right) c_{mn}^* \varphi_m(x) \psi_n(y) \right) \mathrm{d}y \,\mathrm{d}x \tag{5.41}$$

$$\overset{\perp}{=} \frac{T}{2} \frac{B_p'}{2} \sum_m \sum_n \left(k_m^2 + \kappa_n^2\right)^2 c_{mn} c_{mn}^*. \tag{5.42}$$

Finally, the external work by the applied force (equation (5.11)) is integrated:

$$\int_0^T \mathcal{W} \,\mathrm{d}t = \int_0^T F_0 \cos(\omega t) \, w(x_0, y_0, t) \,\mathrm{d}t \tag{5.43}$$

$$= \frac{T}{2} F_0 \sum_m \sum_n \mathrm{Re}\{c_{mn}\} \varphi_m(x_0) \psi_n(y_0). \tag{5.44}$$

5.3.2.1 An eigenvalue problem

In order to solve the problem at hand by numerical methods, we need to truncate it.

$$n = 1, \ldots, N \quad \text{and} \quad m = 1, \ldots, M. \tag{5.45}$$

Define coefficient vectors by arranging the coefficients c_{mn} and c_{mj} of equations (5.17) and (5.18), such that m becomes the 'outer' loop:

$$\mathbf{c} = \begin{bmatrix} c_{11} \\ c_{12} \\ \vdots \\ c_{MN} \end{bmatrix}, \quad \mathbf{c}_b = \begin{bmatrix} c^b_{11} \\ c^b_{12} \\ \vdots \\ c^b_{MS} \end{bmatrix}. \tag{5.46}$$

Using matrix multiplication to write equations (5.30) , (5.33), (5.38), (5.42) and (5.44), the action, $\mathcal{S}$, becomes as follows. For the sake of keeping an overview, we have indicated from what each term originates[1]. Since we are only concerned with the variation of $\mathcal{S}$, we disregard the factor $T/2$ that occurs on all terms:

$$\begin{aligned} &\overbrace{\mathbf{c}^{\mathrm{T}} \begin{bmatrix} \ddots & & 0 \\ & \frac{\omega^2}{2} m_p'' & \\ 0 & & \ddots \end{bmatrix} \mathbf{c}^*}^{\mathcal{K}_p} + \overbrace{\mathbf{c}_b^{\mathrm{T}} \begin{bmatrix} \ddots & & 0 \\ & \frac{\omega^2}{2} m_b' & \\ 0 & & \ddots \end{bmatrix} \mathbf{c}_b^*}^{\mathcal{K}_b} + \overbrace{\mathrm{Re}\left\{\mathbf{c}^{\mathrm{T}}\right\} \begin{bmatrix} \vdots \\ \varphi_m(x_0)\psi_n(y_0) \\ \vdots \end{bmatrix}}^{\mathcal{W}} \\ &\underbrace{- \mathbf{c}^{\mathrm{T}} \begin{bmatrix} \ddots & & 0 \\ & \frac{B_p'}{2}(k_m^2 + \kappa_n^2)^2 & \\ 0 & & \ddots \end{bmatrix} \mathbf{c}^*}_{\mathcal{P}_p} \underbrace{- \mathbf{c}_b^{\mathrm{T}} \begin{bmatrix} \ddots & & 0 \\ & \frac{B_b}{2} k_m^4 & \\ 0 & & \ddots \end{bmatrix} \mathbf{c}_b^*}_{\mathcal{P}_b}. \end{aligned} \tag{5.47}$$

Next, we wish to make a coupling between $\mathbf{c}$ and $\mathbf{c}_b$. Let $\mathbf{J}$ be defined such that

$$\mathbf{c}_b = \mathbf{J}\mathbf{c}, \tag{5.48}$$

governed by the fact that

$$\tilde{w}_b(x, j) = \tilde{w}(x, y_j), \tag{5.49}$$

which leads to

$$\sum_m c^b_{mj} \varphi_m(x) = \sum_m \sum_n \varphi_m(x) \psi_n(y_j) \tag{5.50}$$

$$\Rightarrow \quad \int_0^{l_x} \varphi_k(x) \sum_m c^b_{mj} \varphi_m(x) \, \mathrm{d}x = \int_0^{l_x} \varphi_k(x) \sum_m \sum_n \varphi_m(x) \psi_n(y_j) \, \mathrm{d}x \tag{5.51}$$

$$\overset{\perp}{\Rightarrow} \quad c^b_{mj} = \sum_n c_{mn} \psi_n(y_j). \tag{5.52}$$

[1] i.e. the matrix product labelled $\mathcal{K}_p$ is actually $\int_0^T \mathcal{K}_p \, \mathrm{d}t$ as derived in equation (5.38)

Thus,

$$\mathbf{J} = \begin{bmatrix} \ddots & & 0 \\ & \mathbf{J}' & \\ 0 & & \ddots \end{bmatrix}, \tag{5.53}$$

where

$$\mathbf{J}' = \begin{bmatrix} \psi_1(y_1) & \psi_2(y_1) & \dots & \psi_n(y_1) \\ \psi_1(y_2) & \psi_2(y_2) & \dots & \psi_n(y_2) \\ \vdots & & & \\ \psi_1(y_S) & \psi_2(y_S) & \dots & \psi_n(y_S) \end{bmatrix}. \tag{5.54}$$

I order to perform the variation of expression (5.47), we first realize, that it can only be done by varying the coefficients since everything else is fixed by physics. Thus, we use theorem 4.4, and take the partial derivatives with respect to both the real and the imaginary part of c_{mn} and set them equal to zero.

$$\left(\frac{\partial}{\partial \mathrm{Re}\{c_{mn}\}} + \mathrm{i} \frac{\partial}{\partial \mathrm{Im}\{c_{mn}\}} \right) (\mathcal{S}) = 0. \tag{5.55}$$

As a result we obtain a system of $M \cdot N$ equations in $M \cdot N$ complex unknowns.

To simplify the notation, define the following matrices:

$$\mathbf{K}_p = \begin{bmatrix} \ddots & & 0 \\ & B'_p(k_m^2 + \kappa_n^2)^2 & \\ 0 & & \ddots \end{bmatrix}, \quad \mathbf{K}_b = \begin{bmatrix} \ddots & & 0 \\ & B_b k_m^4 & \\ 0 & & \ddots \end{bmatrix}, \tag{5.56}$$

$$\mathbf{M}_p = \begin{bmatrix} \ddots & & 0 \\ & m''_p & \\ 0 & & \ddots \end{bmatrix}, \quad \mathbf{M}_b = \begin{bmatrix} \ddots & & 0 \\ & m'_b & \\ 0 & & \ddots \end{bmatrix}, \tag{5.57}$$

where $\mathbf{K}_p$ and $\mathbf{M}_p$ are both $MN \times MN$ dimensional, and $\mathbf{K}_b$ and $\mathbf{M}_b$ are dimension $MS \times MS$. Throughout the present thesis, m is the outer loop and n is the inner loop, thinking in terms of nested loops. Next, let

$$\mathbf{K} = \mathbf{K}_p + \mathbf{J}^{\mathrm{T}} \mathbf{K}_b \mathbf{J}, \quad \mathbf{M} = \mathbf{M}_p + \mathbf{J}^{\mathrm{T}} \mathbf{M}_b \mathbf{J}. \tag{5.58}$$

The coefficient vector of the forced problem can be derived from

$$(\mathbf{K} - \omega^2 \mathbf{M})\mathbf{c} = \mathbf{F}, \tag{5.59}$$

where the force vector is

$$\mathbf{F} = F_0 \begin{bmatrix} \vdots \\ \varphi_m(x_0)\psi_n(y_0) \\ \vdots \end{bmatrix}. \tag{5.60}$$

Similarly the eigenvalues can be computed from the eigenvalue problem

$$(\mathbf{K} - \omega^2 \mathbf{M})\mathbf{c} = 0 \Rightarrow \mathbf{M}^{-1}\mathbf{K}\mathbf{c} = \omega^2 \mathbf{c}. \tag{5.61}$$

Remark 5.1 (Symmetry of matrices). Both $\mathbf{K}$ and $\mathbf{M}$ are symmetric since

$$\mathbf{K}^{\mathrm{T}} = (\mathbf{K}_p + \mathbf{J}^{\mathrm{T}}\mathbf{K}_b\mathbf{J})^{\mathrm{T}} = \mathbf{K}_P^{\mathrm{T}} + (\mathbf{K}_b\mathbf{J})^{\mathrm{T}}(\mathbf{J}^{\mathrm{T}})^{\mathrm{T}} = \mathbf{K}_p + \mathbf{J}^{\mathrm{T}}\mathbf{K}_b^{\mathrm{T}}\mathbf{J} = \mathbf{K}_p + \mathbf{J}^{\mathrm{T}}\mathbf{K}_b\mathbf{J} = \mathbf{K}, \tag{5.62}$$

and likewise for $\mathbf{M}$. By the uniqueness of the inverse of a square matrix, it can easily be shown that $\mathbf{M}^{-1}$ is also symmetric. However, this does not necessarily imply that the product $\mathbf{M}^{-1}\mathbf{K}$ is symmetric.

5.3.2.2 A modal expression for the forced problem

By solving the eigenvalue problem (5.61) the actual mode shapes of the structure can be determined. These can then be used to express a solution to the forced problem.

Let $\mathbf{c}_i$ be an eigenvector of (5.61) and denote its entries c_{mn}^i. The (complex) mode shape of the i'th mode is:

$$\tilde{\Phi}_i(x,y) = \sum_m \sum_n c_{mn}^i \varphi_m(x)\psi_n(y) = \mathbf{c}_i^{\mathrm{T}}\boldsymbol{\chi}(x,y), \tag{5.63}$$

where $\boldsymbol{\chi}(x,y)$ is the MN dimensional column vector

$$\boldsymbol{\chi}(x,y) = \begin{bmatrix} \vdots \\ \varphi_m(x)\psi_n(y) \\ \vdots \end{bmatrix}. \tag{5.64}$$

Assuming a pressure distribution, $p(x,y)$ is applied to the structure, we can express a solution to the forced problem as:

$$\tilde{w}(x,y) = \sum_i \frac{\tilde{\Phi}_i(x,y)}{\Lambda_i\left(\omega_i^2 - \omega^2\right)} \int_0^{l_x}\int_0^{l_y} p(x,y)\tilde{\Phi}_i(x,y)\,\mathrm{d}y\,\mathrm{d}x \tag{5.65}$$

$$= \sum_i \frac{\tilde{\Phi}_i(x,y)}{\Lambda_i\left(\omega_i^2 - \omega^2\right)} \int_0^{l_x}\int_0^{l_y} F_0\delta_0(x-x_0, y-y_0)\tilde{\Phi}_i(x,y)\,\mathrm{d}y\,\mathrm{d}x \tag{5.66}$$

$$= \sum_i \frac{\tilde{\Phi}_i(x,y)\tilde{\Phi}_i(x_0,y_0)}{\Lambda_i\left(\omega_i^2 - \omega^2\right)} F_0 \tag{5.67}$$

$$= \sum_i \frac{\mathbf{c}_i^{\mathrm{T}}\boldsymbol{\chi}(x,y)\mathbf{c}_i^{\mathrm{T}}\boldsymbol{\chi}(x_0,y_0)}{\Lambda_i\left(\omega_i^2 - \omega^2\right)} F_0, \tag{5.68}$$

where (5.67) is assuming point force excitation, and the norm Λ_i is defined as

$$\Lambda_i = \int_0^{l_x}\int_0^{l_y} m''(x,y)\tilde{\Phi}_i^2(x,y)\,\mathrm{d}y\,\mathrm{d}x. \tag{5.69}$$

The mass per unit area of the system can be calculated as:

$$m''(x,y) = m_p'' + \sum_j^S m_b'\delta_0(y-y_j), \tag{5.70}$$

and therefore Λ_i becomes:

$$\Lambda_i = \int_0^{l_x}\int_0^{l_y} m''\left(\mathbf{c}_i^{\mathrm{T}}\boldsymbol{\chi}\right)^2 \mathrm{d}y\,\mathrm{d}x \tag{5.71}$$

$$= \int_0^{l_x}\int_0^{l_y}\left(m_p'' + \sum_j^S m_b'\delta_0(y-y_j)\right)\left(\mathbf{c}_i^{\mathrm{T}}\boldsymbol{\chi}\right)^2 \mathrm{d}y\,\mathrm{d}x \tag{5.72}$$

$$= \int_0^{l_x}\int_0^{l_y}\left(m_p''\left(\mathbf{c}_i^{\mathrm{T}}\boldsymbol{\chi}\right)^2\right)\mathrm{d}y\,\mathrm{d}x + \int_0^{l_x}\int_0^{l_y}\left(\sum_j^S m_b'\delta_0(y-y_j)\left(\mathbf{c}_i^{\mathrm{T}}\boldsymbol{\chi}\right)^2\right)\mathrm{d}y\,\mathrm{d}x \tag{5.73}$$

$$= \Lambda_{p,i} + \Lambda_{b,i}, \tag{5.74}$$

where $\boldsymbol{\chi} = \boldsymbol{\chi}(x,y)$ and the norms related to the plate and the beams respectively $\Lambda_{p,i}$ and $\Lambda_{b,i}$ are defined as:

$$\Lambda_{p,i} = \int_0^{l_x}\int_0^{l_y}\left(m_p''\left(\mathbf{c}_i^{\mathrm{T}}\boldsymbol{\chi}\right)^2\right)\mathrm{d}y\,\mathrm{d}x \tag{5.75}$$

$$= m_p''\mathbf{c}_i^{\mathrm{T}}\left(\int_0^{l_x}\int_0^{l_y}\left(\boldsymbol{\chi}\boldsymbol{\chi}^{\mathrm{T}}\right)\mathrm{d}y\,\mathrm{d}x\right)\mathbf{c}_i \tag{5.76}$$

$$\triangleq m_p''\mathbf{c}_i^{\mathrm{T}}\mathbf{c}_i, \tag{5.77}$$

and

$$\Lambda_{b,i} = \int_0^{l_x}\int_0^{l_y}\left(\sum_j m_b'\delta_0(y-y_j)\left(\mathbf{c}_i^{\mathrm{T}}\boldsymbol{\chi}\right)^2\right)\mathrm{d}y\,\mathrm{d}x \tag{5.78}$$

$$= \int_0^{l_x}\int_0^{l_y}\sum_j m_b'\delta_0\left(y-y_j\right)\left(\sum_m\sum_n c_{mn}^i\varphi_m(x)\psi_n(y)\right)^2\mathrm{d}y\,\mathrm{d}x \tag{5.79}$$

$$= \sum_j\int_0^{l_y} m_b'\delta_0\left(y-y_j\right)\int_0^{l_x}\left(\sum_m\sum_n c_{mn}^i\varphi_m(x)\psi_n(y)\right)^2\mathrm{d}x\,\mathrm{d}y \tag{5.80}$$

$$= \sum_j\int_0^{l_y}\int_0^{l_x}\left(\sum_m\varphi_m(x)\left(\sum_n c_{mn}\psi_n(y)\right)\right)\left(\sum_m\varphi_m(x)\left(\sum_n c_{mn}\psi_n(y)\right)\right)\mathrm{d}x$$
$$\times\, m_b'\delta_0\left(y-y_j\right)\mathrm{d}y \tag{5.81}$$

$$\triangleq m_b'\sum_j\sum_{\substack{m\\n,n'}} c_{mn}^i c_{mn'}^i\psi_n(y_j)\psi_{n'}(y_j), \tag{5.82}$$

where we make use of the fact that φ_m are orthonormal functions.

5.4 Torsion

One of the major advantages of using Hamilton's Principle without deriving the wave equation of the system, is that we can fairly easily add forces and moments by expressing them as strain potential and kinetic energies. In this section we wish to include torsion of the beams. The rotational kinetic energy from twisting of the beams is:

$$\mathcal{K}_r = \sum_{j=1}^S\int_0^{l_y}\frac{\Theta'}{2}\dot{u}_j(x,t)^2\,\mathrm{d}x, \tag{5.83}$$

where Θ' is the rotational mass moment of inertia [m^2/m] per unit length. The potential strain energy is

$$\mathcal{P}_r = \sum_{j=1}^{S} \int_0^{l_y} \frac{T_r}{2} \left(\frac{\partial u_j(x,t)}{\partial x} \right)^2 \mathrm{d}x, \tag{5.84}$$

where T_r is the rotational stiffness (or torsional stiffness) [Nm^2]. In the following, we will define the rotational mass moment of inertia and the rotational stiffness of a rectangular beam.

5.4.1 Torsional stiffness and rotational mass moment of inertia

First we need to introduce the shear modulus, which can be found in Cremer et al. [9]:

$$G = \frac{E}{2(1+\nu)}, \tag{5.85}$$

where E is the Young's modulus of elasticity and ν is the Poisson ratio. Thus, G has the same unit as E [N/m^2]. Following Cremer et al. [9] we find the rotational stiffness as:

$$T_r = \frac{G b^3 h}{3}, \tag{5.86}$$

where b is the beam width, and h is the height. The mass moment of inertia per unit length of the beam is defined to be:

$$\Theta' = \Theta'_x = \int r^2 \, \mathrm{d}m', \tag{5.87}$$

where r is the distance to the axis of rotation, and m' is the mass per unit length. The calculation for a rectangular beam about its center axis is shown in figure 5.2.

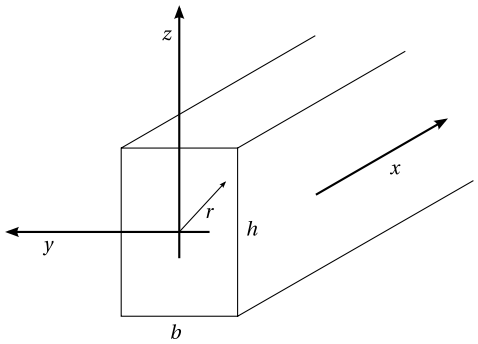

$$r^2 = y^2 + z^2$$

$$\Theta'_x = \int r^2 \, \mathrm{d}m'$$

$$= \int_{-\frac{h}{2}}^{\frac{h}{2}} \rho b z^2 \, \mathrm{d}z + \int_{-\frac{b}{2}}^{\frac{b}{2}} \rho h y^2 \, \mathrm{d}y$$

$$= \frac{\rho \left(b h^3 + h b^3 \right)}{12}$$

Figure 5.2: The mass moment of inertia per unit length. Here calculated of a beam about the x-axis.

Now, that we have described the rotational energies, we can implement them in our model.

5.4.2 Fourier sine series

As done previously we shall describe the rotational motion using Fourier sine series:

$$u(x,j,t) = \mathrm{Re}\left\{ \tilde{u}(x,j) e^{\mathrm{i}\omega t} \right\}, \tag{5.88}$$

where $u = u(x, j, t)$ is the angular displacement of the j'th beam. The complex amplitude has a solution on the form:

$$\tilde{u} = \tilde{u}(x, j) = \sum_m c_{mj}^r \varphi_m(x), \tag{5.89}$$

where c_{mj}^r are complex coefficients. Thus, we can apply the sine series solution to the energies in the same manner as done with the purely transversal motion:

$$\int_0^T \mathcal{K}_r \, \mathrm{d}t \overset{\perp}{=} \frac{T}{2} \frac{\Theta' \omega^2}{2} \sum_m \sum_j c_{mj}^r c_{mj}^{r*}, \tag{5.90}$$

and

$$\int_0^T \mathcal{P}_r \, \mathrm{d}t \overset{\perp}{=} \frac{T}{2} \frac{T_r}{2} \sum_m \sum_j k_m^2 c_{mj}^r c_{mj}^{r*}. \tag{5.91}$$

After doing so, all we need is to make the coupling between the motion of the plate and the rotational motion of the beams.

5.4.3 Coupling between beam and plate

The rotational coupling between the plate and the beams is governed by the fact that

$$\tilde{u}(x, j) = \frac{\partial}{\partial y} \tilde{w}(x, y_j) \tag{5.92}$$

which leads to

$$\sum_m c_{mj}^r \varphi_m(x) = \frac{\partial}{\partial y} \sum_m \sum_n \varphi_m(x) \psi_n(y_j) \tag{5.93}$$

$$\Rightarrow \quad \int_0^{l_x} \varphi_k(x) \sum_m c_{mj}^r \varphi_m(x) \, \mathrm{d}x = \int_0^{l_x} \varphi_k(x) \sum_n \sum_m c_{mn} \varphi_m(x) \kappa_n \sqrt{\frac{2}{l_y}} \cos\left(\kappa_n y_j\right) \mathrm{d}x \tag{5.94}$$

$$\overset{\perp}{\Rightarrow} \quad c_{mj}^r = \sum_n c_{mn} \varphi_m(x) \kappa_n \sqrt{\frac{2}{l_y}} \cos\left(\kappa_n y_j\right). \tag{5.95}$$

Again, we define a vector of coefficients:

$$\mathbf{c}_r = \begin{bmatrix} c_{11}^r \\ c_{12}^r \\ \vdots \\ c_{MJ}^r \end{bmatrix}, \tag{5.96}$$

and let $\mathbf{L}$ be defined such that

$$\mathbf{c}_r = \mathbf{L}\mathbf{c} \tag{5.97}$$

Thus as we have seen before,

$$\mathbf{L} = \begin{bmatrix} \ddots & & 0 \\ & \mathbf{L}' & \\ 0 & & \ddots \end{bmatrix}, \tag{5.98}$$

where

$$\mathbf{L}' = \begin{bmatrix} \frac{\partial}{\partial y}\psi_1(y_1) & \frac{\partial}{\partial y}\psi_2(y_1) & \dots & \frac{\partial}{\partial y}\psi_n(y_1) \\ \frac{\partial}{\partial y}\psi_1(y_2) & \frac{\partial}{\partial y}\psi_2(y_2) & \dots & \frac{\partial}{\partial y}\psi_n(y_2) \\ \vdots & & & \\ \frac{\partial}{\partial y}\psi_1(y_S) & \frac{\partial}{\partial y}\psi_2(y_S) & \dots & \frac{\partial}{\partial y}\psi_n(y_S) \end{bmatrix}, \tag{5.99}$$

which leads to

$$\mathbf{L}' = \begin{bmatrix} \sqrt{\frac{2}{l_y}}\kappa_1 \cos(\kappa_1 y_1) & \sqrt{\frac{2}{l_y}}\kappa_2 \cos(\kappa_2 y_1) & \dots & \sqrt{\frac{2}{l_y}}\kappa_n \cos(\kappa_n y_1) \\ \sqrt{\frac{2}{l_y}}\kappa_1 \cos(\kappa_1 y_2) & \sqrt{\frac{2}{l_y}}\kappa_2 \cos(\kappa_2 y_2) & \dots & \sqrt{\frac{2}{l_y}}\kappa_n \cos(\kappa_n y_2) \\ \vdots & & & \\ \sqrt{\frac{2}{l_y}}\kappa_1 \cos(\kappa_1 y_S) & \sqrt{\frac{2}{l_y}}\kappa_2 \cos(\kappa_2 y_S) & \dots & \sqrt{\frac{2}{l_y}}\kappa_n \cos(\kappa_n y_S) \end{bmatrix}. \tag{5.100}$$

Now, in a similar manner to before, we define stiffness and mass matrices for the rotation:

$$\mathbf{K}_r = \begin{bmatrix} \ddots & & 0 \\ & T_r k_m^2 & \\ 0 & & \ddots \end{bmatrix}, \tag{5.101}$$

$$\mathbf{M}_r = \begin{bmatrix} \ddots & & 0 \\ & \Theta' & \\ 0 & & \ddots \end{bmatrix}, \tag{5.102}$$

where $\mathbf{K}_r$ and $\mathbf{M}_r$ are both $MS \times MS$ dimensional. By letting

$$\mathbf{K} = \mathbf{K}_p + \mathbf{J}^{\mathrm{T}}\mathbf{K}_b\mathbf{J} + \mathbf{L}^{\mathrm{T}}\mathbf{K}_r\mathbf{L}, \quad \mathbf{M} = \mathbf{M}_p + \mathbf{J}^{\mathrm{T}}\mathbf{M}_b\mathbf{J} + \mathbf{L}^{\mathrm{T}}\mathbf{M}_r\mathbf{L}, \tag{5.103}$$

we can include the rotational energies and apply equations 5.59 and 5.61 to solve the forced problem or the eigenvalue problem respectively; that is, the coefficient vector of the forced problem can be derived from

$$(\mathbf{K} - \omega^2\mathbf{M})\mathbf{c} = \mathbf{F}, \tag{5.104}$$

and the eigenvalues can be computed from the eigenvalue problem

$$(\mathbf{K} - \omega^2\mathbf{M})\mathbf{c} = 0 \Rightarrow \mathbf{M}^{-1}\mathbf{K}\mathbf{c} = \omega^2\mathbf{c}. \tag{5.105}$$

When calculating high-frequency responses, a considerable number of modes is needed in the calculations. Since the size of the matrices correspond to the squared number of modes, the computational problem quickly becomes rather complex. In the next chapter, we will describe how the model has been implemented in MATLAB.

CHAPTER

6 Calculation with MATLAB

In order to calculate the vibration of an entire plate, it is necessary to be able to evaluate a number of spatial points simultaneously to obtain acceptable performance. For this purpose we need an operator describing the element-wise multiplication (.*) implemented in MATLAB.

Definition 6.1 (Hadamard product). Let **A** and **B** be matrices of equal dimension. Denote their entries a_{ij} and b_{ij} respectively. The *Hadamard product* (denoted by the operator $\circ$) of **A** and **B** is:

$$\mathbf{A} \circ \mathbf{B} = \begin{bmatrix} a_{11}b_{11} & a_{12}b_{12} & \dots \\ a_{21}b_{21} & a_{22}b_{22} & \dots \\ \vdots & & \end{bmatrix}. \tag{6.1}$$

In a similar manner we will use the operator $\sim$ to denote (right) division element-wise.

$$\mathbf{A} \sim \mathbf{B} = \begin{bmatrix} a_{11}b_{11}^{-1} & a_{12}b_{12}^{-1} & \dots \\ a_{21}b_{21}^{-1} & a_{22}b_{22}^{-1} & \dots \\ \vdots & & \end{bmatrix}. \tag{6.2}$$

The Hadamard product is commutative.

The goal of the present section is to sketch an implementation of equation (5.68) on page 41, such that the displacement of the entire plate can be calculated at once.

First, let $x = (x_1, x_2, ..., x_X)$ and $y = (y_1, y_2, ..., y_Y)$ define the spatial points (x, y) that are to be evaluated. Then, define the following matrices:

$$\boldsymbol{\varphi} = \begin{bmatrix} \varphi_1(x_1) & \varphi_1(x_1) & \dots & \varphi_2(x_1) & \varphi_2(x_1) & \dots & \varphi_M(x_1) \\ \varphi_1(x_2) & \varphi_1(x_2) & \dots & \varphi_2(x_2) & \varphi_2(x_2) & \dots & \varphi_M(x_2) \\ \vdots & & & \vdots & & & \vdots \\ \varphi_1(x_X) & \varphi_1(x_X) & \dots & \varphi_2(x_X) & \varphi_2(x_X) & \dots & \varphi_M(x_X) \\ \vdots & & & \vdots & & & \vdots \end{bmatrix}_{X \times MN} \tag{6.3}$$

and

$$\boldsymbol{\psi} = \begin{bmatrix} \psi_1(y_1) & \psi_1(y_2) & \dots & \psi_1(y_Y) & \dots \\ \psi_2(y_1) & \psi_2(y_2) & \dots & \psi_2(y_Y) & \dots \\ \vdots & & & \vdots & \\ \psi_N(y_1) & \psi_N(y_2) & \dots & \psi_N(y_Y) & \dots \\ \vdots & & & \vdots & \\ \psi_1(y_1) & \psi_1(y_2) & \dots & \psi_1(y_Y) & \dots \\ \psi_2(y_1) & \psi_2(y_2) & \dots & \psi_2(y_Y) & \dots \\ \vdots & & & \vdots & \end{bmatrix}_{MN\times Y} \tag{6.4}$$

Define $\mathbf{C}$ to be a matrix containing the eigenvectors, $\mathbf{c}_i$. These can be obtained in MATLAB by numerically solving the eigenvalue problem (5.61) on page 40.[1]

$$\mathbf{C} = \begin{bmatrix} \vdots & \vdots & & \vdots \\ \mathbf{c}_1 & \mathbf{c}_2 & \dots & \mathbf{c}_{MN} \\ \vdots & \vdots & & \vdots \end{bmatrix}. \tag{6.5}$$

Recall the definition (5.64). In the point of excitation, (x_0, y_0) we have:

$$\boldsymbol{\chi}(x_0, y_0) = \begin{bmatrix} \vdots \\ \varphi_m(x_0)\psi_n(y_0) \\ \vdots \end{bmatrix}. \tag{6.6}$$

Therefore the matrix product

$$\mathbf{C}^{\mathrm{T}}\boldsymbol{\chi}(x_0, y_0) \tag{6.7}$$

is a column vector containing the product $\mathbf{c}_i^{\mathrm{T}}\boldsymbol{\chi}(x_0, y_0)$ for all eigenvectors, $\mathbf{c}_i$.

Definition 6.2 (Diagonal function). Let diag$(\cdot)$ be a function on the space of square matrices, extracting the main diagonal into a column vector; that is,

$$\operatorname{diag}(\mathbf{A}) = \begin{bmatrix} a_{11} \\ a_{22} \\ \vdots \end{bmatrix}, \quad \mathbf{A} = \begin{bmatrix} a_{ij} \end{bmatrix}. \tag{6.8}$$

We can now express Λ_i for all i. First we put equations (5.75) and (5.78) into MN-dimensional vectors.

$$\boldsymbol{\Lambda}_p = \begin{bmatrix} \vdots \\ \Lambda_{p,i} \\ \vdots \end{bmatrix} = \begin{bmatrix} \vdots \\ m_p'' \mathbf{c}_i^{\mathrm{T}} \mathbf{c}_i \\ \vdots \end{bmatrix} = m_p'' \operatorname{diag}(\mathbf{C}^{\mathrm{T}}\mathbf{C}). \tag{6.9}$$

[1] One way of doing this is shown in the MATLAB code included in appendix C. For further details on specific syntax, see the MathWorks™ documentation `http://www.mathworks.com`.

The contribution from the beams (5.78) is a bit more tricky. First, we reshape the eigenvectors $\mathbf{c}_i$ into $M \times N$ matrices:

$$\begin{bmatrix} c_{11}^i \\ c_{12}^i \\ \vdots \\ c_{MN}^i \end{bmatrix} \longmapsto \begin{bmatrix} c_{11}^i & c_{12}^i & \dots & c_{1N}^i \\ \vdots & \vdots & \vdots & \vdots \\ c_{M1}^i & c_{M2}^i & \dots & c_{MN}^i \end{bmatrix}. \tag{6.10}$$

Then, we evaluate the sum of the beams and formulate a new family of matrices $\mathbf{H}_i$ using an Hadamard product:

$$\mathbf{H}_i = \begin{bmatrix} c_{11}^i & c_{12}^i & \dots & c_{1N}^i \\ \vdots & \vdots & \vdots & \vdots \\ c_{M1}^i & c_{M2}^i & \dots & c_{MN}^i \end{bmatrix} \circ \begin{bmatrix} \sum_j \psi_1(y_j) & \sum_j \psi_2(y_j) & \dots & \sum_j \psi_N(y_j) \\ \vdots & \vdots & \vdots & \vdots \\ \sum_j \psi_1(y_j) & \sum_j \psi_2(y_j) & \dots & \sum_j \psi_N(y_j). \end{bmatrix}, \tag{6.11}$$

where the matrix on the right has M identical rows. We can now express the sums of (5.78) as the sum of all elements in the matrix produced by multiplying $\mathbf{H}_i$ by its own transpose from the left.

$$\mathbf{G}_i = \left[g_{nn'}^i \right] = \mathbf{H}_i^{\mathrm{T}} \mathbf{H}_i. \tag{6.12}$$

We obtain the following expression:

$$m_b' \sum_j \sum_{\substack{m \\ n,n'}} c_{mn}^i c_{mn'}^i \psi_n(y_j) \psi_{n'}(y_j) = m_b' \sum_{n,n'} g_{nn'}^i. \tag{6.13}$$

We do this for all the eigenvectors:

$$\mathbf{\Lambda}_b = m_b' \begin{bmatrix} \vdots \\ \sum_{n,n'} g_{nn'}^i \\ \vdots \end{bmatrix}, \tag{6.14}$$

and finally we add the contribution from the plate and beams respectively:

$$\mathbf{\Lambda} = \mathbf{\Lambda}_p + \mathbf{\Lambda}_b. \tag{6.15}$$

Remark 6.3 (Nested loops vs. matrix operations). During the development of the MATLAB code used in the present thesis, Λ_i was first implemented (for test purposes) using nested loops as there is little risk of error when writing sums as loops. However, as the code was tested it turned out that it would be a matter of weeks to iterate through 10.000 Λ_i values. Expressing the summation using matrix operations took about ten minutes, and the computer spent approximately ten seconds calculating all 10.000 values afterwards.

We write the term $(\omega_i^2 - \omega^2)$ as a column vector with entries for all eigenvalues:

$$\mathbf{\Omega} = \begin{bmatrix} \vdots \\ \omega_i^2 - \omega^2 \\ \vdots \end{bmatrix}. \tag{6.16}$$

In order to calculate the displacement as given in equation (5.68), we must first recognize that the sum

$$\sum_m \sum_n c_{mn} \varphi_m(x) \psi_n(y) \tag{6.17}$$

can be calculated for all (x, y), where $x = (x_1, x_2, ..., x_X)$ and $y = (y_1, y_2, ..., y_Y)$, by diagonalizing the coefficients and multiplying by the matrices $\boldsymbol{\varphi}$ and $\boldsymbol{\psi}$ (equations (6.3) and (6.4) respectively):

$$\begin{bmatrix} \sum_m \sum_n c_{mn} \varphi_m(x_1) \psi_n(y_1) & \dots & \sum_m \sum_n c_{mn} \varphi_m(x_1) \psi_n(y_Y) \\ \vdots & & \vdots \\ \sum_m \sum_n c_{mn} \varphi_m(x_X) \psi_n(y_1) & \dots & \sum_m \sum_n c_{mn} \varphi_m(x_X) \psi_n(y_Y) \end{bmatrix} \tag{6.18}$$

$$= \boldsymbol{\varphi} \begin{bmatrix} \ddots & & \\ & c_{mn} & \\ & & \ddots \end{bmatrix} \boldsymbol{\psi}. \tag{6.19}$$

Therefore by defining a 'coefficient' matrix (note that this matrix include the contributions from all the eigenvectors)

$$\mathbf{Q} = \mathbf{C}^{\mathrm{T}} \circ \overbrace{\begin{bmatrix} \vdots & \vdots & \\ (\mathbf{C}^{\mathrm{T}} \boldsymbol{\chi}(x_0, y_0)) \sim (\boldsymbol{\Lambda} \circ \boldsymbol{\Omega}) & (\mathbf{C}^{\mathrm{T}} \boldsymbol{\chi}(x_0, y_0)) \sim (\boldsymbol{\Lambda} \circ \boldsymbol{\Omega}) & \cdots \\ \vdots & \vdots & \end{bmatrix}}^{MN \text{ identical columns}}, \tag{6.20}$$

and denoting its entries q_{ij}, we can calculate the displacement using the diagonal matrix:

$$\boldsymbol{\Xi} = \begin{bmatrix} \ddots & & 0 \\ & \sum_j q_{ij} & \\ 0 & & \ddots \end{bmatrix}. \tag{6.21}$$

We can express equation (5.68) as the product:

$$\tilde{\mathbf{w}}_{x,y} = \boldsymbol{\varphi} \boldsymbol{\Xi} \boldsymbol{\psi}. \tag{6.22}$$

The advantage of using eigenvectors to compute the forced displacement is, that the heavy parts of the process; that is, computing the eigenvalues and the actual mode shapes of the system, need only be carried out once. Having done these calculations, changing the frequency or the excitation is a rather simple matter.

Displacement vs. excitation frequency Calculating and plotting the displacement of the forced problem in a single point as a funciton of excitation frequency may be carried out in MATLAB using matrix operations. Consider equation (5.68) and let (x_1, y_1) be the point at which we wish to study the displacement. Then,

$$\tilde{w}_{x_1,y_1}(\omega) = \sum_i \frac{\mathbf{c}_i^{\mathrm{T}} \boldsymbol{\chi}(x_1, y_1) \mathbf{c}_i^{\mathrm{T}} \boldsymbol{\chi}(x_0, y_0)}{\Lambda_i \left(\omega_i^2 - \omega^2\right)} F_0, \tag{6.23}$$

where both $\boldsymbol{\chi}(x_0, y_0)$ and $\boldsymbol{\chi}(x_1, y_1)$ are MN dimensional column vectors. Let $\boldsymbol{\omega}_f$ be a row vector containing the excitation frequencies $(\omega_{f1}, \omega_{f2}, \ldots)$ to be investigated. We now define a matrix:

$$\boldsymbol{\Omega} = \begin{bmatrix} \vdots & \vdots & \\ \omega_i^2 - \omega_{f1}^2 & \omega_i^2 - \omega_{f2}^2 & \cdots \\ \vdots & \vdots & \end{bmatrix}, \tag{6.24}$$

and a coefficient vector:

$$\mathbf{q} = F_0 \left(\mathbf{C}^{\mathrm{T}} \boldsymbol{\chi}(x_1, y_1) \right) \circ \left(\mathbf{C}^{\mathrm{T}} \boldsymbol{\chi}(x_0, y_0) \right) \sim \boldsymbol{\Lambda}, \tag{6.25}$$

where $\boldsymbol{\Lambda}$ is defined as in (6.15). In MATLAB we can now calculate a vector containing the displacement at (x_1, y_1) for different excitation frequencies as

$$\tilde{\mathbf{w}}_{\boldsymbol{\omega}_f} = \mathbf{q}^{\mathrm{T}} \left(\mathbf{1} \sim \boldsymbol{\Omega} \right), \tag{6.26}$$

where $\mathbf{1}$ is a matrix containing ones in all positions.

6.1 Computational aspects

The matrix system derived in section 5.3.2.1 provides a very neat way of computing the complex coefficients, but the matrices involved quickly become very large as the number of modes included is increased. The purpose of this section is to divide the problem into smaller parts, that can be solved numerically by using several computers running parallel calculations. This can be done rather easily, as the large $(MN \times MN)$ matrices are structured as M matrices of dimension $N \times N$ on a diagonal, and zeros elsewhere. This is because of the block diagonal nature of the coupling matrix $\mathbf{J}$, as will be formulated formally in theorem 6.5. The claim is, that the large $MN \times MN$ matrices are structured as follows:

$$\begin{bmatrix} [\ ]_{N\times N} & & 0 & \\ & [\ ]_{N\times N} & & 0 \\ 0 & & [\ ]_{N\times N} & \\ & 0 & & \ddots \end{bmatrix}_{MN\times MN} \tag{6.27}$$

In the following section, we shall prove that each of the $N \times N$ submatrices can be treated independently of the rest.

6.1.1 Block diagonal matrices

First, consider the following definition:

Definition 6.4 (Block diagonal matrix). We define a block diagonal matrix to be a matrix on the form

$$\mathbf{A} = \begin{bmatrix} \mathbf{S}_1 & & 0 & \\ & \mathbf{S}_2 & & 0 \\ 0 & & \ddots & \\ & 0 & & \mathbf{S}_N \end{bmatrix}, \tag{6.28}$$

where $\dim(\mathbf{S}_1) = \dim(\mathbf{S}_2) = \ldots = \dim(\mathbf{S}_N)$. We refer to $\mathbf{S}_n$ as the blocks of $\mathbf{A}$.

By the definition of the matrix product, the following theorem is trivial. The keyword is that the two matrices have an equal number of blocks such that the matrix products of the blocks are well defined.

Theorem 6.5 (The product of two block diagonal matrices). Let $\mathbf{A}$ and $\mathbf{B}$ be block diagonal matrices with blocks $\mathbf{S}_n^a$ and $\mathbf{S}_n^b$ respectively, such that both of the matrix products $\mathbf{AB}$ and $\mathbf{S}_n^a\mathbf{S}_n^b$ are well defined; that is, the number of blocks in $\mathbf{A}$ equals the number of blocks in $\mathbf{B}$.

Then, the matrix product $\mathbf{AB}$ is a block diagonal matrix on the form

$$\mathbf{AB} = \begin{bmatrix} \ddots & & \\ & \mathbf{S}_n^a\mathbf{S}_n^b & \\ & & \ddots \end{bmatrix}, \tag{6.29}$$

where the elements outside the blocks $\mathbf{S}_n^a\mathbf{S}_n^b$ are all zero.

Note that a diagonal matrix can be considered a block diagonal matrix of an arbitrary number of (diagonal) blocks. Thus, the matrix product of the block diagonal matrix $\mathbf{J}$ and any diagonal matrix is again block diagonal.

From theorem 6.5 we can show how the inverse, the determinant and the eigenvalues of a square block diagonal matrix with square blocks can be found by considering the blocks one by one.

Theorem 6.6 (Properties of a square block diagonal matrix). Let $\mathbf{A}$ be a square block diagonal matrix with square blocks. Then,

1.
$$\mathbf{A}^{-1} = \begin{bmatrix} \mathbf{S}_1^{-1} & & 0 & \\ & \mathbf{S}_2^{-1} & & 0 \\ 0 & & \ddots & \\ & 0 & & \mathbf{S}_N^{-1} \end{bmatrix}, \tag{6.30}$$

2.
$$\det(\mathbf{A}) = \det(\mathbf{S}_1)\cdot\det(\mathbf{S}_2)\cdot\ldots\cdot\det(\mathbf{S}_N), \tag{6.31}$$

3.
$$\lambda \text{ is an eigenvalue of } \mathbf{A} \Leftrightarrow \exists n \in \{1,\cdots,N\}\colon \lambda \text{ is an eigenvalue of } \mathbf{S}_n, \tag{6.32}$$

where $\mathbf{S}_n$ are the blocks of $\mathbf{A}$.

The above theorem is essential, as we wish to calculate both inverses and eigenvalues of rather large block diagonal matrices to solve equations (5.59) and (5.61). Calculation of eigenvalues in MATLAB is a rather heavy task, and the gain from splitting up the problem is significant.

In the following we prove the three parts of theorem 6.6 one by one.

Proof 6.7 (Theorem 6.6. Part 1. The inverse). We shall prove the theorem by using theorem 6.5 and the uniqueness of matrix inverses. Let

$$\mathbf{A} = \begin{bmatrix} \mathbf{S}_1 & & 0 & \\ & \mathbf{S}_2 & & 0 \\ 0 & & \ddots & \\ & 0 & & \mathbf{S}_N \end{bmatrix}, \quad \mathbf{C} = \begin{bmatrix} \mathbf{S}_1^{-1} & & 0 & \\ & \mathbf{S}_2^{-1} & & 0 \\ 0 & & \ddots & \\ & 0 & & \mathbf{S}_N^{-1} \end{bmatrix}, \tag{6.33}$$

then by theorem 6.5

$$\mathbf{AC} = \begin{bmatrix} \mathbf{S}_1\mathbf{S}_1^{-1} & & 0 & \\ & \mathbf{S}_2\mathbf{S}_2^{-1} & & 0 \\ 0 & & \ddots & \\ & 0 & & \mathbf{S}_N\mathbf{S}_N^{-1} \end{bmatrix} = \begin{bmatrix} 1 & & 0 & \\ & 1 & & 0 \\ 0 & & \ddots & \\ & 0 & & 1 \end{bmatrix} \tag{6.34}$$

$$= \begin{bmatrix} \mathbf{S}_1^{-1}\mathbf{S}_1 & & 0 & \\ & \mathbf{S}_2^{-1}\mathbf{S}_2 & & 0 \\ 0 & & \ddots & \\ & 0 & & \mathbf{S}_N^{-1}\mathbf{S}_N \end{bmatrix} = \mathbf{CA}. \tag{6.35}$$

Thus, $\mathbf{C} = \mathbf{A}^{-1}$.

Proof 6.8 (Theorem 6.6. Part 2. The determinant). Again, we use theorem 6.5:

$$\mathbf{A} = \begin{bmatrix} \mathbf{S}_1 & & 0 & \\ & \mathbf{S}_2 & & 0 \\ 0 & & \ddots & \\ & 0 & & \mathbf{S}_N \end{bmatrix} = \begin{bmatrix} \mathbf{S}_1\mathbf{I} & & 0 & \\ & \mathbf{S}_2\mathbf{I} & & 0 \\ 0 & & \ddots & \\ & 0 & & \mathbf{S}_N\mathbf{I} \end{bmatrix} \tag{6.36}$$

$$= \begin{bmatrix} \mathbf{S}_1 & & 0 & \\ & \mathbf{I} & & 0 \\ 0 & & \ddots & \\ & 0 & & \mathbf{I} \end{bmatrix} \begin{bmatrix} \mathbf{I} & & 0 & \\ & \mathbf{S}_2 & & 0 \\ 0 & & \ddots & \\ & 0 & & \mathbf{I} \end{bmatrix} \cdots \begin{bmatrix} \mathbf{I} & & 0 & \\ & \mathbf{I} & & 0 \\ 0 & & \ddots & \\ & 0 & & \mathbf{S}_N \end{bmatrix}, \tag{6.37}$$

where $\mathbf{I}$ is the identity matrix of the same dimension as $\mathbf{S}_n$. By the multiplicative property of determinants we have

$$\det(\mathbf{A}) = \prod_{n=1}^{N} \det(\mathbf{S}_n), \tag{6.38}$$

since expansion by minors, with respect to the rows containing only ones on the diagonal yields

$$\det\left(\begin{bmatrix} \mathbf{I} & & 0 & \\ & \ddots & & 0 \\ 0 & & \mathbf{S}_n & 0 \\ & 0 & & \ddots \\ & & 0 & \mathbf{I} \end{bmatrix}\right) = \left(\prod_{\substack{i=1 \\ i \notin N'}}^{MN} (-1)^{2i}\right) \det(\mathbf{S}_n) = \det(\mathbf{S}_n), \tag{6.39}$$

where MN is the number of rows in $\mathbf{A}$ and N' contains the row numbers of the block $\mathbf{S}_n$.

Proof 6.9 (Theorem 6.6. Part 3. Eigenvalues). Consider the characteristic polynomial, $p(\lambda)$ of $\mathbf{A}$.

$$\det(\mathbf{A} - \lambda\mathbf{I}) = p(\lambda), \tag{6.40}$$

It is well known that the eigenvalues of $\mathbf{A}$ are the roots (counted with multiplicity) of the characteristic polynomial (see Fraleigh and Beauregard [11]). By theorem 6.5 we have:

$$p(\lambda) = \det(\mathbf{A} - \lambda\mathbf{I}) = \det\left(\begin{bmatrix} \mathbf{S}_1 - \lambda\mathbf{I} & & 0 & \\ & \mathbf{S}_2 - \lambda\mathbf{I} & & 0 \\ 0 & & \ddots & \\ & 0 & & \mathbf{S}_N - \lambda\mathbf{I} \end{bmatrix}\right) \tag{6.41}$$

$$= \prod_{n=1}^{N} \det(\mathbf{S}_n - \lambda\mathbf{I}) = \prod_{n=1}^{N} p_n(\lambda), \tag{6.42}$$

where $\mathbf{I}$ is the identity matrix of suitable dimension (there is no risk of confusion) and $p_n(\lambda)$ is the characteristic polynomial of $\mathbf{S}_n$. Thus, the roots of $p(\lambda)$ are exactly those of the $p_n(\lambda)$'s, which proves that the eigenvalues of $\mathbf{A}$ are in fact those of its blocks.

We have now proven that we can treat each block separately when solving for the coefficients in equations (5.59) and (5.61) on page 40.

CHAPTER

7 Statistical Energy Analysis

Prediction of the sound transmission in structures, like between building elements, can be a rather cumbersome and time consuming task. Often, a numerical analysis requires rather large amounts of computational power, along with time consuming analysis of the system parameters that are needed, for instance when defining a finite element model. In statistical energy analysis (SEA) the mean vibrational energy flow is calculated, on the contrary to more traditional approaches based on the wave equation [33]. SEA is based on power balance equations, using the flow of energy to provide a spatially and time averaged frequency mean value response. Thus, SEA provides a computationally easy and quick estimate on the overall vibration. Quite often such an estimate can be a valuable tool, as for instance when designing houses, a more detailed model is both too expensive and too time consuming to implement. Further, there may be stages in a design project, where the exact details of a specific construction are still unknown, but where enough is known to perform an SEA estimate of the overall vibration response of a structure [21].

Due to the time consuming work of understanding and implementing the modal model, as presented in chapters 5 and 6, the topic of SEA will only be briefly introduced in the present thesis. Investigation of parameters, calculations and development of an SEA based model adapted to spatially periodic structures, all belong to the section of future work.

7.1 Assumptions of SEA

SEA is based on statistical room acoustics, and therefore many of the same assumptions and considerations apply, see Ohlrich [30]:

- The excitation is broadband,
- all propagation and reflection angles are equally probable as frequency averages (diffuseness),
- all natural frequencies of the room are equally well excited,
- the detailed form of the room is without importance.

The latter point being one of the major advantages of using SEA-based estimates as an estimate of the supplied power to a finite structure can be based on the point mobility of an infinite one [30].

In general, statistical room acoustics uses two different approaches; one using a modal model, and another using a wave based model. In some cases it may be advantageous to combine the two models as the each have both advantages and drawbacks. The difference between these approaches is outside the scope of the present thesis, as we are concerned only with the modal approach.

One of the requirements of SEA is a fairly high density of modes in each frequency band. This assumption is one of the reasons why SEA of today is not suitable for periodic structures, as we shall see later on. For rib reinforced plates as dealt with in the present investigation, the ribs introduce an orthotropic behavior of the plate because the stiffness in one direction is increased. Further, the modes of spatially periodic structures are not uniformly distributed, but tend to group together in so-called pass bands. Bands without any modes are called stop bands. Thus, the modal density is no longer a smooth function, but instead a comb-shaped function. In the 2D case as investigated here, the pass band/stop band grouping will not be as distinct as for the 1D case, since the considered structure is only spatially periodic in one of its dimensions.

Other disagreements, between standard SEA methods and lightweight (spatially periodic) building structures are; high spatial attenuation in the direction perpendicular to the ribs, and lack of diffuseness in the vibration field of the structure. Further, determining the coupling loss factor can cause difficulties, as the radiation efficiency of this type of structure is not always an easy task.

7.2 SEA of today

Statistical Energy Analysis has been subject to many discussions about its validity, as it yields very poor results for certain kinds of structures. Among these structures are ribbed plates as investigated in the present thesis. However, when predicting high frequency responses of structural vibration, other methods, such as the finite element method, are not computationally practical since the short wavelength requires a considerable number of elements. Thus, a statistical model may be advantageous.

SEA has been shown to provide good results on a number of structures, and therefore effort is still put into adapting and developing SEA methods to suit a broader range of applications with greater precision.

One attempt to improve standard SEA is the Wave Intensity Analysis (WIA) by Langley (see [18] and [19]), in which the wave field is decomposed into directional wave intensity components using Fourier series. WIA is a natural extension to SEA, and it has been demonstrated to provide better result than conventional SEA when applied on both panel arrays [18] and stiffened plates [19].

Langley, Smith, and Fahy [20] models a stiffened plate as a damped coupling element between two SEA subsystems, incorporating the periodic effects in the transmission and absorption coefficients. They compare the result to those of both conventional SEA and WIA, neither of which are able to describe the phase effects and the pass band/stop band behavior.

One of the advantages of WIA is that it relaxes the assumption of diffuseness. This makes it possible to predict not only high-frequency vibration as with SEA, but extend

the prediction into the mid-frequency range. This has been investigated by Nishino and Ohlrich [27], [28].

7.3 Flanking transmission

Cremer et al. [9] describes how built-up structures, like buildings and ships, are affected by flanking transmission. Airborne sound is transmitted between different partitions not only directly through the partitioning element, but also via flanking elements. As building techniques improve, the direct transmission is decreased, and thus including the flanking transmission in the calculations becomes a necessity. Cremer et al. [9] even goes as far as to say, that it can be anticipated, that the flanking transmission dominates in the case of the primary partitioning structure being a high quality double wall with the sidewalls and ceilings are homogeneous plates. Figure 7.1 shows a rough sketch of the transmission paths between neighboring rooms. Flanking transmission may occur not only through walls, but also floors, ceilings or even ducts and pipes.

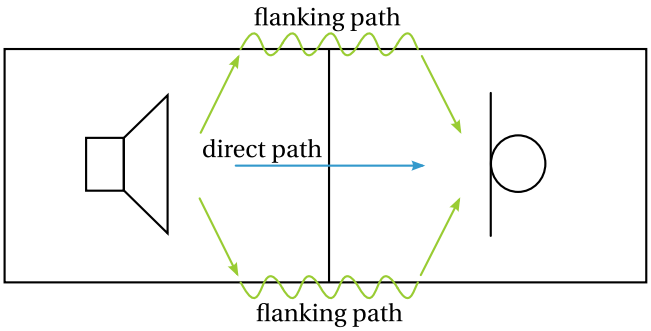

Figure 7.1: Airborne sound is transmitted between different partitions not only directly through the partitioning element, but also via flanking elements.

Including flanking transmission in calculations of sound transmission is not a straight forward task, since flanking transmission – unlike transmission along the direct path – can be hard to determine in a laboratory. Prediction models for flanking transmission of homogeneous structures exists, but in most lightweight building constructions these are not usable.

7.4 SEA subsystems

One of the major uses of SEA is to predict the vibration response of one structural component caused by energy transferred through couplings with other components. Such an analysis is carried out by separating the structural components into *subsystems*. Simply put, SEA deals with the flow and storage of dynamical energy between coupled subsystems. The energy storage is related to the modal density, whereas the energy transfer depends on the damping loss factor and the coupling loss factor along with the impedances needed to determine the input power, see Lyon and DeJong [21]. The key assumption in this approach is, that the energy flow between connected subsystems is proportional to the difference in modal energies of the subsystems [20]. Following Ohlrich [30], the time-averaged supplied power from a point force, $F_0(t)$ can be expressed as

$$P = \overline{F_0^2}\,\mathrm{Re}\left\{\tilde{Y}_\infty\right\} = M\langle\overline{v^2}\rangle\omega\eta, \tag{7.1}$$

where P is the power supplied by the point force $F_0(t)$, $\tilde{Y}_\infty$ is the complex point mobility of the corresponding infinite structure, M is the total mass, $\langle \overline{v^2} \rangle$ is the mean square spatially averaged vibration velocity, ω is the angular frequency, and η is the damping loss factor.

7.5 Periodic structures

When attempting to model ribbed plates using SEA based theory, many different approaches has been investigated. One extreme is modelling each panel (the part of the plate lying between two beams) as a separate subsystem describing the effect of the beams by means of coupling properties. However, such an approach would result in a ridiculously large model when describing complex structures. Further, the number of modes in each panel may not satisfy the assumptions of SEA, and finally this sort of model would not incorporate periodic effects such as pass band/stop band behavior [20].

The other extreme is to consider the ribbed plate as a single subsystem, smearing out the effect of the beams to produce what Langley et al. [20] refers to as an "equivalent orthotropic plate". Again, this approach does not account for the spatial periodicity of the beams. Further, Langley states that this approach can only be successful if the bending stiffness of the beams is low compared to that of the plate, and further that the spacing of the beams must be small compared to the wavelength [20]. Mace [22], [23] finds that a periodically stiffened plate can be treated as an orthotropic plate when the stiffener spacing is less than one third of the wavelength in the plate.

Incorporation of pass band/stop band behavior has been done by both Keane and Price [14] and Tso and Hansen [38], but in both cases rather specific structures are considered, and further work needs to be done to adapt the theory to more general periodic structures.

In the system proposed by Brunskog [5], the ribbed plate is described by two SEA subsystems; one that represents the waves travelling perpendicular to the beams, and incorporating the periodic effect introduced by the ribs, and another describing the waves travelling parallel to the beams. The latter subsystem does not include periodic behavior. It should be recognized that each subsystem contains both plate and beams. The proposed model is shown in figure 7.2.

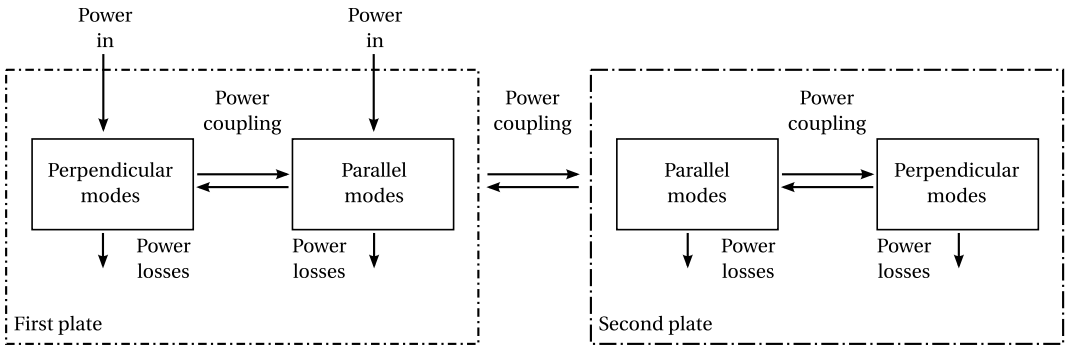

Figure 7.2: The proposed SEA subsystems. Each plate is divided in two separate subsystems; one that represents the waves travelling perpendicular to the beams, and incorporating the periodic effect introduced by the ribs, and another describing the waves travelling parallel to the beams. Redrawn from [5].

The idea is to investigate the modal energies of each subsystem, and this way determine how the input power is divided between the parallel modes and the perpendicular modes. How the subsystems of the proposed model are coupled to each other need to be investigated, as knowing this coupling is a necessity in order to apply the proposed subsystem configuration.

In chapter 9 a possible method of separating the modes into a perpendicular group and a parallel group is investigated.

Part III

Results and overall discussion

CHAPTER

8 Results of the model

In the following chapters, the MATLAB model will be used to simulate the behavior of several lightweight structures. Initially the input to the model was based on parameters given by Sjökvist et al. [34], but later in the process of writing this thesis, other structures has been investigated as well; that is, a wooden structure and a steel structure. The wooden structure has been investigated further by varying the distance between the beams as well as the beam dimensions. The investigation focuses on the effect of including rotational energies in the model, as this seems to have a great influence on the pass band/stop band behavior which we expect from periodic structures. In the present chapter, we focus on the calculations of model density, which has been done by numerically solving the eigenvalue problem described in section 5.

Figures that are not directly discussed, but which may still be of interest to the reader (and serve as documentation of the model), will be put in appendix B. In the case where similar, but slightly different, figures may be found in the appendix, there will be a reference to those figures in the text.

If not clearly stated otherwise, truncation of the infinite sums are done using $M = 200$ and $N = 150$, as the resulting 30.000 modes turn out to be sufficient, yet computationally quick. The criterion of being 'sufficient' is that when the number of modes up to a given frequency is plotted as a function of frequency, the graph should be equal to the same calculation performed with more terms included.

In general a considerably higher number of modes need to be included in the calculations when predicting the forced response of the system. This is because the higher order modes influence the response, as can be seen from equation (5.68) on page 41.

8.1 Description of the system

By means of the model previously described, the eigenvalues of several plates are found. The structures are:

- A wooden structure. The plate is 5 m by 6 m made from 22 mm chipboard. The beams are made of douglas fir, with cross sectional dimensions 50 mm by 100 mm, evenly spaced with a distance of 600 mm, which is a typical spacing for a floor construction.

- A similar chipboard plate, but with 1 m distance between the beams.
- Again, a similar chipboard plate, but with larger beams. The beams are still made from douglas fir, but have cross sectional dimensions 70 mm by 250 mm. The spacing is kept at 600 mm.
- A steel construction. The plate is 5 m by 6 m steel with a thickness of 6 mm. The beams are simple rectangular beams with a height of 100 mm. 10 mm thickness is used for the beams.
- An unknown construction (from now on LGS) based on the parameters used by Sjökvist et al. [34]. The data for the plate are consistent with 18 mm plywood using material properties found in [30]. The plate is 4 m by 6 m, and the beams are spaced 500 mm.

The before mentioned assumptions of thin plates, slender beams and simple support still apply. In table 8.1 the material properties of the investigated systems are shown. It can be seen that the beams used by Sjökvist are quite different from the rectangular beams used in the other constructions. The bending stiffness B_b of LGS is fairly high compared to the others, while neither the torsional stiffness T_r nor the mass per unit length m'_b are significantly different from the range of the others. Most outstanding is the mass moment of inertia, Θ', which is much higher than for any of the other beam configurations.

In the table only the real parts of the material properties are shown. In the model, damping is introduced as a complex Young's Modulus, which makes both shear modulus, bending stiffness and rotational stiffness complex as well. The complex Young's Modulus is calculated as $E(1+i\eta)$. The damping coefficient η of both beams and plate can be found in the table 8.1.

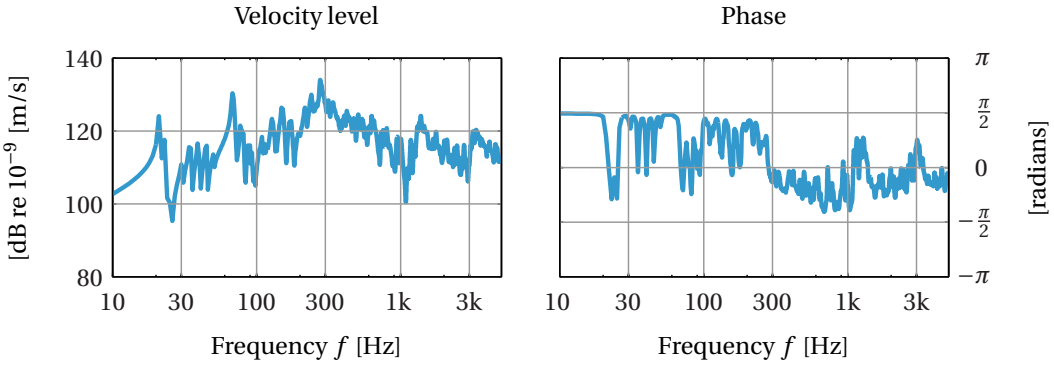

Figure 8.1: Structure "LGS". Frequency response in the driving point $(x_0, y_0) = (1.32, 1)$. On the left is the amplitude, and on the right is the phase.

8.2 Input mobility

To begin with, we present a figure showing the frequency response of one of the modelled constructions. For driving force is 1 N. In the figure 8.1 the input mobility of the structure "LGS" is shown. It can be seen that the phase at low frequencies has a 90° lead, as expected because the system acts spring-like at low frequencies. This is merely meant

System	Wood	Wood (1 m)	Wood (heavy)	Steel	LGS
l_x [m]	5	5	5	5	4
l_y [m]	6	6	6	6	6
l_b [m]	$600{\cdot}10^{-3}$	1	$600{\cdot}10^{-3}$	$600{\cdot}10^{-3}$	$500{\cdot}10^{-3}$
Plate	chipboard	chipboard	chipboard	steel	
h_p [m]	$22{\cdot}10^{-3}$	$22{\cdot}10^{-3}$	$22{\cdot}10^{-3}$	$6{\cdot}10^{-3}$	-
ρ_p [kg/m^3]	650	650	650	$7.80{\cdot}10^{3}$	-
ν_p [·]	$300{\cdot}10^{-3}$	$300{\cdot}10^{-3}$	$300{\cdot}10^{-3}$	$280{\cdot}10^{-3}$	$300{\cdot}10^{-3}$
E_p [N/m^2]	$4.60{\cdot}10^{9}$	$4.60{\cdot}10^{9}$	$4.60{\cdot}10^{9}$	$200{\cdot}10^{9}$	-
η_p [·]	$20{\cdot}10^{-3}$	$20{\cdot}10^{-3}$	$20{\cdot}10^{-3}$	$10{\cdot}10^{-3}$	$20{\cdot}10^{-3}$
B'_p [Nm]	$4.49{\cdot}10^{3}$	$4.49{\cdot}10^{3}$	$4.49{\cdot}10^{3}$	$3.91{\cdot}10^{3}$	$2.80{\cdot}10^{3}$
m''_p [kg/m^2]	14.30	14.30	14.30	46.80	10.80
Max f [Hz]	$6.38{\cdot}10^{3}$	$6.38{\cdot}10^{3}$	$6.38{\cdot}10^{3}$	$44.27{\cdot}10^{3}$	
Beams	douglas fir	douglas fir	douglas fir	steel	
h_b [m]	$100{\cdot}10^{-3}$	$100{\cdot}10^{-3}$	$250{\cdot}10^{-3}$	$100{\cdot}10^{-3}$	-
b [m]	$50{\cdot}10^{-3}$	$50{\cdot}10^{-3}$	$70{\cdot}10^{-3}$	$10{\cdot}10^{-3}$	-
ρ_b [kg/m^3]	520	520	520	$7.80{\cdot}10^{3}$	-
ν_b [·]	$300{\cdot}10^{-3}$	$300{\cdot}10^{-3}$	$300{\cdot}10^{-3}$	$300{\cdot}10^{-3}$	$300{\cdot}10^{-3}$
E_b [N/m^2]	$12{\cdot}10^{9}$	$12{\cdot}10^{9}$	$12{\cdot}10^{9}$	$200{\cdot}10^{9}$	-
η_b [·]	$20{\cdot}10^{-3}$	$20{\cdot}10^{-3}$	$20{\cdot}10^{-3}$	$10{\cdot}10^{-3}$	$20{\cdot}10^{-3}$
B_b [Nm^2]	$50{\cdot}10^{3}$	$50{\cdot}10^{3}$	$1.09{\cdot}10^{6}$	$166.67{\cdot}10^{3}$	$1.35{\cdot}10^{6}$
m'_b [kg/m]	2.60	2.60	9.10	7.80	6.75
G [N/m^2]	$4.62{\cdot}10^{9}$	$4.62{\cdot}10^{9}$	$4.62{\cdot}10^{9}$	$76.92{\cdot}10^{9}$	-
T_r [Nm^2]	$19.23{\cdot}10^{3}$	$19.23{\cdot}10^{3}$	$131.92{\cdot}10^{3}$	$2.56{\cdot}10^{3}$	$12.90{\cdot}10^{3}$
Θ' [kgm]	$2.71{\cdot}10^{-3}$	$2.71{\cdot}10^{-3}$	$51.11{\cdot}10^{-3}$	$6.57{\cdot}10^{-3}$	$200{\cdot}10^{-3}$
Max f [Hz]	$2.42{\cdot}10^{3}$	$2.42{\cdot}10^{3}$	967.64	$2.55{\cdot}10^{3}$	-

Table 8.1: Input parameters for the initial investigation of the modal density. Three slightly varied wooden systems are investigated; one with greater separation between the beams, and another with larger beams. Further, a steel construction and a construction based on Sjökvist et al. [34] has been investigated. The complex terms from damping are not included in the table. The rows marked "Max f" are calculations of the greatest frequency fulfilling the rule off thumb, saying that the bending wavelength should not exceed six times the thickness/height when assuming thin plates and slender beams [9]. The density and Young's modulus of fir are found on allmeasures.com. The other material properties are from Ohlrich [30].

as a partial validity test of the model. The input mobilities of the other structures can be found in the appendix, figures B.1-B.4.

Later we shall investigate the vibration patterns of ribbed plates, but first we will look into the modal density.

8.3 Modal density

The modal density, here relative to the frequency (some authors use the angular frequency instead), $\Delta N/\Delta f$ with N being the number of modes, is calculated by counting the number of modes occurring within a given frequency band and dividing by the bandwidth. Both a fixed bandwith (10 Hz) and an exponential bandwidth (1/6th octaves) have been used. The results are shown in figures 8.2-8.5.

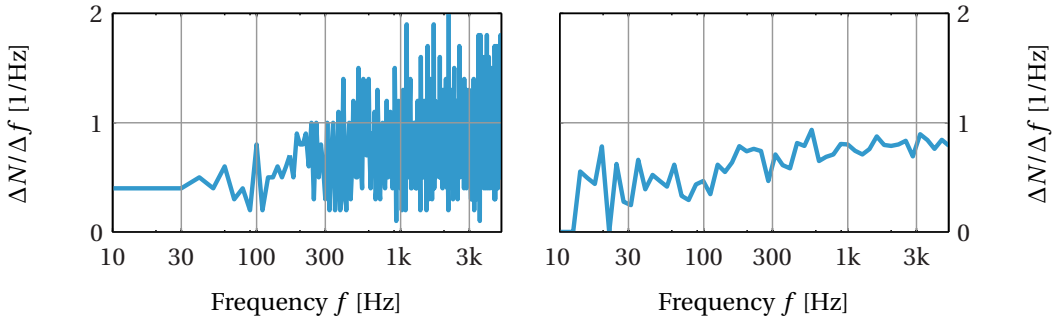

Figure 8.2: Modal density of the structure "wood". On the left a constant bandwidth of 10 Hz is shown, and on the right 1/6th octave bands. The 1/6th octave figure shows small fluctuations towards higher frequencies, but no dominating pass band/stop band behavior can be seen. The low frequency is best seen at the left figure, as the 1/6th octaves are simply too narrow at the low end, and thus the fluctuation is not necessarily a matter of grouping modes, but rather because of the number of modes being very low at the low end of the frequency scale.

In figure 8.2 the results of the system "wood" is shown. The 1/6th octave analysis shows small fluctuations towards higher frequencies, but no dominating pass band/stop band behavior can be seen. The low frequency is best seen using constant bandwidth, as the 1/6th octaves are simply too narrow towards the low end, and thus the fluctuation is not necessarily a matter of grouping modes, but rather because of the number of modes being very low at the low end of the frequency scale.

Figure 8.3 shows the results of a wooden structure with slightly larger spacing between the beams. Very similar results to those with only 600 mm spacing between the beams are seen, except the fluctuations in the 1/6th octave analysis are even smaller towards higher frequencies, compared to figure 8.2.

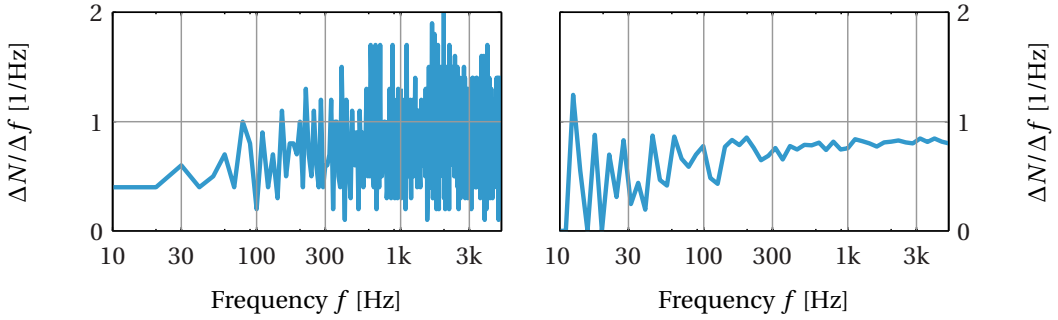

Figure 8.3: Modal density of the structure "wood (1 m)". On the left a constant bandwidth of 10 Hz is shown, and on the right 1/6th octave bands. The 1/6th octave figure becomes nearly constant towards higher frequencies. Otherwise, the result is very similar to that of figure 8.2.

By making the beams larger, it is expected that the influence of periodicity will be greater. That this is the case can be seen in figure 8.4, which shows the modal density when using 70×250 mm^2 cross sectional area for the beams. Because of the rather large height of the beams, the rule-of-thumb saying that slender beam theory can only be applied when the bending wavelength is larger than six times the height of the beams, implies that the model of this structure is only valid up until approximately 1 kHz. The figure shows fluctuations indicating that the modes tend to group (periodically) in certain fre-

quency bands. As the 2D structure is only spatially periodic in one of its dimensions, we do not expect to see a zero modal density in the stop bands, but rather a fluctuation as in the present case. Later on we shall try to divide the modes into two groups, such that one group shows no periodic effects, whereas the other has pass bands and stop bands like in the one dimensional case.

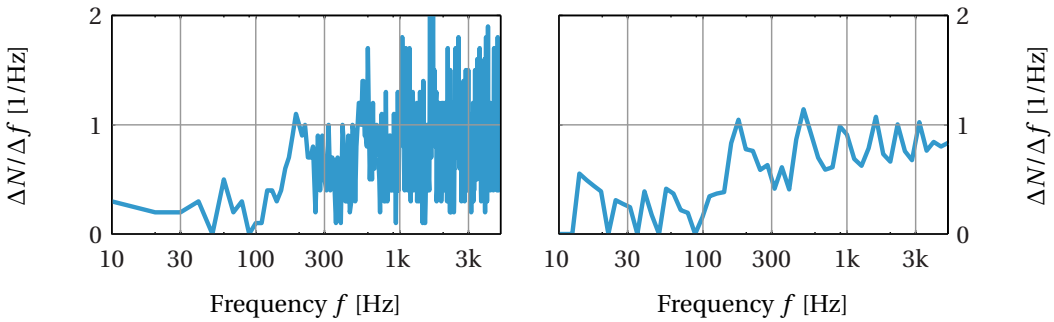

Figure 8.4: Modal density of the structure "wood (heavy)". On the left a constant bandwidth of 10 Hz is shown, and on the right 1/6th octave bands. Be aware that the assumption of slender beams is only valid up to approximately 1 kHz (see table 8.1). Compared to figures 8.2 and 8.3 fluctuations indicating grouping modes are seen.

A figure showing similar results for the steel construction can be found in the appendix (figure B.5). As was the case of the simple wooden structures in figure 8.2 and 8.3 no apparent grouping of modes can be seen.

The last system, "LGS", shows significant grouping of the modes. This is shown in figure 8.5. By comparing the material properties of "LGS" and "wood (heavy)" to the others, we are led to believe that the periodic behavior becomes significant as the bending stiffness and the rotational mass moment of inertia increases. If so, this would not be unexpected, as the periodicity is introduced by the beams, and thus the more stiff and heavy these are, the greater the impact.

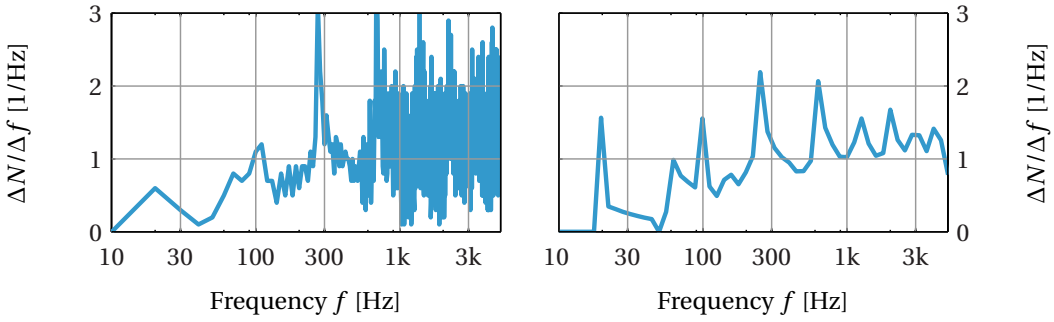

Figure 8.5: Modal density of the structure "LGS". On the left a constant bandwidth of 10 Hz is shown, and on the right 1/6th octave bands. Clear indications of modes grouping together in bands can be seen.

The effect of bending stiffness and rotational mass moment of inertia of the beams is investigated in figure 8.6, where the modal density of the "wood" structure is shown for different modified parameters. Multiplying the bending stiffness by 1000 does not have a great influence on the fluctuation at higher frequencies, whereas a factor of 100 on the rotational mass moment of inertia is seen to have a huge impact. Finally, the rotational stiffness has been multiplied by 1000. This is seen to affect the fluctuation as well. This

supports the thought that the fluctuation is caused by the periodicity in the direction across the beams, since the bending stiffness of the beams act in the direction parallel to the beams, whereas the rotation acts across them. Further, it is seen that the position of the fluctuation peaks does not change when comparing the modified rotational mass moment of inertia to the modified rotational stiffness. This suggests that the position of the pass bands depend on the geometry; that is, the distance between the beams. A parameter study where the wooden structures with different spacing are compared will help investigate this suggestion. However, the parameters must be modified, such that fluctuations are clearly seen. Thus, we multiply both the rotational mass moment of inertia and the rotational stiffness by a factor of 100. The result is shown in figure 8.7. Looking at 1 kHz it is clearly seen that the position of the peaks depend on the distance between the beams.

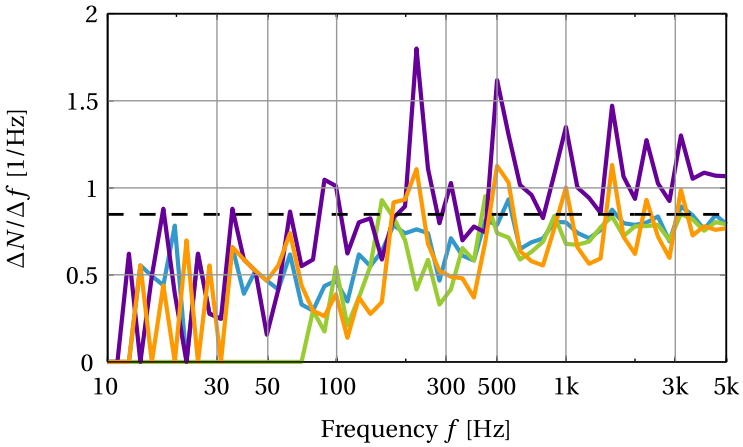

Figure 8.6: Modified "wood" structure. The modal density is shown in 1/6th octave bands. (—) unmodified "wood" structure, (—) beam stiffness increased by a factor of 1000, (—) rotational mass moment of inertia increased by a factor of 100, (—) rotational stiffness increased by a factor of 1000, (– –) frequency averaged modal density of an infinite plate. It is seen that the fluctuation is mainly depending on the rotational mass moment of inertia and the rotational stiffness of the beams, whereas their bending stiffness is without greater influence on the fluctuation. The added bending stiffness influences the low frequency behavior.

In the model that we use in the present thesis, the plate is modelled by a plane, and the beams by lines. As such, the beams have neither width nor height, and thus vertical symmetry relative to the plate is not considered. However, as we define dimensions of the beams in order to calculate stiffnesses and masses the vertical location of the beams need to be considered when calculating the rotational mass moment of inertia. In the above calculations the axis of rotation is the center line of the beam, but when considering for instance a floor construction, the plate will usually be positioned on top of the beams, and thus the axis of rotation would be centered at the top of the beam. When calculating the mass moment of inertia relative to this axis, the rotating mass is four times higher than when using the center axis.

In the original model by Chung [3] the effects of rotational energies are not included, but as the previously discussed results suggest that these energies may play an important role in our model, relative to the grouping of modes, we shall perform a comparison of calculations with and without rotational energies. Further, we will investigate how

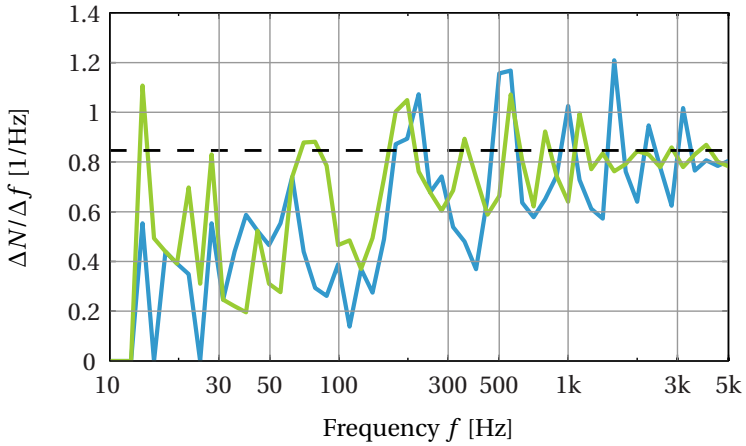

Figure 8.7: Modified "wood" and "wood (1 m)" structures. The modal density is shown in 1/6th octave bands. The structures are both modified by multiplying a factor of 100 to both rotational mass moment of inertia and rotational stiffness. (—) modified "wood" structure, (—) modified "wood (1 m)" structure. The position of the peaks is seen to depend on the beam separation distance. This is especially clear when looking at 1 kHz, where one configuration has a valley while the other has a peak.

the periodic behavior is affected by using the higher rotational mass moment of inertia caused by the beams being located underneath the plate contrary to being centered vertically.

8.4 Effect of torsion

In the following section we make comparisons of the modal densities, with rotational energy using centered beams, with rotational energy using off-center beams (the plate lying on top of the beams), without rotational energies, and without beams at all. The latter calculation serve as a partial validation of the model, as it is directly comparable to the frequency averaged modal density of an infinite plate, as given in equation (3.12) on page 18.

Figure 8.8 shows the modal density of the system "LGS". 1/6th octave bands are chosen to get some smoothing of the results. As pointed out earlier, the 1/6th octave bands are too narrow at low frequencies to obtain the desired smoothing. The figure shows very different results with and without the rotational energies of the beams included in the calculations. Some fluctuation is seen without including torsion, but it seems that the grouping is opposite of that including the torsion. The calculation including torsion shows much bigger fluctuations than when calculated without these energies. The calculation for the plate alone shows good agreement with the theoretical frequency averaged modal density of an infinite plate. Clearly, this figure proves that the rotational energies cannot be neglected for this particular structure.

Figure 8.9 shows the modal density of the system "steel" using 1/6th octave bands as before. This figure shows very little fluctuation when the rotational energies are not included in the calculation, but if any, looking at the higher frequency range, it seems that the modes have the opposite grouping compared to the calculations including torsion, just as the case seen in figure 8.8. Thus the torsion cannot be neglected for this structure either. The effect of using the rotational mass moment of inertia about an axis centered

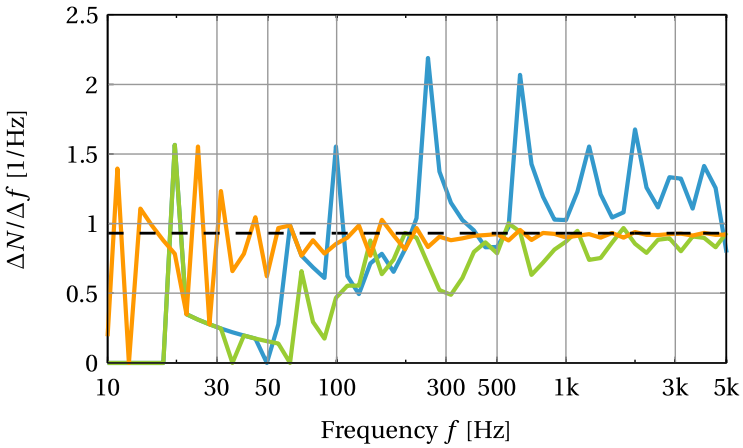

Figure 8.8: Modal density of the system "LGS" calculated in 1/6th octave bands. (—) Without rotational energies, (—) with rotational energies, (—) plate without beams, (– –) frequency averaged modal density of an infinite plate. The effect of including rotational energies in the calculation are clearly seen; the fluctuation becomes much larger compared to the calculation without these energies. The calculation of the plate alone shows good agreement with the theoretical frequency averaged value

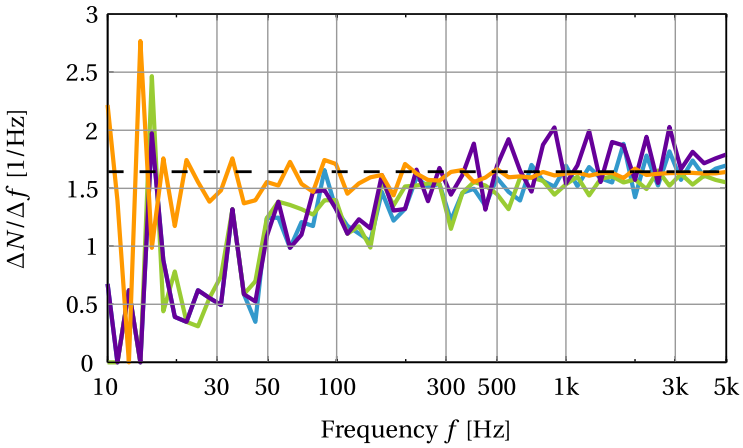

Figure 8.9: Modal density of the system "steel" calculated in 1/6th octave bands. (—) Without rotational energies, (—) with rotational energies, (—) using mass moment of inertia about the top of the beams, (—) plate without beams, (– –) frequency averaged modal density of an infinite plate. The effect of including rotational energies in the calculation are clearly seen; the fluctuation becomes much larger compared to the calculation without these energies. The calculation of the plate alone shows good agreement with the theoretical frequency averaged value

(compared to a centered axis) at the top of each beam is pronounced in this figure at higher frequencies. Again, the calculation for the plate alone shows good agreement with the theoretical frequency averaged modal density of an infinite plate.

Similar figures for the three wooden systems are included in the appendix (figures B.6-B.8). Except for the system with the heavy beams, these show almost no tendency of mode grouping. The system with the heavy beams show such tendencies, but mostly above the limiting frequency of slender beam theory.

Next, we will try varying the dimensions of the plate slightly, while keeping the area constant. The idea is to see how such small imperfections influence the modal densities.

8.5 Small variations of plate dimensions

To investigate the effect of small variations of the plate dimension, the modal densities of 3000 nominally identical plates has been calculated. This has been done for several of the investigated systems. The results are shown as mean values with standard deviation error bars using 1/6th octave bands. These results are depicted in figure 8.10 and 8.11.

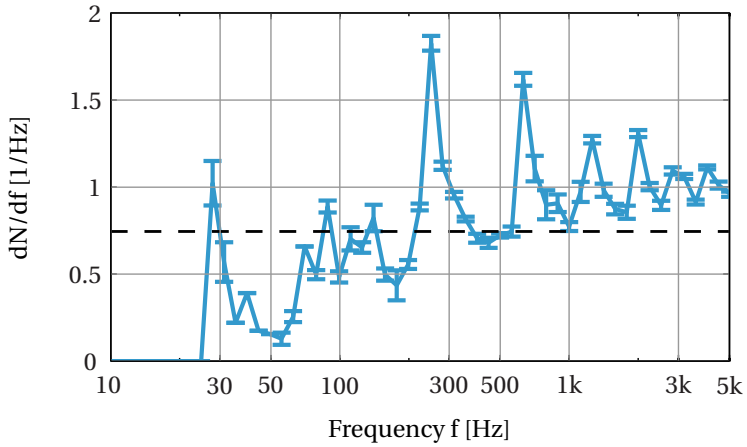

Figure 8.10: Modal density of the structure "LGS" calculated in 1/6th octave bands. The depicted result is an average of 3000 nominally identical plates; that is the plate dimensions are varied randomly with up to 10 cm in each direction, but keeping the area constant. Standard deviations are shown as error bars.

It is seen that in general the standard deviations are rather small, and thus small variations in the width and/or lenght of the plate are not crucial in the calculations. However, at low frequencies large deviations may be seen as the 1/6th octave bands become very narrow and the modal density is fairly low.

A similar calculation has been carried out for the "wood" structure. The figure B.10 can be found in the appendix.

8.6 Summary

In the present chapter, we have seen that:

- The phase of the input mobility is leading 90° at low frequencies. Since we expect spring like behavior at sufficiently low frequencies, the result is in agreement with the expectation.

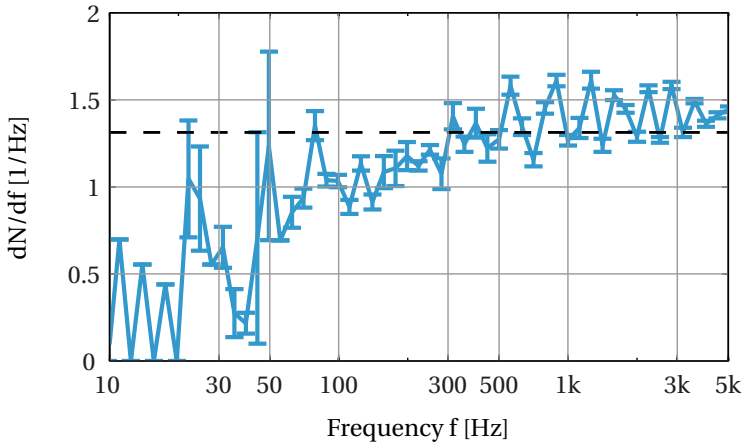

Figure 8.11: Modal density of the structure "steel" calculated in 1/6th octave bands. The depicted result is an average of 3000 nominally identical plates; that is the plate dimensions are varied randomly with up to 10 cm in each direction, but keeping the area constant. Standard deviations are shown as error bars.

- Good overall agreement between the calculated modal densities of the unstiffened plates compared to the theoretical values from equation (3.12).
- The modal density of the investigated systems show fluctuations toward higher frequencies. This behavior is most pronounced for the "LGS", "steel" and "wood (heavy)" systems.
- High values of the bending stiffness and the mass moment of inertia of the beams seem to lead to greater fluctuation. When investigated closer by varying the parameters, it is discovered that the rotational mass moment of inertia is determining the magnitude of the fluctuations along with the rotational stiffness, whereas the added bending stiffness only affects the low frequency behavior.
- Two systems with different distances between the beams (but otherwise equal parameters) are compared. The resulting modal density plots show that the positions of the peaks depend on the separation distance between the beams.
- Comparison of the modal densities with and without including rotational energies of the beams shows, that including these energies is essential to the grouping of the modes (the fluctuations seen at higher frequencies). This comes as no surprise since the rotational parameters has just shown to be critical to these fluctuations.
- The factor of four, that is the difference between using a centered axis and an axis at the top of the beams, is significant when calculating the rotational mass moment of inertia of the beams.
- When varying the plate dimensions up to 10 cm in both length and width (keeping the area constant) the modal density only shows small variations. The standard deviation is fairly low (except for the very low frequencies) when using 1/6th octave bands for analysis.

CHAPTER

9 Grouping the fundamental modes

Our goal is to divide the fundamental modes into two groups; one which we shall call the perpendicular modes, and another which we term the parallel modes.

9.1 An angular approach

In our search for possible ways to group the modes, we consider the following geometrical approach. In equation (5.63) it has been shown, that each mode shape of the ribbed plate is a linear combination of the sinusoidal mode shapes of the plate alone, $\varphi_m(x)\psi_n(y)$. Further, we have seen that each eigenvector contains the coefficients of equation (5.63). Now, the idea that we wish to investigate, is to reshape each eigenvector into an $M \times N$ matrix and the putting the corresponding mode into one of the two groups (either perpendicular or parallel) depending on where it has its dominant coefficients, relative to an angle θ, as depicted in figure 9.1.

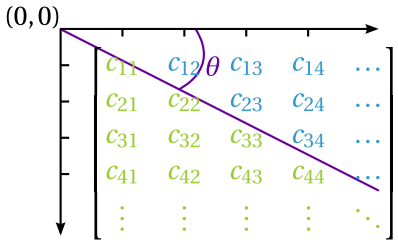

Figure 9.1: Angular separation approach. The modes are each put into the group that contains the most dominant coefficients for that particular mode. Colors: Perpendicular modes and parallel modes.

Let $c_i^{\perp}$ be the coefficients above the separation angle, and likewise let $c_j^{\parallel}$ be the coefficients below the separation angle. If

$$\left| \sum_i \left(c_i^{\perp} \right)^2 \right| > \left| \sum_j \left(c_j^{\parallel} \right)^2 \right|, \tag{9.1}$$

we consider the given mode to belong to the perpendicular group of modes. If (9.1) is not fulfilled, we let the mode belong to the parallel group of modes.

The goal is to investigate if such a separation approach can lead to the modal density of one group showing pass-band/stop-band behavior while the other group does not show this kind of behavior. We do so, by writing a MATLAB script, that for a given angle does the separation and displays the modal densities graphically.

For each column we use the product of the column number and the tangent of the angle, to determine how many of the coefficients should be counted as perpendicular. I.e. in the n'th column the first $n \cdot \tan\theta$ (see fig. 9.2) coefficients are included in the sum of perpendicular coefficients in equation (9.1), whereas the rest are counted as parallel.

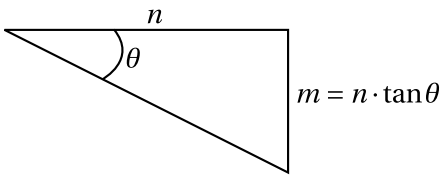

Figure 9.2: In the n'th column the first $n \cdot \tan\theta$ coefficients are included in the sum of perpendicular coefficients

9.2 Results of the angular approach

By using the angular approach described above, grouping of the modes have been attempted for the "LGS" structure and the "steel" structure, as these show fluctuations indicating that the modes tend to be more dense in some frequency bands compared to others.

Finding the optimal angle has been done simply by plotting the resulting modal densities of all angles from 5° to 85° in steps of 5 degrees. Then, by looking at the generated figures, the optimal angles regarding a division such that one group shows pass-band/stop-band behavior while the other group does not, has been determined.

We have no reason to expect the optimal angles for two different systems to be equal, and as we shall see in the following, they are not.

When investigating the "LGS" structure, an angle of 35° has been found as the optimal angle. The results are shown in figures 9.3 and 9.4. The perpendicular modes show clear pass-band/stop-band behavior, while the parallel modes show a fairly flat modal density towards the higher frequencies. At lower frequencies the perpendicular modes are dominating.

The results of the "steel" structure are shown in figures 9.5 and 9.6. For this structure, an angle of 15° turned out to provide the best result. It can be seen from the figures, that the perpendicular modes show clear pass-band/stop-band behavior at frequencies above 500 Hz, while the parallel modes show a fairly flat modal density at these frequencies. At lower frequencies the parallel modes are dominating and show fluctuating behavior.

Inspired by the clear periodicity of the perpendicular modes seen in figure 9.6, we will investigate the repetition rate in the following section.

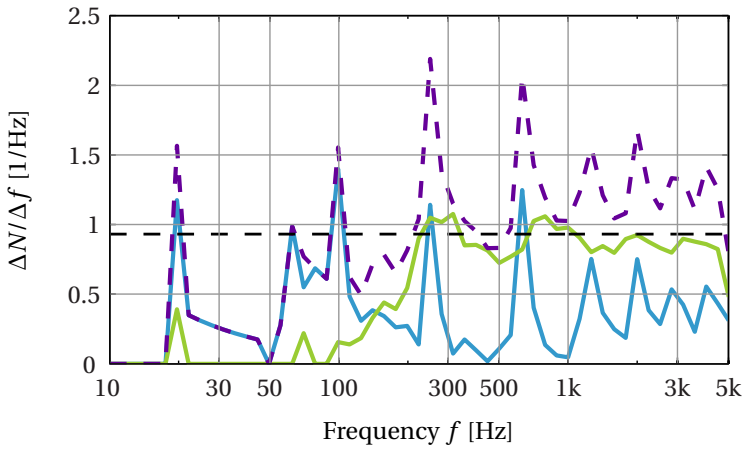

Figure 9.3: Grouping of the modes in structure "LGS". The optimal angle is found to be $\theta = 35°$. 1/6th octave bands. (—) Perpendicular modes, (—) parallel modes, (– –) total modal density, and (– –) frequency averaged modal density of an infinite plate. The perpendicular modes show clear pass-band/stop-band behavior, while the parallel modes show a fairly flat modal density towards the higher frequencies. At lower frequencies the perpendicular modes are dominating.

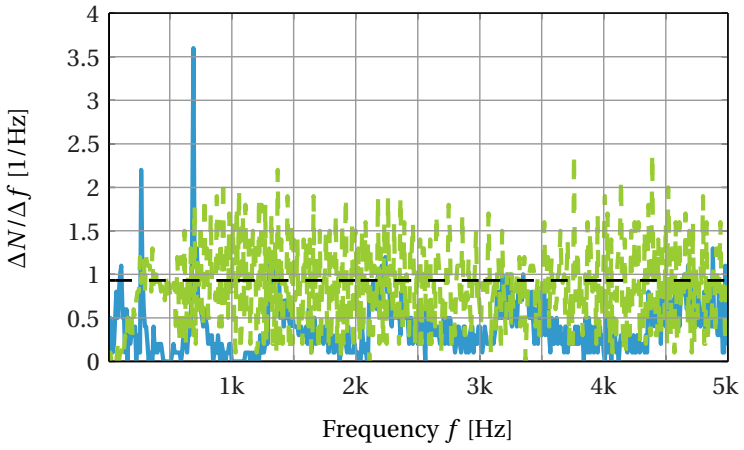

Figure 9.4: Grouping of the modes in structure "LGS". The optimal angle is found to be $\theta = 35°$. 10 Hz constant bandwidth depicted on a linear scale. (—) Perpendicular modes, (—) parallel modes, and (– –) frequency averaged modal density of an infinite plate. The periodic behavior of the perpendicular modes is clearly seen.

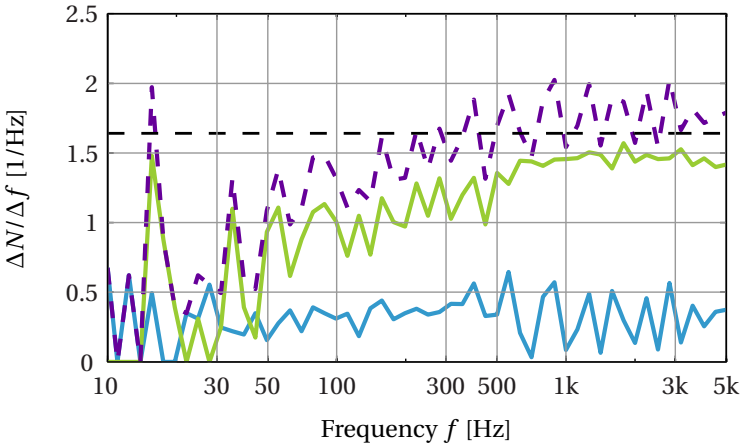

Figure 9.5: Grouping of the modes in structure "steel". The optimal angle is found to be $\theta = 15°$. 1/6th octave bands. (—) Perpendicular modes, (—) parallel modes, (– –) total modal density, and (– –) frequency averaged modal density of an infinite plate. The perpendicular modes show clear pass-band/stop-band behavior at frequencies above 500 Hz, while the parallel modes show a fairly flat modal density at these frequencies. At lower frequencies the parallel modes are dominating and show fluctuating behavior.

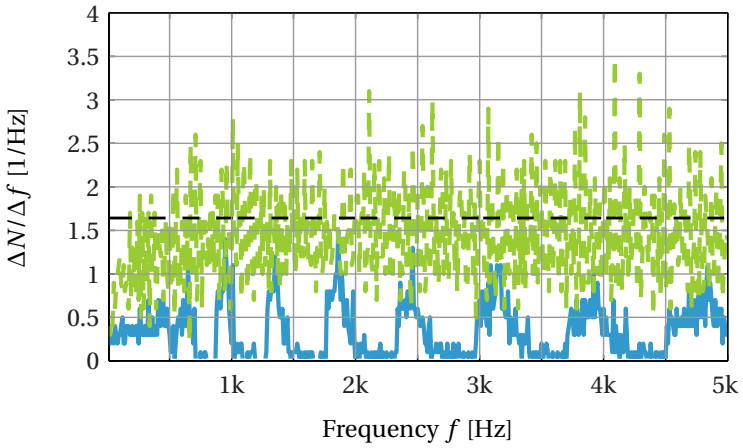

Figure 9.6: Grouping of the modes in structure "steel". The optimal angle is found to be $\theta = 15°$. 10 Hz constant bandwidth depicted on a linear scale. (—) Perpendicular modes, (—) parallel modes, and (– –) frequency averaged modal density of an infinite plate. The periodic behavior of the perpendicular modes is clearly seen. As the linear scaling tends to hide what is happening at low frequencies the fluctuation in the parallel modes at low frequencies is not seen as clearly in this figure compared to figure 9.5.

9.2.1 Investigation of the perpendicular modes

First, we use MATLAB to trace the on-set frequencies of the pass bands seen in the perpendicular modes depicted in figure 9.6. The frequencies are listed in table 9.1. Cremer et al. [9] suggest that the pass band/stop band behavior is periodic in kl. Since $kl \sim \sqrt{f}$ we plot the square root of the onset frequencies as a function of the period number. The result is seen in figure 9.7. Next, we use polynomial fitting to see if the data are positioned on a straight line. As can be seen in the figure, the modal density of the perpendicular modes is clearly fluctuating with a period proportional to kl.

On-set number	On-set frequency [Hz]
1	870
2	1280
3	1760
4	2330
5	2960
6	3700
7	4500

Table 9.1: On-set frequencies found by tracing the perpendicular modes in figure 9.6. The frequencies in the table are used to verify that the periodicity is proportional to kl, see fig. 9.7.

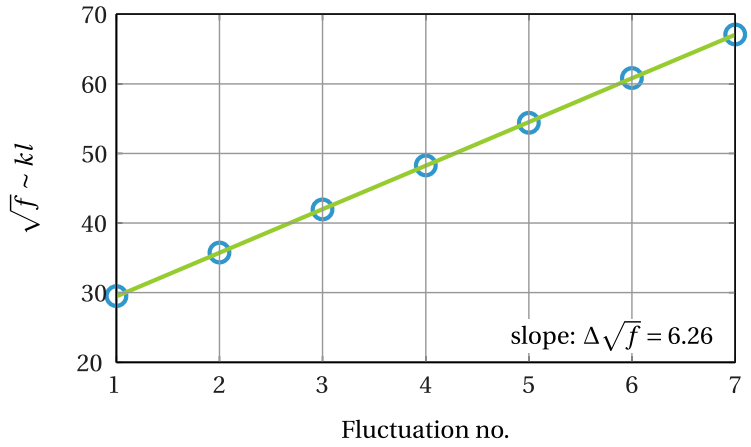

Figure 9.7: Periodicity in kl. Data from the perpendicular modes of the structure "steel". The plot shows square root of the on-set frequencies from figure 9.6 as a function of the period number, see table 9.1. It can be seen that the periods are proportional to kl as the data are on a straight line.

The modal density of the perpendicular modes of the structure "steel" are plotted as a function of $\sqrt{f}/2\pi$ using 10 Hz bandwidth in figure 9.8. A similar figure showing the perpendicular modes found for the "LGS" structure can be found in the appendix, figure B.9.

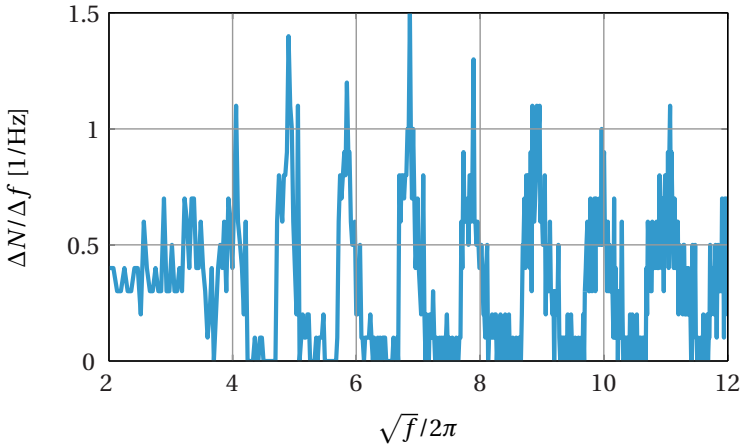

Figure 9.8: Modal density of the perpendicular modes of the structure "steel". 10 Hz bandwidth is used. It can be seen that the periods have equal width in $\sqrt{f} \sim kl$.

9.3 Summary

On an overall level, the angular approach may not be the best solution when trying to group the modes into two; one group showing pass-band/stop-band behavior, and another showing an even distribution of modes. However, it has been shown that an angular approach can indeed be used to obtain such grouping at higher frequencies where the structures behave nicely in a periodic sense. By using the term 'nicely' we mean, that though there may be fluctuations towards lower frequencies they tend to be more random in their distribution.

It has been found, that the optimal angle of separation differs from system to system. How the angle is related to the material properties and configuration of the structure is yet to be determined. Actually, in an SEA sense the angle is not really of importance – the modal density of each of the two groups is what is interesting. It would be expected that the modal density of the perpendicular beams can be found, by studying how similarly spatially periodic 1D structures behave. Likewise, the parallel modes should be distributed somewhat like the well known theoretical frequency averaged modal density of an infinite plate. However, the added stiffness caused by the beams need to be included in the calculations of such a distribution.

In short, we have seen that:

- The angular approach makes it possible to separate the modes into two groups; one that shows periodic behavior and one that does not.
- The angle of separation differs from structure to structure.
- The period of the modal density of perpendicular modes is proportional to kl.

CHAPTER

10 Vibration pattern

In the present chapter, we will look at vibration patterns of both mode shapes and forced vibrations. The reason for investigating such figures is, that by looking at the vibration pattern, information about directional propagation can be obtained.

10.1 A few mode shapes

In figures 10.1 and 10.2 a few of the actual mode shapes of the steel structure are shown. It can be seen from figure 10.1 that the mode shapes are composed from sinusoids. By looking at figure 10.2 it can be seen that there is only little variation within each bay, whereas the variation between different bays may be greater. This tendency is not as pronounced at lower frequencies, as can be seen at the 200 Hz mode depicted in figure 10.1.

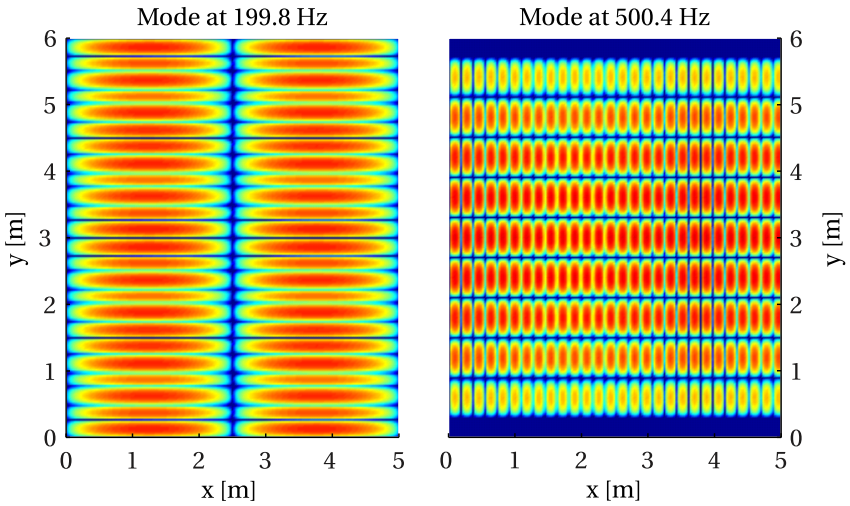

Figure 10.1: A couple of actual mode shapes of the "steel" structure. The plate is here seen from above. Blue colors are low displacements, red colors are high displacements.

Similar figures for the "LGS" structure can be found in the appendix (figures B.11 and B.12).

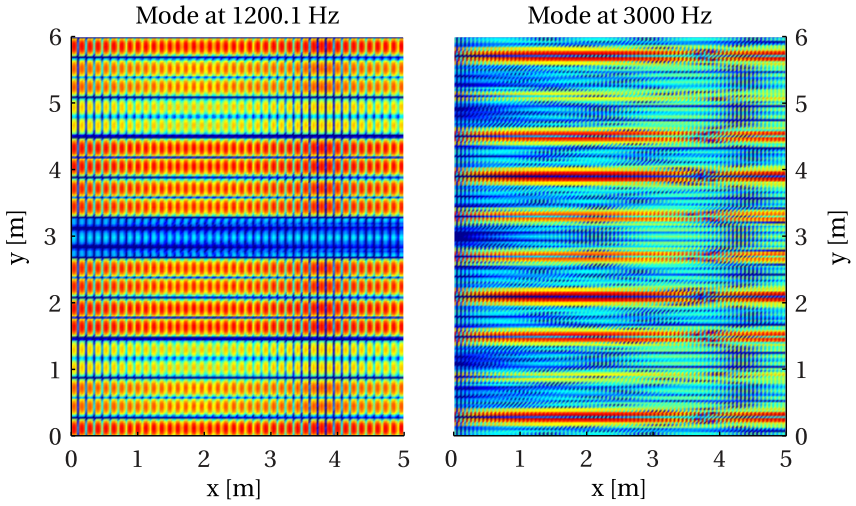

Figure 10.2: A couple of actual mode shapes of the "steel" structure. The plate is here seen from above. Blue colors are low displacements, red colors are high displacements.

10.2 Forced vibration

As explained earlier, the vibration response caused by forced excitation depend on the higher order modes as well as the lower ones. Thus, one should always make sure that sufficiently many modes are included in the calculation when simulating a forced response. In the following, the number of modes necessary is determined by trial-and-error; that is, by increasing the number of modes until the generated figure shows no difference from the previous one.

The figures in the present section are calculated with truncation $M = N = 500$, as these values are found to be sufficiently large.

Figure 10.3 shows forced vibration of the "steel" structure at 1/3 octave bands centered at 1 kHz and 4 kHz respectively. The plate is excited with a 1 N point force at $(x, y) = (1.32, 1.2)$. The response shown is an average of ten random frequencies within a 1/3 octave band. The average is obtained by averaging the squared velocities and converting to decibels afterwards. Strong attenuation across the beams – especially between the excited bay and the neighboring ones – is seen, whereas the attenuation within each bay is seen to be low. Similar results of the "LGS" structure are depicted in figure 10.4.

Looking at figure 10.3 strong attenuation in the direction perpendicular to the beams is seen, whereas only relatively little attenuation is seen within each bay. In figure 10.4 dominating modes parallel to the beams are clearly seen in the 1/3 octave band at 1 kHz, but still the figure shows strong attenuation across the beams compared to the parallel direction when considering the bays close to the excitation point. This observation agrees with the results of Sjökvist [33].

A figure by Sjökvist showing the forced vibration of the "LGS" structure is included in appendix, see figure A.1. The figure shows strong directionality, which indicates that the pass bands are highly directional. When averaging over random frequencies within a 1/3 octave band, we do not see the same kind of directionality in the results presented here.

Forced vibration at lower frequencies is shown in the appendix, where a series of figures showing forced vibration of the "LGS" structure is given. The low-frequency response is less interesting in terms of SEA, as the modal density is too low for SEA pre-

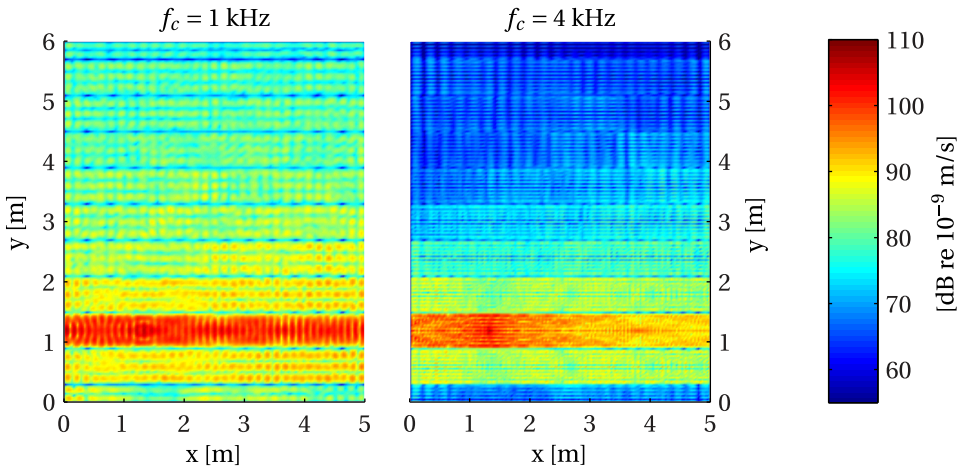

Figure 10.3: Forced vibration of the "steel" structure. The plate is here seen from above. Blue colors are low velocity levels, red colors are high ones. Truncation at $M = 500$, $N = 500$ has been used for the calculation. The figures show RMS averages of 10 random frequencies within a 1/3 octave band centered at 1 kHz (left) and 4 kHz (right) respectively. The beams are spaced 600 mm starting at $y = 0.3$. The plate is excited with a 1 N point force at $(x, y) = (1.32, 1.2)$. Strong attenuation across the beams – especially between the excited bay and the neighboring ones – is seen, whereas the attenuation within each bay is seen to be low.

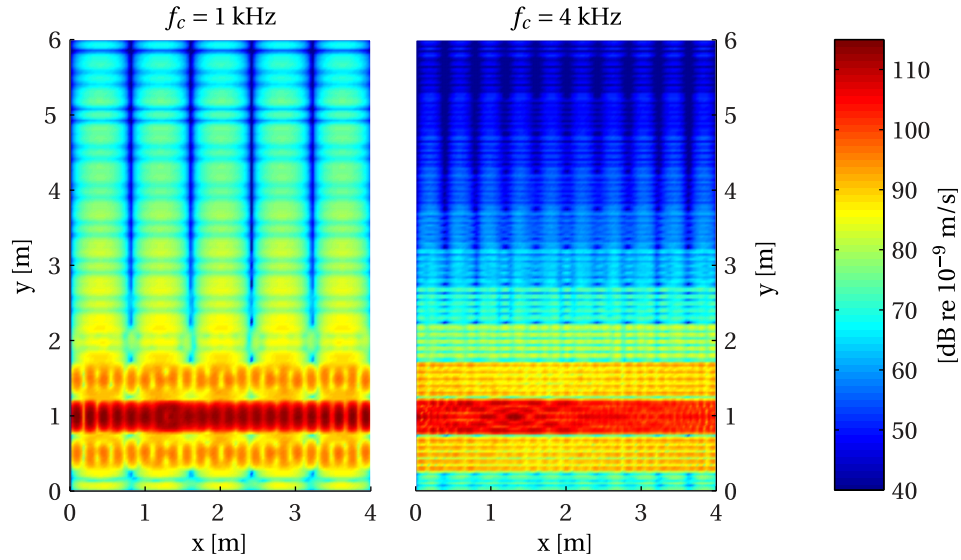

Figure 10.4: Forced vibration of the "LGS" structure. The plate is here seen from above. Blue colors are low velocity levels, red colors are high ones. Truncation at $M = 500$, $N = 500$ has been used for the calculation. The figures show RMS averages of 10 random frequencies within a 1/3 octave band centered at 1 kHz (left) and 4 kHz (right) respectively. The beams are spaced 500 mm starting at $y = 0.25$. The plate is excited with a 1 N point force at $(x, y) = (1.32, 1)$. Strong attenuation between the excited bay and the neighbouring bays is seen. Away from the excitation, dominant modes in the direction along the bays is seen.

dictions. Further, low frequency response can be obtained by other methods like finite element modelling. Figures B.13-B.22 show forced vibration at various frequencies. To apply some smoothing, each figure is the mean result of 50 random frequencies within a 1/6th octave band. Each figure is composed of two plots, both showing the plate from above. The plot on the left is a calculation including rotational energies, whereas the plot on the right does not include this effect. As discovered when investigating modal density there is a significant difference between the results with and without rotational energies.

10.3 Summary

We have demonstrated how some of the actual mode shapes of a rib reinforced plate looks. Further, we have shown how the model predicts the forced vibration response, when excited with a time harmonic point force at various frequencies. We have seen that:

- A high number of modes is necessary to calculate the forced vibration response at high frequencies.
- The rib reinforced plate has strong attenuation across the beams, whereas
- only relatively little attenuation within each bay is seen.

Part IV

Summary and conclusions

CHAPTER

11 Summary

It the present thesis a modal model of a rib reinforced plate has been presented. In chapter 1 a brief introduction is given, followed by a quick walk-through of some basic principles in chapter 2. The theory in chapter 2 should not be new to the reader, but is merely presented as a reminder, since these principles are fundamental in order to understand the model presented at a later stage.

Chapter 3 primarily deals with the bending wave equation of beams and plates. A solution to the bending wave equation of a simply supported beam is found. Further, the concept of modes, natural frequencies and mode shapes is introduced. This chapter concludes the introductory part of the thesis.

The next part of the thesis deals with the theory behind the model, and later the implementation in MATLAB. First, an introduction to Hamilton's principle is given in chapter 4 starting with the calculus of variations and the variational delta operator. Hamilton's principle is then introduced, and finally adapted to the use of complex exponential notation.

Chapter 5 deals with the modal model. By describing the plate and beams separately, using the mechanical motion to calculate the kinetic and elastic potential energies of each component, Hamilton's principle is applied and an expression for the forced deflection of the combined system is found. Further, an eigenvalue problem is derived. By numerically solving the eigenvalue problem, the natural frequencies and corresponding mode shapes can be found. In chapter 6 linear algebra is used to simplify the matrices describing the system. The chapter describes how both the forced problem and the eigenvalue problem can be solved in MATLAB. The procedure is made such that the problem can be divided into smaller pieces that can be solved using parallel computing. This makes it possible to solve the problem for frequencies, that would otherwise be very difficult to deal with, as the number of modes to include in the calculations increases rapidly with the frequency.

In chapter 7 provides a brief introduction to statistical energy analysis. Further, a proposal to an SEA model by Brunskog is presented. This model is the reason for the investigation of mode groups in chapter 9.

After introducing SEA, results of the implemented modal model are presented and discussed. Chapter 8 deals with the modal density of different ribbed plates, simulated using the model. A parameter study of the various inputs to the model is performed by

varying them one by one. It is found that the rotational energies are important to the pass band/stop band behavior seen as fluctuations in the modal density. The positions of the peaks in the fluctuation depends on the distance between the beams.

Next, in chapter 9 the goal is to separate the modes into two groups, such that one shows periodic behavior, while the other one does not. A geometrical approach is investigated, and it is successfully implemented. Looking closer at the group of perpendicular modes; that is, the group of modes showing pass band/stop band behavior, it is seen that the periodicity is evenly spaced in terms of kl. Details, such as how to determine the angle of separation for a given structure are still to be investigated. Further, in terms of SEA, a method to predict the modal densities of the two groups, without implementing a modal model, need to be developed.

Finally, a few of the actual mode shapes and some forced vibration patterns are presented in chapter 10. Strong attenuation in the direction perpendicular to the beams is seen, whereas the attenuation in the direction along them is relatively little in comparison.

CHAPTER

12 Conclusion

The main outcome of the thesis at hand, is the modal model presented in chapter 5. Understanding the underlying theory and implementing the model has taken a considerable amount of time. As writing a thesis includes meeting a deadline, the findings listed in the section below are therefore not necessarily all that can be obtained from the model; that is, given more time, further details of the behavior of a simply supported ribbed plate could be investigated using the present model.

12.1 Findings in the thesis

From the investigations carried out in chapters 8-10 it has been shown that the modes of a spatially periodic ribbed plate can be divided in two groups; one showing periodic behavior in terms of pass bands and stop bands, and another that does not show such behavior. We have seen that the rotational mass moment of inertia and the rotational stiffness are important to the pass band/stop band behavior. Further, simulations show that the frequencies of the pass bands are determined primarily by the distance between the beams. The period of the modal density of the perpendicular modes is proportional to kl.

Small variations of the plate dimensions has shown to be non-critical, when the distance between the beams is fixed and the area of the plate kept constant.

Investigation of mode shapes and forced vibration responses of different plate configurations has revealed that the spatial attenuation in the direction across the beams is strong, whereas it is small within each bay in comparison.

12.2 Future work

The work presented in this thesis is only part of a greater goal; namely the development of an SEA based model describing the vibrational behavior of coupled spatially periodic structures. Continuing the work in that direction could be done by a number of different investigations:

- Expansion of the model by including for instance the slippage that occurs in the coupling between the plate and the beams. This is described by Chung [3] as a

spring potential energy.

- Implementation of point coupling of the beams to the plate, as would be the case with a wooden floor screwed onto the beams.
- Validation of the model by comparing to measured experimental results. Preferably well defined and homogeneous materials like lexan or metal should be used.
- Validation by comparing to other calculation methods, such as the finite element approach.
- Development of an expression for the modal density of perpendicular modes and parallel modes respectively. Such an expression will be needed for SEA adaptation. As will further investigation of the basic assumptions of SEA.
- Investigation of how minor changes in the material properties affect the vibrational response. In order for a prediction tool to be useful for wooden constructions, it must not be too sensitive to changes in the material properties, as these have a great variation between different samples of wood. Nor is wood nearly as homogeneous as for instance steel.
- Consideration of near-periodicity.
- Determination of coupling loss factors and transmission coefficients of coupled periodic structures. How to handle coupling that is neither strong nor weak should be determined.

As can be seen from the above suggestions and considerations, there is plenty of work yet to be done.

Part V

Appendices

APPENDIX

A Figures from various sources

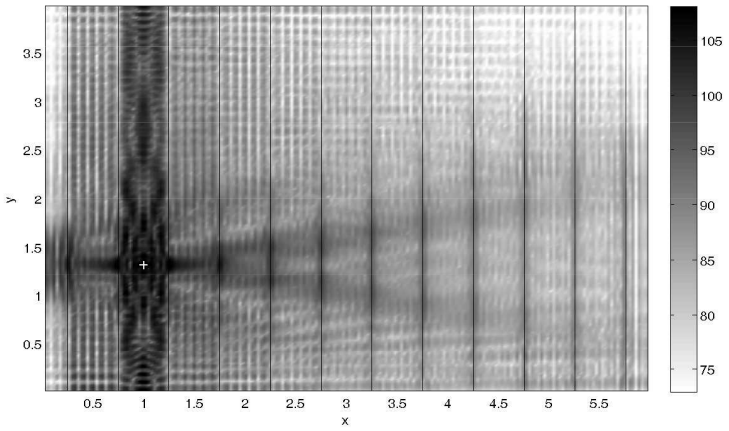

Figure A.1: From [33, p.79, fig.4]. Original caption: *"The plate seen from above. The position of the beams is marked with black lines and the excitation point is marked with a white '+' sign. The vibration level for the 5000 Hz one-third octave band is displayed by grey scale, where darker means more vibration; see the bar at the right side of the figure."*

APPENDIX

B Additional figures

In the following appendix, additional figures from the model is shown. These figures are not directly discussed, but may still be of interest.

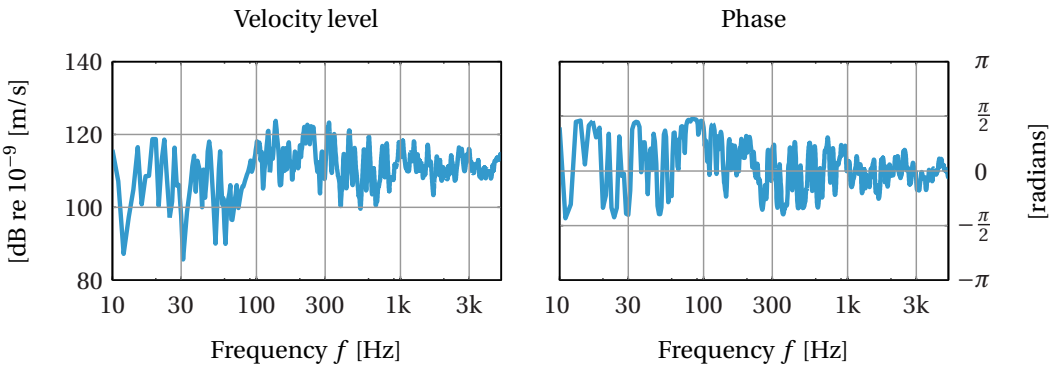

Figure B.1: Structure "wood". Frequency response in the driving point $(x_0, y_0) = (1.32, 1.2)$. On the left is the amplitude, and on the right is the phase.

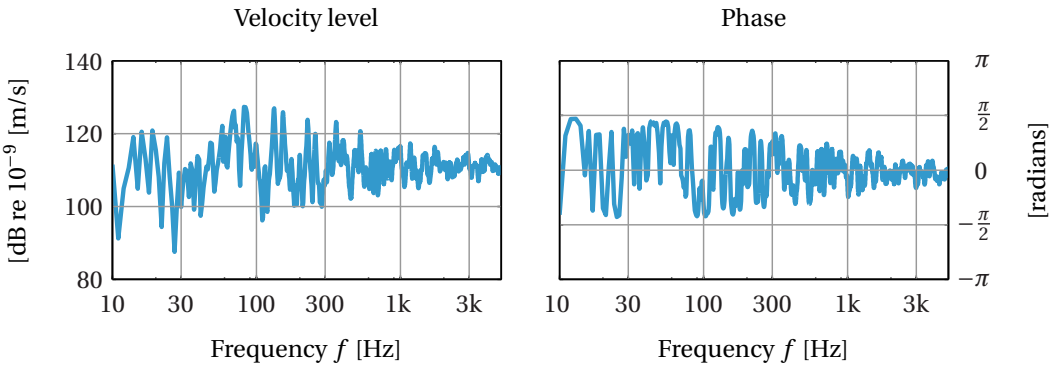

Figure B.2: Structure "wood (1 m)". Frequency response in the driving point $(x_0, y_0) = (1.32, 1)$. On the left is the amplitude, and on the right is the phase.

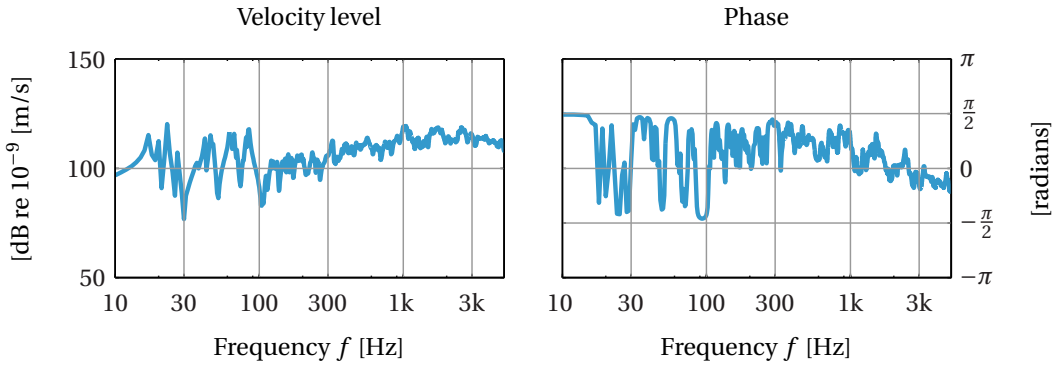

Figure B.3: Structure "wood (heavy)". Frequency response in the driving point $(x_0, y_0) = (1.32, 1.2)$. On the left is the amplitude, and on the right is the phase.

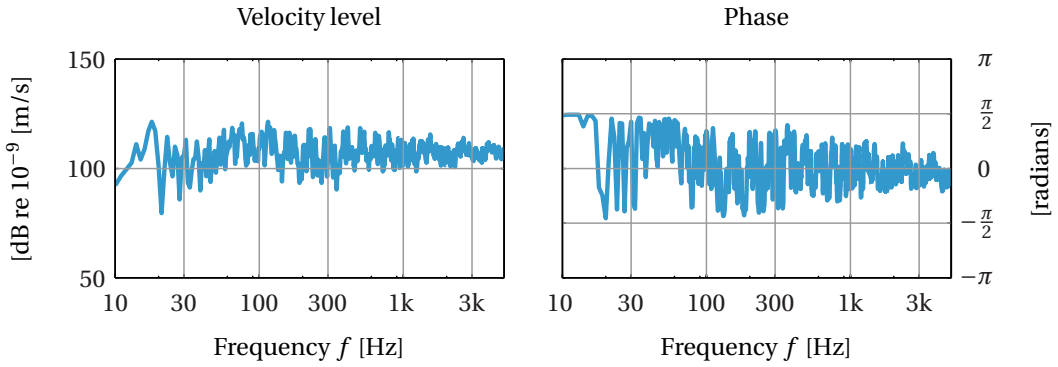

Figure B.4: Structure "steel". Frequency response in the driving point $(x_0, y_0) = (1.32, 1.2)$. On the left is the amplitude, and on the right is the phase.

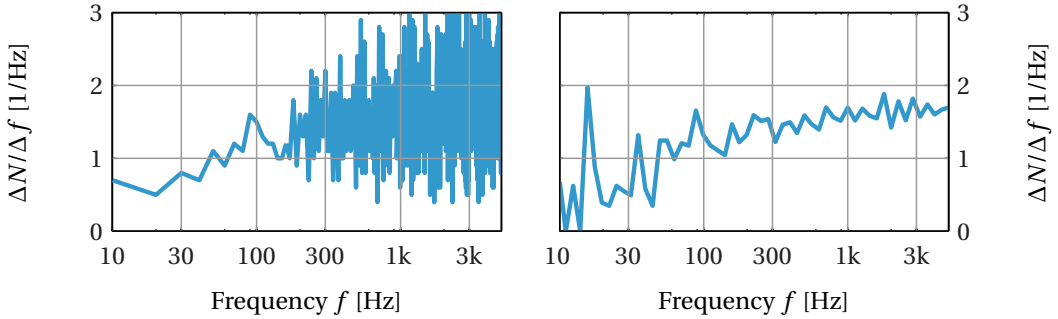

Figure B.5: Modal density of the structure "steel". On the left a constant bandwidth of 10 Hz is shown, and on the right 1/6th octave bands are used. As was the case in figures 8.2 and 8.3, no apparent pass-band/stop-band behavior can be seen.

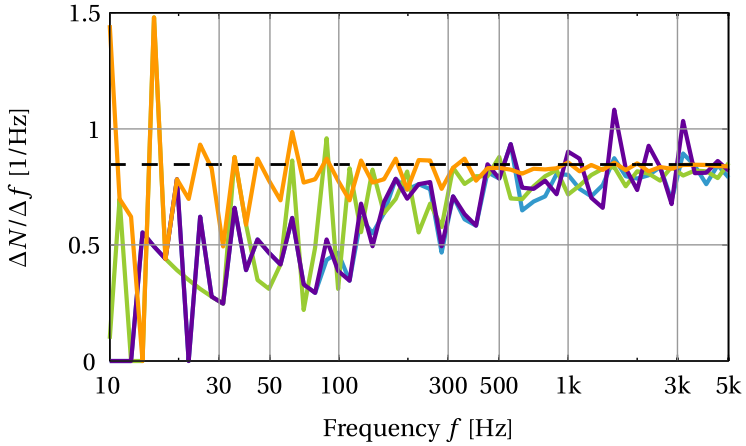

Figure B.6: Modal density of the system "wood" calculated in 1/6th octave bands. (—) Without rotational energies, (—) with rotational energies, (—) using mass moment of inertia about the top of the beams, (—) plate without beams, (– –) frequency averaged modal density of an infinite plate. The effect of including rotational energies in the calculation are clearly seen; the fluctuation becomes much larger compared to the calculation without these energies. The calculation of the plate alone shows good agreement with the theoretical frequency averaged value

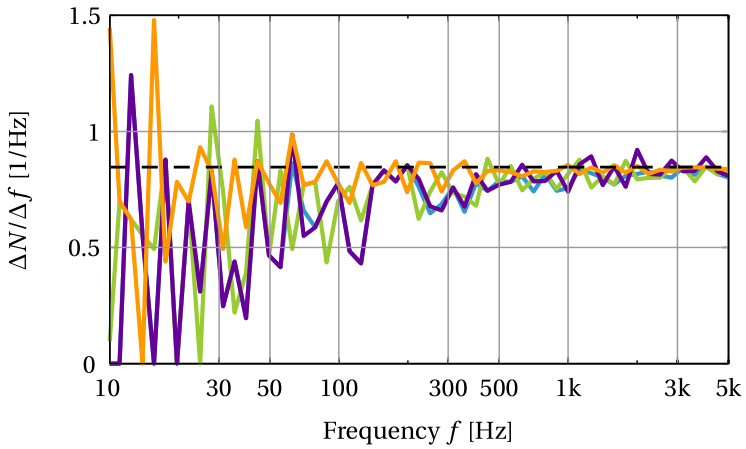

Figure B.7: Modal density of the system "wood (1 m)" calculated in 1/6th octave bands. (—) Without rotational energies, (—) with rotational energies, (—) using mass moment of inertia about the top of the beams, (—) plate without beams, (– –) frequency averaged modal density of an infinite plate. The effect of including rotational energies in the calculation are clearly seen; the fluctuation becomes much larger compared to the calculation without these energies. The calculation of the plate alone shows good agreement with the theoretical frequency averaged value

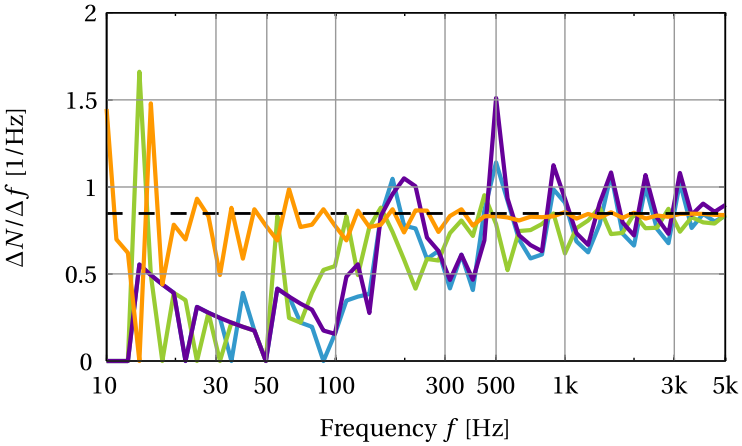

Figure B.8: Modal density of the system "wood (heavy)" calculated in 1/6th octave bands. (—) Without rotational energies, (—) with rotational energies, (—) using mass moment of inertia about the top of the beams, (—) plate without beams, (– –) frequency averaged modal density of an infinite plate. The effect of including rotational energies in the calculation are clearly seen; the fluctuation becomes much larger compared to the calculation without these energies. The calculation of the plate alone shows good agreement with the theoretical frequency averaged value.

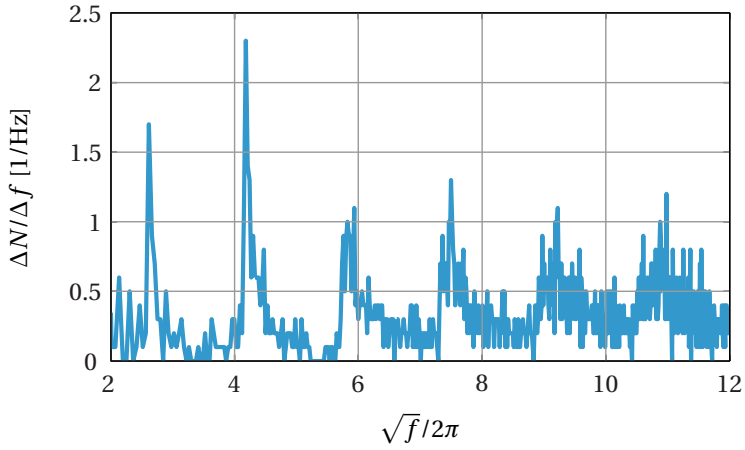

Figure B.9: Modal density of the perpendicular modes of the structure "LGS". 10 Hz bandwidth is used. It can be seen that the periods have equal width in $\sqrt{f} \sim kl$.

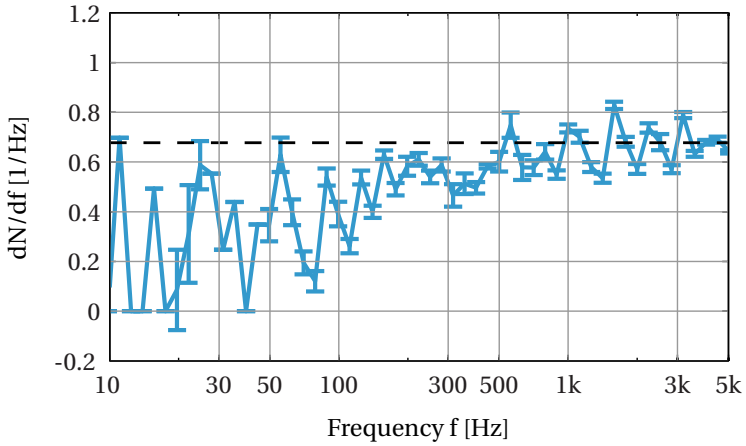

Figure B.10: Modal density of the structure "wood" calculated in 1/6th octave bands. The depicted result is an average of 3000 nominally identical plates; that is the plate dimensions are varied randomly with up to 10 cm in each direction, but keeping the area constant. Standard deviations are shown as error bars.

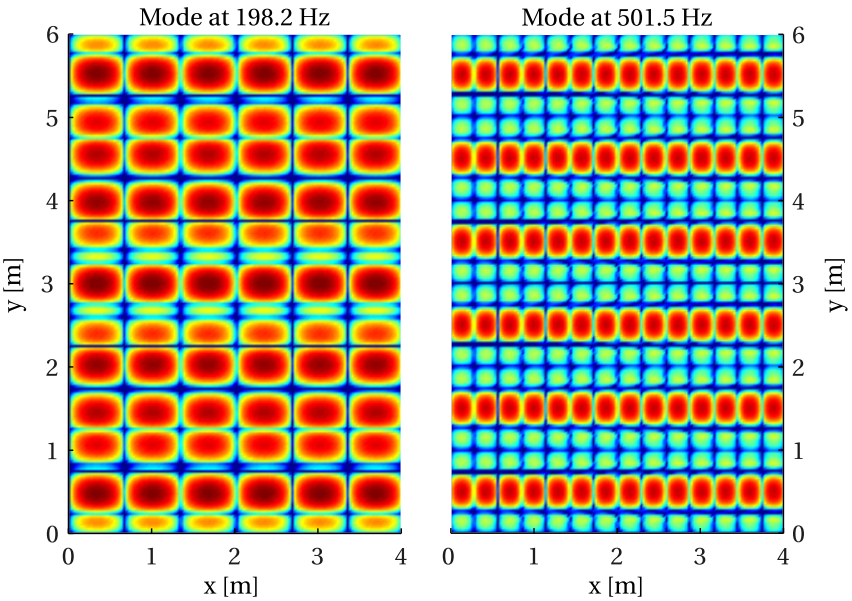

Figure B.11: A couple of actual mode shapes of the "LGS" structure. The plate is here seen from above. Blue colors are low displacements, red colors are high displacements.

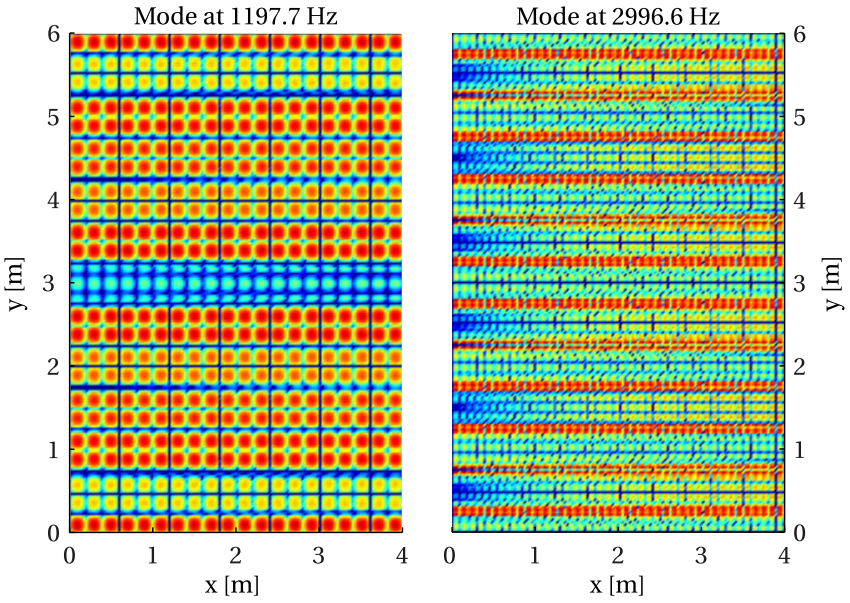

Figure B.12: A couple of actual mode shapes of the "LGS" structure. The plate is here seen from above. Blue colors are low displacements, red colors are high displacements.

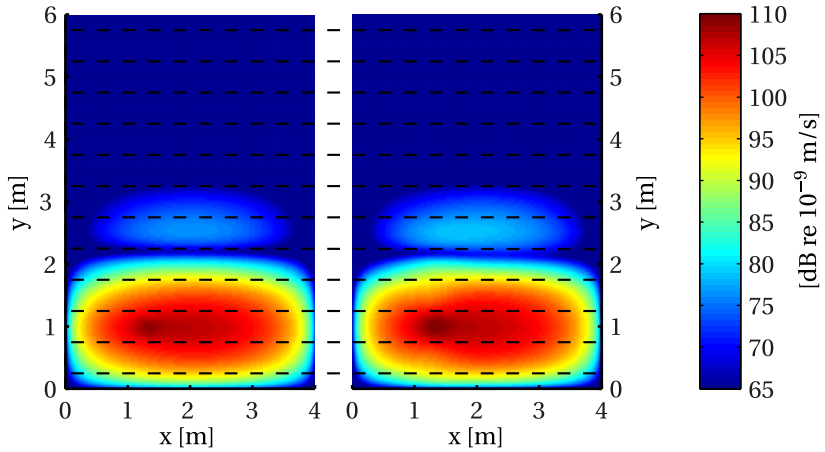

Figure B.13: Comparison of the vibration pattern with and without torsion included in the model. On the left the torsion is included, and on the right it is not. The positions of the beams are indicated by the broken lines across both figures. The excitation is a 1 N time harmonic point force at $x = 1.32$ m and $y = 1$ m. The vibration pattern shown is an average of the response caused by 50 random excitation frequencies within a 1/6th octave band centered at 28 Hz.

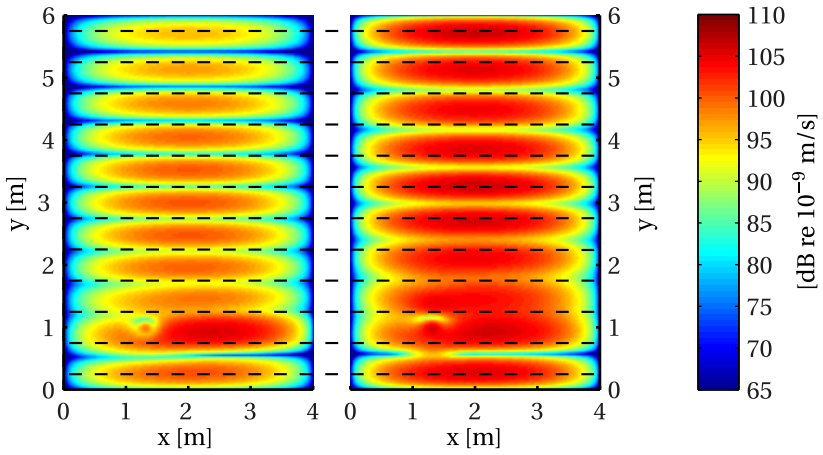

Figure B.14: Comparison of the vibration pattern with and without torsion included in the model. On the left the torsion is included, and on the right it is not. The positions of the beams are indicated by the broken lines across both figures. The excitation is a 1 N time harmonic point force at $x = 1.32$ m and $y = 1$ m. The vibration pattern shown is an average of the response caused by 50 random excitation frequencies within a 1/6th octave band centered at 56 Hz.

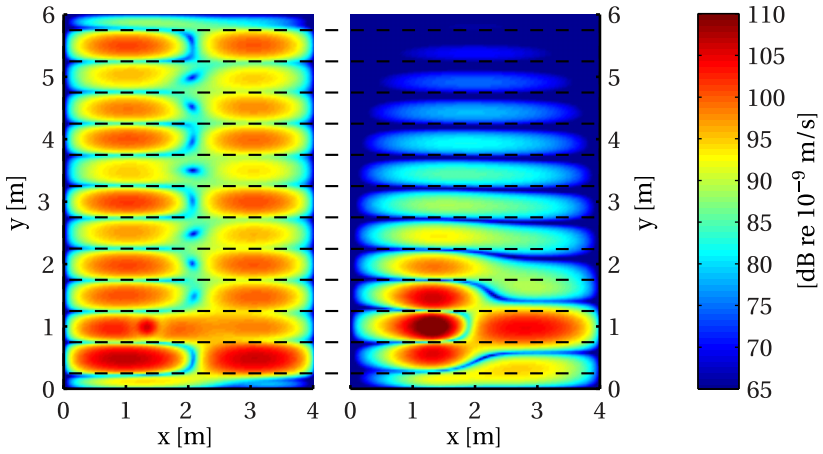

Figure B.15: Comparison of the vibration pattern with and without torsion included in the model. On the left the torsion is included, and on the right it is not. The positions of the beams are indicated by the broken lines across both figures. The excitation is a 1 N time harmonic point force at $x = 1.32$ m and $y = 1$ m. The vibration pattern shown is an average of the response caused by 50 random excitation frequencies within a 1/6th octave band centered at 90 Hz.

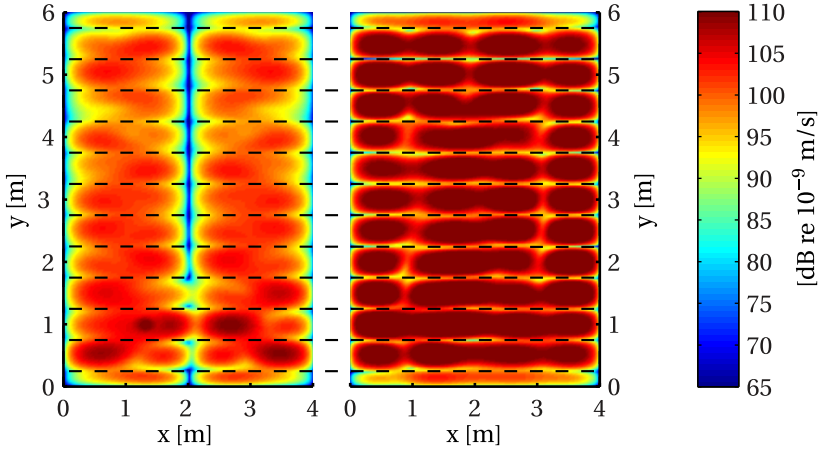

Figure B.16: Comparison of the vibration pattern with and without torsion included in the model. On the left the torsion is included, and on the right it is not. The positions of the beams are indicated by the broken lines across both figures. The excitation is a 1 N time harmonic point force at $x = 1.32$ m and $y = 1$ m. The vibration pattern shown is an average of the response caused by 50 random excitation frequencies within a 1/6th octave band centered at 140 Hz.

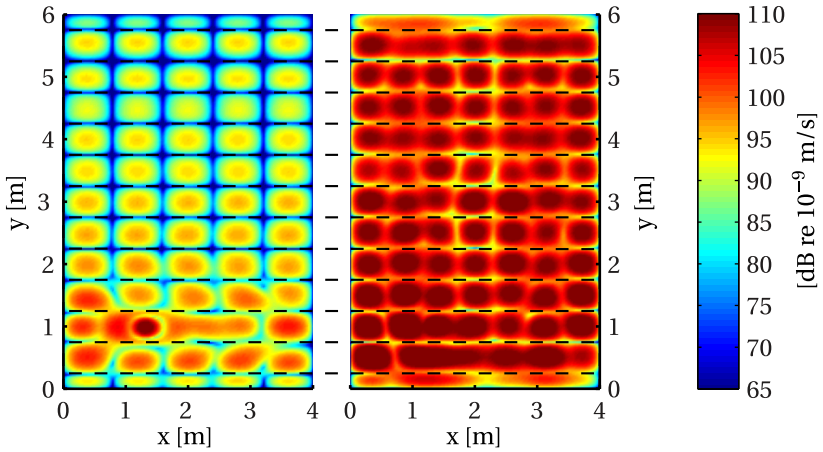

Figure B.17: Comparison of the vibration pattern with and without torsion included in the model. On the left the torsion is included, and on the right it is not. The positions of the beams are indicated by the broken lines across both figures. The excitation is a 1 N time harmonic point force at $x = 1.32$ m and $y = 1$ m. The vibration pattern shown is an average of the response caused by 50 random excitation frequencies within a 1/6th octave band centered at 180 Hz.

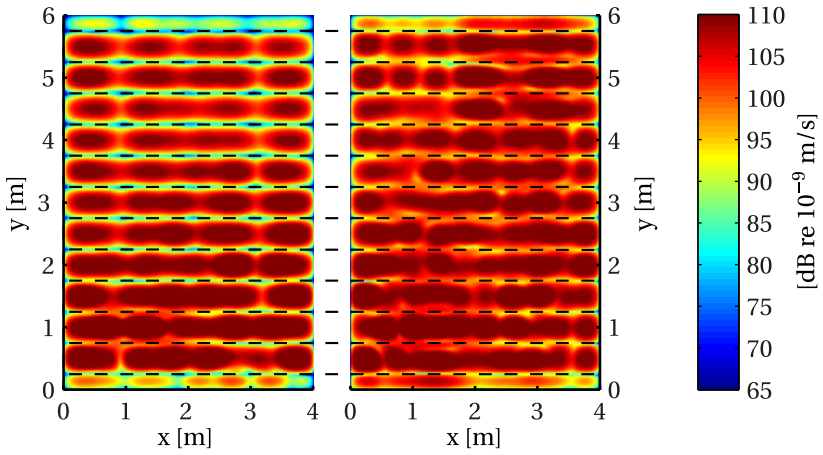

Figure B.18: Comparison of the vibration pattern with and without torsion included in the model. On the left the torsion is included, and on the right it is not. The positions of the beams are indicated by the broken lines across both figures. The excitation is a 1 N time harmonic point force at $x = 1.32$ m and $y = 1$ m. The vibration pattern shown is an average of the response caused by 50 random excitation frequencies within a 1/6th octave band centered at 250 Hz.

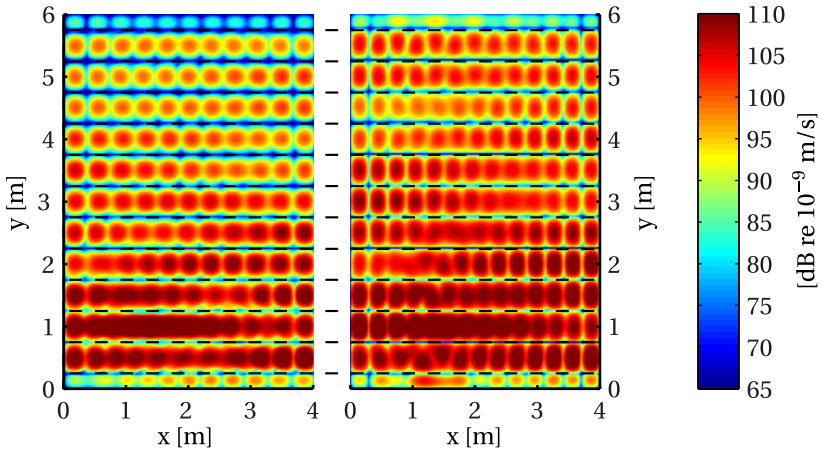

Figure B.19: Comparison of the vibration pattern with and without torsion included in the model. On the left the torsion is included, and on the right it is not. The positions of the beams are indicated by the broken lines across both figures. The excitation is a 1 N time harmonic point force at $x = 1.32$ m and $y = 1$ m. The vibration pattern shown is an average of the response caused by 50 random excitation frequencies within a 1/6th octave band centered at 400 Hz.

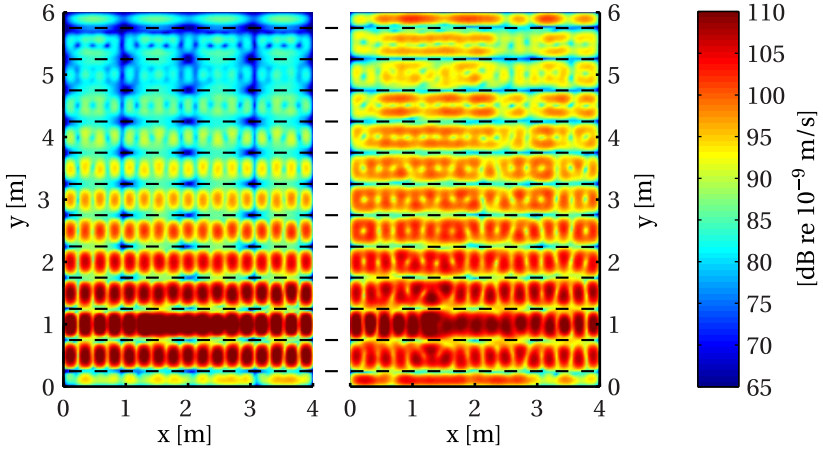

Figure B.20: Comparison of the vibration pattern with and without torsion included in the model. On the left the torsion is included, and on the right it is not. The positions of the beams are indicated by the broken lines across both figures. The excitation is a 1 N time harmonic point force at $x = 1.32$ m and $y = 1$ m. The vibration pattern shown is an average of the response caused by 50 random excitation frequencies within a 1/6th octave band centered at 630 Hz.

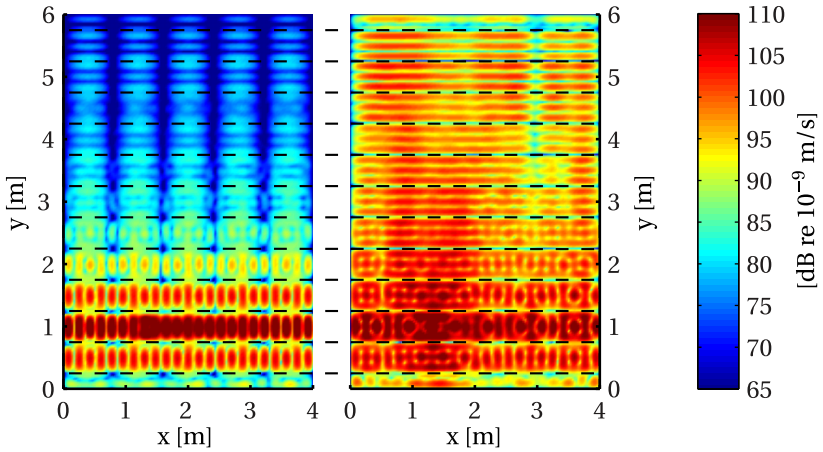

Figure B.21: Comparison of the vibration pattern with and without torsion included in the model. On the left the torsion is included, and on the right it is not. The positions of the beams are indicated by the broken lines across both figures. The excitation is a 1 N time harmonic point force at $x = 1.32$ m and $y = 1$ m. The vibration pattern shown is an average of the response caused by 50 random excitation frequencies within a 1/6th octave band centered at 1000 Hz.

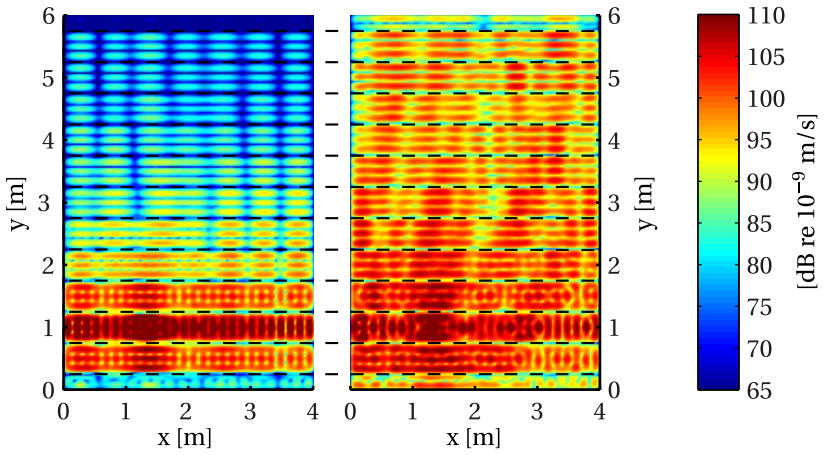

Figure B.22: Comparison of the vibration pattern with and without torsion included in the model. On the left the torsion is included, and on the right it is not. The positions of the beams are indicated by the broken lines across both figures. The excitation is a 1 N time harmonic point force at $x = 1.32$ m and $y = 1$ m. The vibration pattern shown is an average of the response caused by 50 random excitation frequencies within a 1/6th octave band centered at 1250 Hz.

APPENDIX

C MATLAB scripts

In the present appendix, the MATLAB scripts, that have been used to produce figures and numerical results presented in this thesis, are included. The scripts are merely provided as a documentation of the findings, and the reader should be warned, that they were not written with publishing in mind – writing nice and easy-to-read scripts can be a time consuming and demanding task, even for a trained programmer (which this author is not).

C.1 MATLAB version

For the numerical calculations in the present thesis, the following version of MATLAB has been used. It has been running on DTU gbar linux servers (glint00-glint17), and has been accessed through ThinLinc client software. Of course only a few of the installed packages has actually been used, as can be seen from the included scripts.

```
--------------------------------------------------------------------------------
MATLAB Version 7.7.0.471 (R2008b)
MATLAB License Number: 167507
Operating System: Linux 2.6.18-92.1.6.el5 #1 SMP Wed Jun 25 12:38:37 EDT 2008 x86_64
Java VM Version: Java 1.6.0_04 with Sun Microsystems Inc. Java HotSpot(TM) 64-Bit Server VM mixed mode
--------------------------------------------------------------------------------
MATLAB                                                Version 7.7       (R2008b)
Simulink                                              Version 7.2       (R2008b)
Aerospace Blockset                                    Version 3.2       (R2008b)
Aerospace Toolbox                                     Version 2.2       (R2008b)
Bioinformatics Toolbox                                Version 3.2       (R2008b)
Communications Blockset                               Version 4.1       (R2008b)
Communications Toolbox                                Version 4.2       (R2008b)
Control System Toolbox                                Version 8.2       (R2008b)
Curve Fitting Toolbox                                 Version 1.2.2     (R2008b)
Database Toolbox                                      Version 3.5       (R2008b)
Datafeed Toolbox                                      Version 3.2       (R2008b)
EDA Simulator Link DS                                 Version 2.0       (R2008b)
Econometrics Toolbox                                  Version 1.0       (R2008b)
Filter Design Toolbox                                 Version 4.4       (R2008b)
Financial Derivatives Toolbox                         Version 5.3       (R2008b)
Financial Toolbox                                     Version 3.5       (R2008b)
Fixed-Income Toolbox                                  Version 1.6       (R2008b)
Fixed-Point Toolbox                                   Version 2.3       (R2008b)
Fuzzy Logic Toolbox                                   Version 2.2.8     (R2008b)
Genetic Algorithm and Direct Search Toolbox           Version 2.4       (R2008b)
Image Processing Toolbox                              Version 6.2       (R2008b)
Instrument Control Toolbox                            Version 2.7       (R2008b)
MATLAB Builder JA                                     Version 2.0.2     (R2008b)
MATLAB Compiler                                       Version 4.9       (R2008b)
MATLAB Distributed Computing Server                   Version 4.0       (R2008b)
MATLAB Report Generator                               Version 3.4       (R2008b)
Mapping Toolbox                                       Version 2.7.1     (R2008b)
```

```
Model Predictive Control Toolbox                Version 3.0       (R2008b)
Neural Network Toolbox                          Version 6.0.1     (R2008b)
Optimization Toolbox                            Version 4.1       (R2008b)
Parallel Computing Toolbox                      Version 4.0       (R2008b)
Partial Differential Equation Toolbox           Version 1.0.13    (R2008b)
RF Blockset                                     Version 2.3       (R2008b)
RF Toolbox                                      Version 2.4       (R2008b)
Real-Time Workshop                              Version 7.2       (R2008b)
Real-Time Workshop Embedded Coder               Version 5.2       (R2008b)
Robust Control Toolbox                          Version 3.3.2     (R2008b)
Signal Processing Blockset                      Version 6.8       (R2008b)
Signal Processing Toolbox                       Version 6.10      (R2008b)
SimBiology                                      Version 2.4       (R2008b)
SimDriveline                                    Version 1.5.1     (R2008b)
SimElectronics                                  Version 1.1       (R2008b)
SimEvents                                       Version 2.3       (R2008b)
SimHydraulics                                   Version 1.4       (R2008b)
SimMechanics                                    Version 3.0       (R2008b)
SimPowerSystems                                 Version 5.0       (R2008b)
Simscape                                        Version 3.0       (R2008b)
Simulink Control Design                         Version 2.4       (R2008b)
Simulink Design Verifier                        Version 1.3       (R2008b)
Simulink Fixed Point                            Version 6.0       (R2008b)
Simulink Parameter Estimation                   Version 1.2.3     (R2008b)
Simulink Report Generator                       Version 3.4       (R2008b)
Simulink Response Optimization                  Version 3.2       (R2008b)
Simulink Verification and Validation            Version 2.4       (R2008b)
Spline Toolbox                                  Version 3.3.5     (R2008b)
Stateflow                                       Version 7.2       (R2008b)
Stateflow Coder                                 Version 7.2       (R2008b)
Statistics Toolbox                              Version 7.0       (R2008b)
Symbolic Math Toolbox                           Version 5.1       (R2008b)
System Identification Toolbox                   Version 7.2.1     (R2008b)
SystemTest                                      Version 2.2       (R2008b)
Video and Image Processing Blockset             Version 2.6       (R2008b)
Virtual Reality Toolbox                         Version 4.8       (R2008b)
Wavelet Toolbox                                 Version 4.3       (R2008b)
```

C.2 Solving the eigenvalue problem

In this section, a script that solves the eigenvalue problem and store the results for later analysis is presented. Further some scripts for calculating and plotting the modal density are provided.

C.2.1 modalmodelEVP.m

This script solves the eigenvalue problem and stores the data for later analysis.

```
1  % Modal model implemented from the draft paper
2  % "Non-diffuse bending waves in lightweight ribbed plates"
3  % by Jonas Brunskog and Hyuck Chung.
4
5  % Author: Kristoffer A. Dickow
6  % Part of MSc project, DTU 2009
7
8  % Calculates the eigenvalues and eigenvectors and saves them in a file.
9
10 clear all; clc; close all;
11
12 savefile = 'filename'; % enter filename here
13
14 t0 = clock; % needed to measure calculation time
15
16 lx=5; % Plate dimension
17 ly=6; % Plate dimension
18
19 M = 200; % Truncation of m
```

```
20 N = 150; % Truncation of n
21
22 yj = .3:.6:1y; % Position of beams
23 %yj = .5:1:1y; % Position of beams
24 %yj = .25:.5:1y; % Position of beams
25
26 %%%%% 22mm chipboard on fir beams
27
28 % constants plate
29 hp=22e-3; % thickness
30 rhop=6.5e2; % density
31 nup=.3; % poisson ratio
32 Ep=4.6e9*(1+1i*.02); % Young's modulus
33
34 Bp=Ep*hp^3/(12*(1-nup^2)); % plate bending stiffness pr unit width
35 mp=rhop*hp; % plate mass per unit area
36
37 % constants beam
38 bb=5e-2; % width of beams
39 hb=10e-2; % height of beams
40 rhob=5.2e2; % density of beams
41 Eb=1.2e10*(1+1i*.02); % Young's modulus
42 nub=.3; % poisson
43
44 Bb=Eb*bb*hb^3/12; % beam bending stiffness
45 mb=rhob*(bb*hb); % beam mass per unit length
46 Gb=Eb/(2+2*nub); % Shear modulus
47 Tr = Gb*bb^3*hb/3; % Torsional stiffness
48 Theta = rhob*bb*hb^3/12; % Rotational mass moment of intertia
49 %Theta=Theta*4; % place the rotation axis at the end instead of centered
50
51 %%% STEEL CONSTRUCTION
52
53 % % constants plate
54 % hp=6e-3;%18e-3; % thickness
55 % rhop=7.8e3;%6.5e2; % density
56 % nup=.28;%.3; % poisson ratio
57 % Ep=2e11*(1+1i*.01);%4.6e9*(1+1i*.02); % Young's modulus
58 %
59 %
60 % Bp=Ep*hp^3/(12*(1-nup^2)); % plate bending stiffness pr unit width
61 % mp=rhop*hp; % plate mass per unit area
62 %
63 % % constants beam
64 % bb=10e-3;%5e-2; % width of beams
65 % hb=100e-3;%10e-2; % height of beams
66 % rhob=rhop;%5.3e-2; % density of beams
67 % Eb=Ep;%1.2e10*(1+1i*.02); % Young's modulus
68 % nub=nup;%.3; % poisson
69 %
70 % Bb=Eb*bb*hb^3/12; % beam bending stiffness
71 % mb=rhob*(bb*hb); % beam mass per unit length
72 % Gb=Eb/(2+2*nub); % Shear modulus
73 % Tr = Gb*bb^3*hb/3; % Torsional stiffness
74 % Theta = rhob*bb*hb^3/12; % Rotational mass moment of intertia
75 % %Theta=Theta*4; % place the rotation axis at the end instead of centered
76 %%%%%%%%%%%
77
78 %LGS:
79 % Bb=1.35e6*(1+1i*.02);
80 % Bp=2800*(1+1i*.02);
81 % mb=6.75;
82 % mp=10.8;
83 % Theta=.2;
84 % Tr=1.29e4*(1+1i*.02);
85
86 m = (1:M)';    % Column vector
87 n = (1:N);     % Row vector
```

```
88
89  km = pi*m/lx;  % Column w/ modes in x direction
90  kappan = pi*n/ly;% Row w/ modes in y direction
91
92  clear m n
93
94  S = length(yj);
95
96  Kpmn = Bp*(repmat(km.^2,1,N)+repmat(kappan.^2,M,1)).^2; % MxN matrix
97
98  Jdiag = sqrt(2/ly)*sin(yj'*kappan); % J-matrix is diagonal with M
99                                      % Jdiag's on the diagonal
100
101 Idiag = sqrt(2/ly)*cos(yj'*kappan).*repmat(kappan,S,1);
102
103 % Allocate memory
104 Di = zeros(M*N,1);
105 V = sparse(zeros(M*N));
106
107 for ii=1:M;
108     Km = diag(Kpmn(ii,:))+Jdiag'*(Bb*km(ii)^4*eye(S))*Jdiag+Idiag'*(Tr*km(ii)^2*eye(S))*Idiag;
109     Mm = mp*eye(N)+Jdiag'*(mb*eye(S))*Jdiag+Idiag'*(Theta*eye(S))*Idiag;
110     [Vm Dm] = eig(Mm\Km);
111     V((ii-1)*N+1:ii*N,(ii-1)*N+1:ii*N) = Vm;
112     Di((ii-1)*N+1:ii*N) = diag(Dm);
113 end
114
115 % V is an MN by MN matrix with eigenvectors as columns
116 % Di is a coloumn vector with corresponding eigenvalues
117
118 disp(['Calculation time: ',num2str(etime(clock,t0)),' seconds'])
119 clear Dm Jdiag Idiag Km Kpmn Mm S Vm ii t0
120 save(savefile);
```

C.2.2 modaldensity.m

This script plots the modal density of one or more systems.

```
1  % Author: Kristoffer A. Dickow
2  % Part of MSc project, DTU 2009
3
4  clc;clear all; close all;
5  % requires that modalmodelEVP has been run first.
6  % requires newsemilogfig.m - if not available search and replace
7  % newsemilogfig with figure()
8  % same for newloglogfig.m and newlinfig.m
9  % requires mygrid.m, otherwise remove mygrid-calls
10
11 t0 = clock; % needed to measure calculation time
12
13 % Initialize figures
14 fig1=newloglogfig; % mode count, log scale
15 fig2=newlinfig;   % density in 10 Hz bands, linear scale
16 fig3=newsemilogfig; % density in 1/6 octaves, log scale
17 [fig4 fig4l fig4r]=newdoublesemilogfig; % constant bandwith and 1/6 octave. Log scales
18
19 for data={'wood100torsion' 'wood1m100torsion'}
20
21 load(char(data));
22
23 slopeplate = real(lx*ly*mp/(2*sqrt(Bp*mp))); % modal density of a plate from MO 7022
24
25 [Di I] = sort(real(Di)); % sort eigenvalues
26 Di = sqrt(Di)/(2*pi); % eigenfrequencies
27
```

```
f=0:0.5:10e3;
Nm = cumsum(histc(Di,f)); % cumulative histogram
figure(fig1);
plot(Di,1:length(Di));

df = 10; % Hz
ff=0:df:10e3;

figure(fig2);
DNr=histc(Di,ff)/df;
plot(ff,DNr);
figure(fig4)
subplot(fig4l)
plot(ff,DNr);

% calculate 1/6 octave bands from 10 Hz to 5 kHz
freqs=[0 0];
cf = 1000*2^(1/12); % upper cut off
count = 0;
while cf>2
    count = count+1;
    freqs(count)=cf;
    cf=cf/2^(1/6);
end
freqs=fliplr(freqs);
cf = 1000*2^(1/6)*2^(1/12); % upper cut off
while cf<10000
    count = count+1;
    freqs(count)=cf;
    cf=cf*2^(1/6);
end
[rows cols] = size(Di);

DNr=histc(Di,freqs)./(repmat(freqs*(2^(1/6)-1),cols,1))';

figure(fig3)
plot(freqs/2^(1/12),DNr);
figure(fig4)
subplot(fig4r)
plot(freqs/2^(1/12),DNr);
end


% add legends and theoretical average value for just a plate w/o ribs
figure(fig1);
plot(10:5000,polyval([slopeplate 0],10:5000),'LineStyle', '--', 'LineWidth', 1, 'Color', [0 0 0]);
xlabel('Frequency $f$ [Hz]');
ylabel('Cumulative mode number');
mygrid;
%legend('with torsion','without torsion');
figure(fig2);
plot(ff,ones(size(ff))*slopeplate,'LineStyle', '--', 'LineWidth', 1, 'Color', [0 0 0]);
xlabel('Frequency $f$ [Hz]');
ylabel('$\Delta N/\Delta f$ [1/Hz]');
mygrid;
%legend('with torsion','without torsion');
figure(fig3);
plot(ff,ones(size(ff))*slopeplate,'LineStyle', '--', 'LineWidth', 1, 'Color', [0 0 0]);
xlabel('Frequency $f$ [Hz]');
ylabel('$\Delta N/\Delta f$ [1/Hz]');

mygrid;
%legend('with torsion','without torsion');
figure(fig4);
subplot(fig4l);
ylim([0 2]);
xlabel('Frequency $f$ [Hz]');
ylabel('$\Delta N/\Delta f$ [1/Hz]');
```

```
mygrid;
subplot(fig4r);
ylim([0 2]);
xlabel('Frequency $f$ [Hz]');
ylabel('$\Delta N/\Delta f$ [1/Hz]');
mygrid;
```

C.2.3 devideModes.m

This script implements the geometrical approach described in section 9.1

```
% this script loads eigenvalues and eigenvectors and devides the modes into
% two groups determined by a separation-angle.

clc; clear all; close all;

load('lgsEVPdata')

slopeplate = real(lx*ly*mp/(2*sqrt(Bp*mp))); % modal density of a plate from MO 7022

% idea: choose an angle, find perpendicular modes (above the angle)
% plot the modal density of these modes, observe grouping in pass- and stop
% bands (hopefully).

% for each eigenvector, determine if it's normal or perpendicular and
% create an index-vactor that can be used to find related eigenvalues.

separationAngle = 35;%15:5:20; % [degree] separation angle

for sepAng=separationAngle;

separationVector = zeros(M*N,1); % 0 if below separation, 1 if above
rows = 1:M; % all rows

cols = min(N,floor(rows*tand(90-sepAng)));% columns to count below separation

for ii = rows
    colsBelow = cols(ii);
    separationVector(N*(ii-1)+1:N*ii)=[zeros(colsBelow,1);ones(N-colsBelow,1)];
end

separationIndex = zeros(M*N,1);

for ii = 1:M*N
    eigenvector = V(:,ii);
    below=abs(sum(eigenvector(¬separationVector).^2));
    above=abs(sum(eigenvector(¬¬separationVector).^2));
    if below<above
        separationIndex(ii)=1;
    end
end

eigenfreqBelow = sort(sqrt(real(Di(¬separationIndex)))/(2*pi));
eigenfreqAbove = sort(sqrt(real(Di(¬¬separationIndex)))/(2*pi));
eigenfreqAll  = sort(sqrt(real(Di))/(2*pi));

%%% fig1

fig1=newloglogfig;
plot(eigenfreqAbove,1:length(eigenfreqAbove))
plot(eigenfreqBelow,1:length(eigenfreqBelow))
plot(eigenfreqAll,1:length(eigenfreqAll),'--')

%%% fig2
df = 10; % Hz
```

```
55  ff=0:df:10e3;
56
57  DNr=histc(eigenfreqAbove,ff)/df;
58
59  fig2=newlinfig;
60  plot(ff,DNr);
61
62  DNr=histc(eigenfreqBelow,ff)/df;
63  plot(ff,DNr);
64
65  DNr=histc(eigenfreqAll,ff)/df;
66  plot(ff,DNr,'--');
67
68  %%% fig3
69  fig3=newsemilogfig;
70
71  % calculate 1/6 octave bands from 10 Hz to 5 kHz
72  freqs=[0 0];
73  cf = 1000*2^(1/12); % upper cut off
74  count = 0;
75  while cf>2
76      count = count+1;
77      freqs(count)=cf;
78      cf=cf/2^(1/6);
79  end
80  freqs=fliplr(freqs);
81  cf = 1000*2^(1/6)*2^(1/12); % upper cut off
82  while cf<10000
83      count = count+1;
84      freqs(count)=cf;
85      cf=cf*2^(1/6);
86  end
87  [rows cols] = size(Di);
88
89  DNr=histc(eigenfreqAbove,freqs)./(repmat(freqs*(2^(1/6)-1),cols,1))';
90  plot(freqs/2^(1/12),DNr);
91
92  DNr=histc(eigenfreqBelow,freqs)./(repmat(freqs*(2^(1/6)-1),cols,1))';
93  plot(freqs/2^(1/12),DNr);
94
95  DNr=histc(eigenfreqAll,freqs)./(repmat(freqs*(2^(1/6)-1),cols,1))';
96  plot(freqs/2^(1/12),DNr,'--')
97  %%%
98
99  % add legends and theoretical average value for just a plate w/o ribs
100 figure(fig1);
101 plot(10:5000,polyval([slopeplate 0],10:5000),'LineStyle', '--', 'LineWidth', 1, 'Color', [0 0 0]);
102 xlabel('Frequency $f$ [Hz]');
103 ylabel('Cumulative mode number');
104 mygrid;
105
106 figure(fig2);
107 plot(ff,ones(size(ff))*slopeplate,'LineStyle', '--', 'LineWidth', 1, 'Color', [0 0 0]);
108 xlabel('Frequency $f$ [Hz]');
109 ylabel('$\Delta N/\Delta f$ [1/Hz]');
110 mygrid;
111
112 figure(fig3);
113 plot(ff,ones(size(ff))*slopeplate,'LineStyle', '--', 'LineWidth', 1, 'Color', [0 0 0]);
114 xlabel('Frequency $f$ [Hz]');
115 ylabel('$\Delta N/\Delta f$ [1/Hz]');
116 mygrid;
117 end
```

C.3 Solving the forced problem

C.3.1 modalmodelEVP_forced_freq.m

This script produces a frequency response.

```
% Author: Kristoffer A. Dickow
% Part of MSc project, DTU 2009

clc;clear all; close all;
% requires that modalmodelEVP has been run first.
% plots deflection at a single point as a function of excitation frequency

t0 = clock; % needed to measure calculation time

load('woodbig')

% define observation point
x1 = 1.32;
y1 = 1;

%%% Calculation of deflection %%%

x0=1.32; % excitation point
y0=1;   % excitation point
f=10:5000; % frequency range

phimx0 = sqrt(2/lx)*sin(km*x0); % phi_m(x0)
psiny0 = sqrt(2/ly)*sin(kappan*y0);% psi_n(y0)

[Psix0 Psiy] = meshgrid(phimx0,psiny0);

Psix0 = Psix0.*Psiy;
Psix0 = Psix0(:);

phimx1 = sqrt(2/lx)*sin(km*x1); % phi_m(x1)
psiny1 = sqrt(2/ly)*sin(kappan*y1);% psi_n(y1)

[Psix1 Psiy] = meshgrid(phimx1,psiny1);

Psix1 = Psix1.*Psiy;
Psix1 = Psix1(:);

omega = f*2*pi;

Lambda_p = mp*diag(V'*conj(V));


%%%%%% calculate Lambda_b
psiyj=zeros(length(yj),N);
for jj=1:length(yj)
   psiyj(jj,:)=sqrt(2/ly)*sin(pi*yj(jj)/ly*(1:N));
end
psiyj=sum(psiyj,1);
Lambda_b=zeros(M*N,1);
for ii=1:M*N
    ci=V(:,ii);
    ci=reshape(ci,N,M)'.*repmat(psiyj,M,1);
    Lambda_b(ii)=mb*sum(sum(ci'*ci));
end

Lambda=Lambda_p+Lambda_b;

q = (V'*Psix1).*(V'*Psix0)./Lambda;

[Omega Omegay] = meshgrid(omega.^2, Di);
```

```
61
62 Omega = Omegay - Omega;
63
64 w=q'*(1./Omega);
65 v=1i*omega.*w;
66
67 disp(['Calculation time: ',num2str(etime(clock,t0)),' seconds'])
68
69 [fig1 fig1l fig1r]=newdoublesemilogfig;
70
71 subplot(fig1l)
72 plot(omega/(2*pi),10*log10(abs(v.^2)/(sqrt(2)*1E-9)^2))
73 xlabel('Frequency f [Hz]');
74 title('Velocity level');
75 ylabel('[dB re 10^-9 [m/s]');
76 mygrid
77
78 subplot(fig1r)
79 plot(omega/(2*pi),phase(v))
80 ylim([-pi pi]);
81 xlabel('Frequency f [Hz]');
82 title('Phase');
83 ylabel('[radians]');
84 set(gca,'YTick',[-pi -pi/2 0 pi/2 pi],'YTickLabel',...
85     {'-π' ;'-π/2'; '0' ;'π/2' ;'π'});
86 mygrid
```

C.3.2 modalmodelEVP_forced.m

This script plots the forced vibration response based on the eigenvalues and eigenvectors. Further, it plots some of the actual mode shapes.

```
1  % Author: Kristoffer A. Dickow
2  % Part of MSc project, DTU 2009
3
4  clc;clear all; close all;
5  % requires that modalmodelEVP has been run first.
6  % the output is comparable to modalmodelforced.m, but is based on actual
7  % modeshapes calculated by modalmodelEVP.
8
9  t0 = clock; % needed to measure calculation time
10
11 load('steeloffcenter') % file to load
12
13 [x,y]=meshgrid(0:.03:lx,0:.03:ly);
14 x = x(1,:);
15 y = y(:,1);
16
17 %%% Calculation of deflection %%%
18
19 x0=1.32; % excitation point
20 y0=1.2; % excitation point
21 f=1000; % excitation frequency
22
23 phimx0 = sqrt(2/lx)*sin(km*x0); % phi_m(x0)
24 psiny0 = sqrt(2/ly)*sin(kappan*y0);% psi_n(y0)
25
26 [Psix0 Psiy] = meshgrid(phimx0,psiny0);
27
28 Psix0 = Psix0.*Psiy;
29 Psix0 = Psix0(:);
30
31 omega = f*2*pi;
32
```

```
x=x';
y=y';

X = length(x);
Y = length(y);
mrow = round(linspace(1,M,M*N)); % M is the outer variation of MN
ncol = repmat((1:N)',M,1);

phimx = sqrt(2/lx)*sin(repmat(x,1,M*N).*(pi/lx*repmat(mrow,X,1)));
psiny = sqrt(2/ly)*sin(repmat(y,M*N,1).*(pi/ly*repmat(ncol,1,Y)));

Lambda_p = mp*diag(V'*conj(V));


%%%%%% calculate Lambda_b
psiyj=zeros(length(yj),N);
for jj=1:length(yj)
   psiyj(jj,:)=sqrt(2/ly)*sin(pi*yj(jj)/ly*(1:N));
end
psiyj=sum(psiyj,1);
Lambda_b=zeros(M*N,1);
for ii=1:M*N
    ci=V(:,ii);
    ci=reshape(ci,N,M)'.*repmat(psiyj,M,1);
    Lambda_b(ii)=mb*sum(sum(ci'*ci));
end

Lambda=Lambda_p+Lambda_b;

Omega = Di-omega^2;

Q = sum(V'.*repmat((V'*Psix0)./(Lambda.*Omega),1,M*N),1);

w=phimx*diag(Q)*psiny;

v=abs(1i*omega*w)/(sqrt(2)*1E-9);

disp(['Calculation time: ',num2str(etime(clock,t0)),' seconds'])

figure();
v=10*log10(abs(v.^2));
pcolor(x,y,v'); shading interp; hold on;
set(gca,'CLim',[65 110])
%for yjj=yj
%   line([0 lx],[yjj yjj], 'LineStyle', ':', 'LineWidth', 2, 'Color', [0 0 0]);
%end
xlabel('x [m]');
ylabel('y [m]');


[Di I] = sort(real(Di)); % sort eigenvalues
Di = sqrt(Di)/(2*pi); % eigenfrequencies

% plot some of the modes

%find desired frequencies
fdes=[200 500];
[temp f1] = min(abs(Di-fdes(1)));
[temp f2] = min(abs(Di-fdes(2)));
clear temp

[fig left right]=newdoublemodeplot(lx,ly);

eigenvect = V(:,I(f1));
frek = Di(f1);
mode = phimx*diag(eigenvect)*psiny;
subplot(left)
pcolor(x,y,10*log10(abs(mode.^2))'); shading interp; hold on;
```

```
title(['Mode at ',num2str(round(10*frek)/10),' Hz']);

eigenvect = V(:,I(f2));
frek = Di(f2);
mode = phimx*diag(eigenvect)*psiny;
subplot(right)
pcolor(x,y,10*log10(abs(mode.^2))); shading interp; hold on;
title(['Mode at ',num2str(round(10*frek)/10),' Hz']);
```

C.3.3 modalmodelforced.m

This script plots the forced vibration response calculated without using the eigenfunction expansion.

```
% Modal model implemented from the draft paper
% "Non-diffuse bending waves in lightweight ribbed plates"
% by Jonas Brunskog and Hyuck Chung.

% Author: Kristoffer A. Dickow
% Part of MSc project, DTU 2009

% Calculates the forced deflection and creates pcolor plot

clear all; clc; %close all;

t0 = clock; % needed to measure calculation time

savefile=('filename'); % enter filename to save data

averages=1; % how many calculations to perform
octaves=0; % 1 for 1/1 octaves, 3 for 1/3 octaves, etc. (0 for exact frequency)

lx=4; % Plate dimension
ly=6; % Plate dimension

M = 500; % Truncation of m
N = 500; % Truncation of n

yj = .25:.5:ly; % Position of beams

f=1250; % Excitation frequency
x0=1.32; % Driving point
y0=1;% Driving point
F0=1; % Force amplitude

%%%%% 22mm chipboard on fir beams

% constants plate
hp=22e-3; % thickness
rhop=6.5e2; % density
nup=.3; % poisson ratio
Ep=4.6e9*(1+1i*.02); % Young's modulus

Bp=Ep*hp^3/(12*(1-nup^2)); % plate bending stiffness pr unit width
mp=rhop*hp; % plate mass per unit area

% constants beam
bb=5e-2; % width of beams
hb=10e-2; % height of beams
rhob=5.2e2; % density of beams
Eb=1.2e10*(1+1i*.02); % Young's modulus
nub=.3; % poisson

Bb=Eb*bb*hb^3/12; % beam bending stiffness
mb=rhob*(bb*hb); % beam mass per unit length
```

```
Gb=Eb/(2+2*nub); % Shear modulus
Tr = Gb*bb^3*hb/3; % Torsional stiffness
Theta = rhob*bb*hb^3/12; % Rotational mass moment of intertia
%Theta=Theta*4; % place the rotation axis at the end instead of centered

%%% STEEL CONSTRUCTION

% constants plate
hp=6e-3;%18e-3; % thickness
rhop=7.8e3;%6.5e2; % density
nup=.28;%.3; % poisson ratio
Ep=2e11*(1+1i*.01);%4.6e9*(1+1i*.02); % Young's modulus


Bp=Ep*hp^3/(12*(1-nup^2)); % plate bending stiffness pr unit width
mp=rhop*hp; % plate mass per unit area

% constants beam
bb=10e-3;%5e-2; % width of beams
hb=100e-3;%10e-2; % height of beams
rhob=rhop;%5.3e-2; % density of beams
Eb=Ep;%1.2e10*(1+1i*.02); % Young's modulus
nub=nup;%.3; % poisson

Bb=Eb*bb*hb^3/12; % beam bending stiffness
mb=rhob*(bb*hb); % beam mass per unit length
Gb=Eb/(2+2*nub); % Shear modulus
Tr = Gb*bb^3*hb/3; % Torsional stiffness
Theta = rhob*bb*hb^3/12; % Rotational mass moment of intertia
Theta=Theta*4; % place the rotation axis at the end instead of centered
%%%%%%%%%%

%LGS:
Bb=1.35e6*(1+1i*.02);
Bp=2800*(1+1i*.02);
mb=6.75;
mp=10.8;
Theta=.2;
Tr=1.29e4*(1+1i*.02);

[x,y]=meshgrid(0:.03:lx,0:.03:ly);
x = x(1,:);
y = y(:,1);

m = (1:M)';    % Column vector
n = (1:N);     % Row vector

km = pi*m/lx;  % Column w/ modes in x direction
kappan = pi*n/ly;% Row w/ modes in y direction

clear m n

phimx0 = sqrt(2/lx)*sin(km*x0); % phi_m(x0)
psiny0 = sqrt(2/ly)*sin(kappan*y0);% psi_n(y0)

S = length(yj);

Jdiag = sqrt(2/ly)*sin(yj'*kappan); % J-matrix is diagonal with M
                                    % Jdiag's on the diagonal

Idiag = sqrt(2/ly)*cos(yj'*kappan).*repmat(kappan,S,1);

clear yj

F = F0*phimx0*psiny0;
clear phimx0 phimy0

% Allocate memory
```

```
120 v = zeros(length(x),length(y));
121
122 if octaves==0;
123     fmin=f;
124     fmax=f;
125 else
126     fmin = f/2^(1/(2*octaves));
127     fmax = f*2^(1/(2*octaves));
128 end
129
130 for aa=1:averages
131     f=fmin+(fmax-fmin)*rand();
132     omega=f*2*pi;
133
134     % Allocate memory
135     w = zeros(length(x),length(y));
136
137     c = zeros(M,N);
138
139     Ma = Bp*(km.^2*ones(1,N)+ones(M,1)*kappan.^2).^2-mp*omega^2; % MxN matrix
140     Mb = Bb*km.^4*ones(1,S)-mb*omega^2; % MxS matrix
141     Mc = Tr*km.^2*ones(1,S)-Theta*omega^2;
142
143     for ii=1:M
144         Matr = diag(Ma(ii,:))+Jdiag'*diag(Mb(ii,:))*Jdiag;%+Idiag'*diag(Mc(ii,:))*Idiag; % NxN
145         c(ii,:) = Matr\(F(ii,:)');
146     end
147
148     %disp('constants calculated');
149     clear Mb Ma Mc Matr MatrWO
150
151     for ii=1:length(x)
152         for jj=1:length(y)
153             phimx = sqrt(2/lx)*sin(km*x(ii)); % phi_m(x) mode
154             psiny = sqrt(2/ly)*sin(kappan*y(jj));% psi_n(y) mode
155             wxy = phimx*psiny;
156             w(ii,jj) = wxy(:)'*c(:);
157         end
158     end
159
160     v=v+(abs(1i*omega*w)/(sqrt(2)*1E-9)).^2;
161     disp(['loop no. ',num2str(aa),' of ',num2str(averages)])
162     disp(['ETA ',num2str((averages-aa)*etime(clock,t0)/aa),' seconds'])
163 end
164 v=v/averages;
165 v=10*log10(abs(v));
166
167 save(savefile);
168
169 %%%
170 figure();
171 pcolor(x,y,v'); shading interp
172 set(gca,'CLim',[60 100],...
173     'PlotBoxAspectRatio',[lx ly 1])
174 colorbar('Location','EastOutside')
175 xlabel('x [m]');
176 ylabel('y [m]');
```

C.4 Other investigations

C.4.1 platevariation.m

This script calculates the eigenvalues for a number of nominally identical plates. The dimensions of each plate is varied randomly keeping the area constant. The eigenvalues

are stored for later analysis.

```
% Author: Kristoffer A. Dickow
% Part of MSc project, DTU 2009

% Multiple EVP. Small plate variations.
% Calculates the eigenvalues and stores them in a file.

clear all; clc; close all;

t0 = clock; % needed to measure calculation time

lx=4; % Plate dimension
ly=6; % Plate dimension

savefile='lgs1000plates';

M = 200; % Truncation of m
N = 150; % Truncation of n

yj = .3:.6:ly; % Position of beams
%yj = .5:1:ly; % Position of beams
yj = .25:.5:ly; % Position of beams

%%%%% 22mm chipboard on fir beams

% constants plate
hp=22e-3; % thickness
rhop=6.5e2; % density
nup=.3; % poisson ratio
Ep=4.6e9*(1+1i*.02); % Young's modulus

Bp=Ep*hp^3/(12*(1-nup^2)); % plate bending stiffness pr unit width
mp=rhop*hp; % plate mass per unit area

% constants beam
bb=5e-2; % width of beams
hb=10e-2; % height of beams
rhob=5.2e2; % density of beams
Eb=1.2e10*(1+1i*.02); % Young's modulus
nub=.3; % poisson

Bb=Eb*bb*hb^3/12; % beam bending stiffness
mb=rhob*(bb*hb); % beam mass per unit length
Gb=Eb/(2+2*nub); % Shear modulus
Tr = Gb*bb^3*hb/3; % Torsional stiffness
Theta = rhob*bb*hb^3/12; % Rotational mass moment of intertia
Theta=Theta*4; % place the rotation axis at the end instead of centered
%%% STEEL CONSTRUCTION

% constants plate
hp=6e-3;%18e-3; % thickness
rhop=7.8e3;%6.5e2; % density
nup=.28;%.3; % poisson ratio
Ep=2e11*(1+1i*.01);%4.6e9*(1+1i*.02); % Young's modulus


Bp=Ep*hp^3/(12*(1-nup^2)); % plate bending stiffness pr unit width
mp=rhop*hp; % plate mass per unit area

% constants beam
bb=10e-3;%5e-2; % width of beams
hb=100e-3;%10e-2; % height of beams
rhob=rhop;%5.3e-2; % density of beams
Eb=Ep;%1.2e10*(1+1i*.02); % Young's modulus
nub=nup;%.3; % poisson

```

```
Bb=Eb*bb*hb^3/12; % beam bending stiffness
mb=rhob*(bb*hb); % beam mass per unit length
Gb=Eb/(2+2*nub); % Shear modulus
Tr = Gb*bb^3*hb/3; % Torsional stiffness
Theta = rhob*bb*hb^3/12; % Rotational mass moment of intertia
Theta=Theta*4; % place the rotation axis at the end instead of centered
%%%%%%%%%%%

%LGS:
Bb=1.35e6*(1+1i*.02);
Bp=2800*(1+1i*.02);
mb=6.75;
mp=10.8;
Theta=.2;
Tr=1.29e4*(1+1i*.02);

m = (1:M)';    % Column vector
n = (1:N);     % Row vector

S = length(yj);

runs = 3000; % how many variations to perform

% Allocate memory
Di = zeros(M*N,runs);

for jj=1:runs
    lxr=lx+rand/10;
    lyr=lx*ly/lxr;

    km = pi*m/lxr;  % Column w/ modes in x direction
    kappan = pi*n/lyr;% Row w/ modes in y direction

    Kpmn = Bp*(repmat(km.^2,1,N)+repmat(kappan.^2,M,1)).^2; % MxN matrix use meshgrid

    Jdiag = sqrt(2/lyr)*sin(yj'*kappan); % J-matrix is diagonal with M
                                         % Jdiag's on the diagonal
    Idiag = sqrt(2/lyr)*cos(yj'*kappan).*repmat(kappan,S,1);
    for ii=1:M
        Km = diag(Kpmn(ii,:))+Jdiag'*(Bb*km(ii)^4*eye(S))*Jdiag+Idiag'*(Tr*km(ii)^2*eye(S))*Idiag;
        Mm = mp*eye(N)+Jdiag'*(mb*eye(S))*Jdiag+Idiag'*(Theta*eye(S))*Idiag;
        Dm = eig(Mm\Km);
        Di((ii-1)*N+1:ii*N,jj) = Dm;
    end
    disp(['Calculation time (loop ',num2str(jj),'): ',num2str(etime(clock,t0)),' seconds'])
end

% Di is a coloumn vector with eigenvalues

save(savefile);
disp(['Calculation time: ',num2str(etime(clock,t0)),' seconds'])
```

C.4.2 compareeigenvals.m

The script compares the eigenvalues calculated by the previous script, and plots the average modal density in 1/6th octave bands with standard deviation shown as error bars.

```
% devide eigenfreqencies into 1/6 octave bands and calculate mean and
% standard deviation. Input is a matrix with eigenvalues of comparable
% systems as columns
clear all; clc; close all;
load('steel3000plates');
Di = sqrt(real(Di))/(2*pi); % eigenfrequencies

slopeplate = real(lx*ly*mp/(2*sqrt(Bp*mp))); % modal density of a plate from MO 7022
```

```
9
10 % calculate 1/6 octave bands from 10 Hz to 5 kHz
11 freqs=[0 0];
12 cf = 1000*2^(1/12); % upper cut off
13 count = 0;
14 while cf>2
15     count = count+1;
16     freqs(count)=cf;
17     cf=cf/2^(1/6);
18 end
19 freqs=fliplr(freqs);
20 cf = 1000*2^(1/6)*2^(1/12); % upper cut off
21 while cf<10000
22     count = count+1;
23     freqs(count)=cf;
24     cf=cf*2^(1/6);
25 end
26 [rows cols] = size(Di);
27
28 DNr=histc(Di,freqs)./(repmat(freqs*(2^(1/6)-1),cols,1))';
29 y=mean(DNr,2);
30 s=std(DNr,0,2);
31
32 fig1=newsemilogfig;
33 ff=freqs/2^(1/12);
34 errorbar(ff,y,s);
35 plot(ff,ones(size(ff))*slopeplate,'LineStyle', '--', 'LineWidth', 1, 'Color', [0 0 0]);
36 xlabel('Frequency f [Hz]');
37 ylabel('dN/df [1/Hz]');
38 mygrid;
```

C.4.3 straightline.m

This script is used to investigate if the onsets of pass bands are periodic in kl.

```
1  clear all; clc; close all;
2  %%%%%%%%%%%% create fig %%%%%%%%%%%%
3  figure();
4  set(gca,'LineWidth',.5,...
5      'ColorOrder',[.2 .6 .8;.6 .8 .2;.4 0 .6;.2 .8 1;1 .6 0;...
6      0 .6 0;.2 0 .6;0 .4 0;.2 .4 .6],...
7      'PlotBoxAspectRatio',[16 9 9],'Box','on'...
8      );
9  set(gcf,'DefaultLineLineWidth',1.5);
10 %xlim([10 5000]);
11 grid off;
12 hold all;
13 %%%%%%%%%%%%%%%%%%%%%%%%%%%%%%%%%%%%
14
15 f=[870 1280 1760 2330 2960 3700 4500]; % onsets of pass bands
16 plot(sqrt(f),'Marker','o','MarkerSize',7,'LineStyle','none')
17 x=1:length(f);
18 p=polyfit(x,sqrt(f),1);
19 plot(x,p(1)*x+p(2));
20 ylabel('$\sqrt{f} \sim kl$')
21 xlabel('Fluctuation no.')
22
23 mygrid()
```

C.5 Functions to produce the layout of figures

The following functions are not affecting the numerical output of the model, but are only used to create the desired graphical layout.

C.5.1 newlinfig.m

This function creates a new figure with linear scales.

```
function h=newlinfig()
h=figure();
set(gca,'LineWidth',.5,...
     'XTick',(500:500:5000),...
    'XTickLabel',{'','1k','','2k','','3k','','4k','','5k'},...
    'ColorOrder',[.2 .6 .8;.6 .8 .2;.4 0 .6;.2 .8 1;1 .6 0;...
    0 .6 0;.2 0 .6;0 .4 0;.2 .4 .6],...
    'PlotBoxAspectRatio',[16 9 9],'Box','on'...
    );
set(gcf,'DefaultLineLineWidth',1.5);
xlim([10 5000]);
grid off;
hold all;
```

C.5.2 newsemilogfig.m

This function creates a new figure with logarithmic x-scale.

```
function h=newsemilogfig()
h=figure();
set(gca,'LineWidth',.5,'XScale','log',...
    'XTick',[10 30 50 100 300 500 1000 3000 5000],...
    'XTickLabel',{'10','30','50','100','300','500','1k','3k','5k'},...
    'ColorOrder',[.2 .6 .8;.6 .8 .2;.4 0 .6;.2 .8 1;1 .6 0;...
    0 .6 0;.2 0 .6;0 .4 0;.2 .4 .6],...
    'PlotBoxAspectRatio',[16 9 9],'Box','on'...
    );
set(gcf,'DefaultLineLineWidth',1.5);
xlim([10 5000]);
grid off;
hold all;
```

C.5.3 newloglogfig.m

This function creates a new figure with both scales logarithmic.

```
function h=newloglogfig()
h=figure();
set(gca,'LineWidth',.5,'XScale','log','YScale','log',...
    'XTick',[10 30 50 100 300 500 1000 3000 5000],...
    'XTickLabel',{'10','30','50','100','300','500','1k','3k','5k'},...
    'ColorOrder',[.2 .6 .8;.6 .8 .2;.4 0 .6;.2 .8 1;1 .6 0;...
    0 .6 0;.2 0 .6;0 .4 0;.2 .4 .6],...
    'PlotBoxAspectRatio',[16 9 9],'Box','on'...
    );
set(gcf,'DefaultLineLineWidth',1.5);
xlim([10 5000]);
grid off;
hold all;
```

C.5.4 newdoublesemilogfig.m

This function creates a new figure with two semi logarithmic subplots.

```
function [h left right]=newdoublesemilogfig()
h=figure();
left=subplot(1,2,1,'Parent',h);
set(gca,'LineWidth',.5,'XScale','log',...
    'XTick',[10 30 100 300 1000 3000],...
    'XTickLabel',{'10','30','100','300','1k','3k'},...
    'ColorOrder',[.2 .6 .8;.6 .8 .2;.4 0 .6;.2 .8 1;1 .6 0;...
    0 .6 0;.2 0 .6;0 .4 0;.2 .4 .6],...
    'PlotBoxAspectRatio',[16 9 9],'Box','on'...
    );
set(gcf,'DefaultLineLineWidth',1.5);
xlim([10 5000]);
grid off;
geom=get(gca,'Position');
hold all;
right=subplot(1,2,2,'Parent',h);
set(gca,'LineWidth',.5,'XScale','log',...
    'XTick',[10 30 100 300 1000 3000],...
    'XTickLabel',{'10','30','100','300','1k','3k'},...
    'ColorOrder',[.2 .6 .8;.6 .8 .2;.4 0 .6;.2 .8 1;1 .6 0;...
    0 .6 0;.2 0 .6;0 .4 0;.2 .4 .6],...
    'PlotBoxAspectRatio',[16 9 9],'Box','on',...
    'YAxisLocation','right');
set(gcf,'DefaultLineLineWidth',1.5);
set(gca,'Position',geom+[geom(3)+.05 0 0 0])
xlim([10 5000]);
grid off;
hold all;
```

C.5.5 newdoublepcolorfig.m

This function creates a new figure with two color plots.

```
function [h left right]=newdoublepcolorfig(lx,ly,range)
% lx and ly are dimensions
if nargin==0
    lx=4;
    ly=6;
    range=[65 110];
end

h=figure();

left=subplot(1,2,1,'Parent',h);
set(gca,'LineWidth',.5, ...
    'PlotBoxAspectRatio',[lx ly 1],...
    'CLim',range,...
    'YAxisLocation','left');
set(gca,'Position',get(gca,'Position')-[.05 0 0 0])
xlim([0 lx]);
ylim([0 ly]);
xlabel('x [m]');
ylabel('y [m]');
geom=get(gca,'Position');
hold all;
right=subplot(1,2,2,'Parent',h);
set(gca,'LineWidth',.5, ...
    'PlotBoxAspectRatio',[lx ly 1],...
    'CLim',range,...
    'YAxisLocation','right');
```

```
colorbar('Location','EastOutside')
set(gca,'Position',geom+[geom(3)+.05 0 0 0])
xlim([0 lx]);
ylim([0 ly]);
xlabel('x [m]');
ylabel('y [m]');
hold all;
```

C.5.6 newdoublemodeplot.m

Similar to the previous script.

```
function [h left right]=newdoublemodeplot(lx,ly)
% lx and ly are dimensions
if nargin==0
    lx=4;
    ly=6;
end

h=figure();

left=subplot(1,2,1,'Parent',h);
set(gca,'LineWidth',.5, ...
    'PlotBoxAspectRatio',[lx ly 1],...
    'YAxisLocation','left');
set(gca,'Position',get(gca,'Position')-[.05 0 0 0])
xlim([0 lx]);
ylim([0 ly]);
xlabel('x [m]');
ylabel('y [m]');
geom=get(gca,'Position');
hold all;
right=subplot(1,2,2,'Parent',h);
set(gca,'LineWidth',.5, ...
    'PlotBoxAspectRatio',[lx ly 1],...
    'YAxisLocation','right');
set(gca,'Position',geom+[geom(3)+.05 0 0 0])
xlim([0 lx]);
ylim([0 ly]);
xlabel('x [m]');
ylabel('y [m]');
hold all;
```

C.5.7 mygrid.m

This function adds solid grey gridlines to an existing figure.

```
function mygrid(h,col)
if nargin<3
    rightaxes=false;
    if nargin<2
        col=[.6 .6 .6];
        if nargin==0
            h=gcf;
        end
    end
end
figure(h);
limX=get(gca,'XLim');
limY=get(gca,'YLim');
tickX=get(gca,'XTick');
tickY=get(gca,'YTick');
```

```
16
17 for ii=tickX;
18     line([ii ii],limY,'Color',col,'LineWidth',.5);
19 end
20 for ii=tickY;
21     line(limX,[ii ii],'Color',col,'LineWidth',.5);
22 end
23 line(limX,[limY(1) limY(1)],'Color',[0 0 0],'LineWidth',.5);
24 line(limX,[limY(2) limY(2)],'Color',[0 0 0],'LineWidth',.5);
25 line([limX(1) limX(1)],limY,'Color',[0 0 0],'LineWidth',.5);
26 line([limX(2) limX(2)],limY,'Color',[0 0 0],'LineWidth',.5);
```

List of Symbols

List of symbols

$\tilde{A}, A$	Amplitude
b, b_b	Beam width [m]
B_b	Bending stiffness (beam) [Nm^2]
B'_p	Bending stiffness per unit width (plate) [Nm]
$c_b, c_{b,b}, c_{b,p}$	Bending wave speed [m/s]
$\mathbf{c}, \mathbf{c}_b, \mathbf{c}_r$	Coefficient vectors
$c_{mn}, c^b_{mj}, c^r_{mj}$	Complex coefficients for plate, beam (transverse) and beam (rotation) respectively
$\mathbf{C}$	Matrix containing eigenvectors, see equation (6.5)
e	base of the natural logarithm
E, E_p, E_b	Young's modulus of elasticity [$\mathrm{N/m}^2$]
f	Frequency [Hz]
$\tilde{F}, F$	Force [N]
F	A function (chapter 4)
$\mathbf{F}$	Force vector
G	Shear modulus [$\mathrm{N/m}^2$]
$\mathbf{G}_i$	Matrix, see equation (6.12)
h, h_p	Plate thickness [m]
h, h_b	Beam height [m]
$\mathbf{H}_i$	Matrix, see equation (6.11)
i	Imaginary unit
I	A functional (chapter 4)
I, I_y	Second area moment of inertia [m^4]
j	Beam number
$\mathbf{J}$	Coupling matrix
$k_b, k_{b,b}, k_{b,p}$	Structural wavenumber for bending waves [m^{-1}]
k_m	Used for mode shapes. See equation (5.20)
$\mathcal{K}, \mathcal{K}_p, \mathcal{K}_b$	Kinetic energy [J]
$\mathbf{K}, \mathbf{K}_p, \mathbf{K}_b, \mathbf{K}_r$	Stiffness matrices

to be continued

List of symbols (continued)

$\mathbf{L}$	Coupling matrix
l_x, l_y	Length [m]
$\mathcal{L}$	Lagrangian [J]
m, n	Integers used to keep track of modes
m	Mass [kg]
m', m'_b	Mass per unit lenght [kg/m]
m'', m''_p	Mass per unit area [kg/m^2]
M, N	Truncation of Fourier series
M	Total mass (only chapter 7)
$\mathbf{M}, \mathbf{M}_p, \mathbf{M}_b, \mathbf{M}_r$	Mass matrices
p	Pressure [Pa]
P	Time averaged power [W]
$\mathcal{P}, \mathcal{P}_p, \mathcal{P}_b$	Potential energy [J]
$\mathbf{q}$	Coefficient vector, see equation (6.25)
$\mathbf{Q}$	Coefficient matrix, see equation (6.20)
r	Damping constant [kg/s]
s	Spring constant [N/m]
S	Area [m^2]
S	Number of beams (chapter 5 onwards)
$\mathcal{S}$	Action integral
t, t_0, t_1, t_2, T	Time [s]
T_r	Rotational stiffness [Nm^2]
$\tilde{u}_j, u_j$	Angular displacement
$\tilde{v}, v$	Velocity [m/s]
$\tilde{w}, w$	Transverse plate displacement [m]
$\tilde{w}_b, w_b$	Transverse beam displacement [m]
$\mathcal{W}$	Work [J]
x	Displacement [m]
x, y, z	Cartesian coordinates
$\tilde{Y}, Y$	Mechanical mobility [m/Ns]
$\tilde{Z}$	Mechanical impedance [Ns/m
$\boldsymbol{\chi}$	Column vector, see equation (5.64)
δ	Variational operator
$\delta_0(\cdot)$	Dirac delta function
δ_{ij}	Kronecker delta
$\Delta(\cdot)$	Laplacian
$\Delta N/\Delta f$	Modal density [Hz^{-1}]
ε	A small value
η	Damping loss factor
$\gamma(\cdot)$	An arbitrary smooth function
λ	Roots of characteristic equation (chapter 3)
$\Lambda, \Lambda_i, \Lambda_p, \Lambda_b$	Norm
$\nabla(\cdot)$	Del operator, gradient, divergence
ν	Poisson's ratio

to be continued

List of symbols (continued)

κ_n	Used for mode shapes. See equation (5.20)
$\omega, \omega_n, \omega_i$	Angular frequency [rad/s]
$\boldsymbol{\Omega}$	Vector, see equation (6.16). Matrix, see equation (6.24)
$\varphi_m(x)$	Mode shape
$\boldsymbol{\varphi}$	Matrix, see equation (6.3)
$\tilde{\Phi}_i$	Complex mode shape of the i'th mode. See equation (5.63)
Θ'	Rotational mass moment of inertia [m^2/m]
$\psi_n(y)$	Mode shape
$\boldsymbol{\psi}$	Matrix, see equation (6.4)
ρ	mass density [kg/m^3]
$\boldsymbol{\Xi}$	Diagonal matrix, see equation (6.21)
$\overset{\perp}{=}$	Indicates the use of orthogonality
$\overline{x}$	Spatial averaging
$\langle x \rangle$	Time averaging
$\tilde{x}$	Denotes a complex quantity
$\dot{x}$	Time derivative
x^*	Complex conjugate
x^{T}	Transpose

Index

References

[1] N.H. Asmar. *Partial Differential Equations with Fourier Series and Boundary Value Problems*. Pearson Education, Limited, 2nd edition, 2004. ISBN 0-131-48096-0.

[2] I.N. Bronshtein, K.A. Semendyayev, G. Musiol, and H. Muehlig. *Handbook of Mathematics*. Springer-Verlag Berlin Heidelberg, New York, 5th edition, 2007. ISBN 978-3-540-72121-5.

[3] J. Brunskog and H. Chung. *Non-diffuse Bending Waves in Lightweight Ribbed Plates*. Not yet published, 2009. draft.

[4] J. Brunskog and H. Chung. *Lack of Diffuseness in Wave Propagation in Lightweight Joist Floors*. Inter-noise, 2007. 28-31 August 2007, Istanbul, Turkey.

[5] J. Brunskog, K. Dickow, and M. Ohlrich. *Modal Density and Modal Distribution in a Ribbed Plate*. Inter-noise, 2009. 23-26 August 2009, Ottawa, Canada.

[6] H. Chung and E. Grant. *Fourier Series Solutions to the Vibration of Rectangular Lightweight Floor/Ceiling Structures*. *Acta Acoustica united with Acoustica*, 94(3): 401–409, 2008.

[7] H. Chung, G. Dodd, G. Emms, K. McGunnigle, and G. Schmid. *Maximising impact sound resistance of timber framed floor/ceiling systems*. Final report, Report FWPRDC PN04.2005, Forest & Wood Products Research and Development Corporation, Australia, 2006. http://www.fwprdc.org.au.

[8] R. Courant and D. Hilbert. *Methods of Mathematical Physics*. Interscience Publishers, Inc., New York, first english edition, 1953.

[9] L. Cremer, M. Heckl, and B.A.T. Petersson. *Structure-Borne Sound. Structural Vibrations and Sound Radiation at Audio Frequencies*. Springer-Verlag, Berlin Heidelberg, 3rd edition, 2005. ISBN 3-540-22696-6.

[10] F. Fahy. *Foundations of Engineering Acoustics*. Elsevier Academic Press, 2001. ISBN 0-12-247665-4. Reprinted in 2005.

[11] J.B. Fraleigh and R.A. Beauregard. *Linear Algebra*. Addison-Wesley, 3rd edition, 1995. ISBN 0-201-52675-1.

[12] E.L. Hixson. *Harris' Shock and Vibration Handbook*, chapter 10. McGraw-Hill, 5th edition, 2002. ISBN 0-07-137081-1.

[13] F. Jacobsen, T. Poulsen, J.H. Rindel, A.C. Gade, and M. Ohlrich. *Fundamentals of Acoustics and Noise Control*. Lecture note at the Technical University of Denmark, 2007. Note no 31200.

[14] A.J. Keane and W.G. Price. *Statistical Energy Analysis of Periodic Structures. Proceedings of the Royal Society of London, series A*, 423:331–360, 1989.

[15] L.E. Kinsler, A.R. Frey, A.B. Coppens, and J.V. Sanders. *Fundamentals of Acoustics*. John Wiley & Sons, 4th edition, 2000. ISBN 0-471-84789-5.

[16] B.R. Kusse and E.A. Westwig. *Mathematical Physics*. Wiley-VCH, Weinheim, 2nd edition, 2006. ISBN 3-527-40672-7.

[17] C. Lanczos. *The Variational Principles of Mechanics*. University of Toronto Press, Canada, 1949.

[18] R.S. Langley. *A Wave Intensity Technique for the Analysis of High Frequency Vibrations. Journal of Sound and Vibration*, 159(3):483–502, 1992.

[19] R.S. Langley and A.N. Bercin. *Wave Intensity Analysis of High Frequency Vibrations. The Philosophical Transactions of the Royal Society*, 346:489–499, 1994.

[20] R.S. Langley, J.R.D. Smith, and F.J. Fahy. *Statistical Energy Analysis of Periodically Stiffened Damped Plate Structures. Journal of Sound and Vibration*, 208(3):407–426, 1997.

[21] R.H. Lyon and R.G. DeJong. *Theory and Application of Statistical Energy Analysis*. Butterworth-Heinemann, Newton, MA, 2nd edition, 1995. ISBN 0-7506-9111-5.

[22] B. R. Mace. *Periodically Stiffened Fluid-loaded Plates, 1: Response to Convected Harmonic Pressure and Free Wave Propagation. Journal of Sound and Vibration*, 73(4): 473–486, 1980.

[23] B. R. Mace. *Periodically Stiffened Fluid-loaded Plates, 2: Response to Line and Point Forces. Journal of Sound and Vibration*, 73(4):487–504, 1980.

[24] L. Madsen. Introduktion til LaTeX version 3 beta, 2008. `http://www.imf.au.dk/system/latex/bog/`, ID 2008-09-03-16-27.

[25] J. Mørkholt. *Structure-Borne Sound and Vibration. Structural Vibration and Sound Radiation From Plates. Part 3*. Technical University of Denmark, Acoustic Technology, Ørsted•DTU, 2nd edition, 2006.

[26] P.M. Morse and K.U. Ingard. *Theoretical Acoustics*. McGraw-Hill, United States of America, 1968.

[27] H. Nishino and M. Ohlrich. *Prediction of Medium Frequency Vibration by Wave Intensity Analysis*. Proceedings of Int. Conf. on Noise and Vibration Pre-design and Characterisation using Energy Methods, 2000. Lyon, France.

[28] H. Nishino and M. Ohlrich. *Application of Wave Intensity Analysis for Predicting Mid-frequency Vibration Transmission in Extended Plate Structures*. Inter-Noise, 2001. The Hauge, Netherlands.

[29] M. Ohlrich. *Structure-Borne Sound and Vibration. Introduction to Vibration and Waves in Solid Structures at Audible Frequencies. Part 1a*. Technical University of Denmark, Acoustic Technology, Ørsted•DTU, 2005.

[30] M. Ohlrich. *Structure-Borne Sound and Vibration. Vibration and Waves in Solid Structures at Audible Frequencies. Part 2*. Technical University of Denmark, Acoustic Technology, Ørsted•DTU, 2nd edition, 2006.

[31] T.D. Rossing. *Springer Handbook of Acoustics*, chapter 28. Modal Analysis, pages 1127–1138. Springer, 2007. ISBN 978-0-387-30446-5.

[32] I.H. Shames and C.L. Dym. *Energy and Finite Element Methods in Structural Mechanics*. Taylor & Francis, New York, si-units edition, 2003. ISBN 0-89116-942-3.

[33] L.-G. Sjökvist. *Structural Sound transmission and Attenuation in Lightweight Structures*. PhD thesis, Chalmers University of Technology, Department of Civil and Environmental Engineering, Division of Applied Acoustics, 2008.

[34] L.-G. Sjökvist, J. Brunskog, and F. Jacobsen. *Vibrational Behavior of a Rib-stiffened Plate – Theoretical Parameter Survey with a Fourier Series Model*. Included in PhD thesis by Sjökvist. Structural sound transmission and attenuation in lightweight structures. Chalmers University of Technology, Göteborg, Sweden, 2008.

[35] I. Steward and D. Tall. *Complex Analysis*. Cambridge University Press, United Kingdom, 2002 reprint edition, 1983. ISBN 0-521-28763-4.

[36] R. Szilard. *Theories and Applications of Plate Analysis. Classical, Numerical and Engineering Methods*. John Wiley & Sons, Inc., Hoboken, New Jersey, 2004. ISBN 0-471-42989-9.

[37] K.T. Tang. *Mathematical Methods for Engineers and Scientists 3*. Springer-Verlag Berlin Heidelberg, New York, 2007. ISBN 978-3-540-44695-8.

[38] Y.K. Tso and C.H. Hansen. *The Transmission of Vibration Through a Coupled Structure. Journal of Sound and Vibration*, 215(1):63–79, 1998.

[39] D.V. Wallerstein. *A Variational Approach to Structural Analysis*. John Wiley & Sons, New York, 2002. ISBN 0-471-39593-5.

[40] P. Wilson. *The Memoir Class for Configurable Typesetting*. The Herries Press, Normandy Park, WA, 2008.

[41] H.D. Young and R.A. Freedman. *University Physics*. Pearson Addison-Wesley, 12th edition, 2008. ISBN 0-321-50121-7.

www.elektro.dtu.dk

Department of Electrical Engineering
Acoustic Technology
Technical University of Denmark
Ørsteds Plads
Building 348
DK-2800 Kgs. Lyngby
Denmark
Tel: (+45) 45 25 38 00
Fax: (+45) 45 93 16 34
Email: info@elektro.dtu.dk